DISSERTATION

# VASCULAR ENDOTHELIUM GLYCOCALYX-MIMETIC SURFACES DESIGNED FOR BLOOD CONTACTING DEVICES

Submitted by

Jessi Vlcek

School of Biomedical Engineering

In partial fulfillment of the requirements

For the Degree of Doctor of Philosophy

Colorado State University

Fort Collins, Colorado

Fall 2021

Doctoral Committee:

Advisor: Matthew Kipper

Co-Advisor: Melissa Reynolds

Ketul Popat

Christine Olver

Copyright by Jessi Vlcek 2021
All Rights Reserved

# ABSTRACT

## VASCULAR ENDOTHELIUM GLYCOCALYX-MIMETIC SURFACES DESIGNED FOR BLOOD CONTACTING DEVICES

Each year millions of blood-contacting devices are used in clinical scenarios, with contact durations designed to range anywhere from hours to years.[1] Current blood-contacting devices can perform their intended purposes well but require the assistance of systemic drugs to inhibit failure via interactions between the material's surface and the surrounding biology. The drugs used to inhibit failure of these devices are associated with side effects that can cause increased morbidity of patients because of their systemic administration. Thus, there is a need to design materials that can inhibit thrombus, inflammation, and infection locally at the surface of a device.

In this work bio-inspired surfaces were engineered to reduce unfavorable blood-material reactions. The success of the designed surfaces was tested by evaluating their cell-material interactions, whole blood interactions, enzymatic stability, and mechanical durability. The inspiration behind these surfaces is the vascular endothelial glycocalyx, which is the luminal side of blood vessels, and inhibits blood coagulation during hemostasis. The vascular endothelial glycocalyx is a meshwork of glycosaminoglycans (GAGs), proteoglycans (PGs), and glycoproteins which are predominantly negatively charged that acts as mediator between the blood and the underlying tissue. The surfaces proposed in this work are made to mimic the glycocalyx in its topography and

chemistry by adsorbing polyelectrolyte multilayers (PEMs) onto a substrate, and subsequently adsorbing PG mimics on top of the PEMs. There are two different PG mimics used for this project which are: polyelectrolyte complex nanoparticles (PCNs) and proteoglycan mimetic graft copolymers (GC); both of which will present either heparin (HEP) or chondroitin sulfate (CS). Some of the surfaces will also be made to release nitric oxide (NO) from the surfaces through a modified version of chitosan (CHIT). Additionally, further modifications were made to the PEM surfaces to make them more mechanically durable by 1-Ethyl-3-(3-dimethylaminopropyl) carbodiimide (EDC), N-hydroxysuccinimide (NHS) crosslinking of the CHIT and hyaluronan (HA) layers, and the addition of an initial polydopamine (PDA) layer.

In the first chapter of this work outlines the current approaches to blood-contacting materials and their limitations, along with the biological components and processes that they will need to interact. The second chapter evaluates PCN and PEM surfaces that do and do not release NO via their cell-material interactions with key cell types in the processes of thrombosis, inflammation, and infection. Chapter three examines the interactions between two different PG-mimics (PC or GCs) and enzymes when suspended in solution or adsorbed onto PEM surfaces. The fourth chapter includes an evaluation of the mechanical durability of PEM and mechanically improved PEM surfaces, and whole blood evaluations of PG, GC, and modified and unmodified PEM surfaces. Taken together, this work produces multiple bioinspired surfaces that have varying degrees of success in their blood compatibility and longevity.

# ACKNOWLEDGEMENTS

This work could not have been possible without the contribution of others, and I would like to acknowledge all who has mentored, guided, and supported me throughout my PhD. First, I would like to acknowledge my advisor Dr. Matt Kipper and co-advisor Dr. Melissa Reynolds for helping shape me as a scientist and guide the work that is outlined in my dissertation. Matt, thank you for your enthusiasm about science, your unwavering positivity, and your willingness to meet with me about science followed by much needed chit chat. I admire your ability to explore research in topics/fields that you are unfamiliar with and how you continue to pursue knowledge. Melissa, thank you for your organized approach to science, making yourself available despite being located across campus, and always checking up on me as a scientist and as a person. I have enjoyed being mentored by both of you and it has made me a more well-rounded scientist and person. Additionally, thank you for your patience and positive outlook during my last year of graduate school which coincided with the COVID-19 pandemic.

Secondly, I would like to thank my committee members Dr. Ketul Popat and Dr. Christine Olver who helped shape the work outlined in this dissertation. Christine, thank you for your guidance in the monocyte and macrophage experiments I have conducted, and your expertise in clinical relevance. Ketul, thank you for your input on future experiments, creating a collaborative between your lab and Matt's, and mentoring me as a GTF.

I also want to acknowledge all the staff, scientists, and students that helped me through my PhD, and have improved me as a person and scientist. Thank you to all my

colleagues and lab mates who have helped me with my work, gave me feedback on presentations, and were always willing to talk to me about science and life including Dr. Hassan Hedayati, Dr. Liszt Yeltin, Dr. Alec Lutzke, Dr. Bella Neufeld, Dr. Raimundo Romero, Dr. Tara Wigmosta, Dafu Wang, Alyssa Melivn, Dr. Yanyi Zang, Jamie Cuchiaro, Roberta Sabino, and Jon Thai. I want to give a special thanks to Ananya Vajapayajula and Kelly Traller for helping me in the lab and having patients with me as they were the first undergraduate students I have mentored independently. I also want to thank the other undergraduate students: Sarah Igli, Natalie Rapp, and Anugrah Mathew, who helped my work by making PEM surfaces. I would also like to thank Dr. Stu Tobet and Sara Mattern of SBME for helping me navigate the program, Dr. Susan James who allowed me to rotate through her lab, Tim Gonzalez for fixing our equipment, Dr. Ellen Brennan-Pierce for managing the labs in Scott and teaching me more about lab safety, Tina Dihle for helping arrange the blood draws needed for my research, and Patt McCurdy and Rebecca Miller of the CIF.

Lastly, I would like to thank my family that raised me to be independent, and who despite not being scientist, always had a love for science and learning which was instilled in me. A special thank you to my friends that I have made in graduate school. You have helped me through some of the most difficult times of my life and have become like family. Keagan, Kevin, and Jerry thank you all for your never-ending support and making my home a happy one.

# DEDICATION

*To my family given and made.*

TABLE OF CONTENTS

# CHAPTER 1: INTRODUCTION

## Overview

The following sections outline background information for other chapters of this dissertation, approaches to designing blood compatible materials, and the rationale behind the material designs used in following chapters. An overview of blood, its components, and coagulation is first provided followed by a description of the endothelial glycocalyx, which consists of glycosaminoglycans, proteoglycans, glycoproteins, and nitric oxide. The state of hospital borne infections is reviewed and two common bacteria are highlighted: *Staphylococcus aureus*, and *Pseudomonas aeruginosa*. The problem of biomaterial longevity is highlighted. This is followed by overviews of different approaches taken by researchers to design blood-contacting materials. This chapter ends with goals and aims for the rest of the dissertation.

## 1.1. Blood components

Blood is both a fluid and a tissue; it transports nutrients, waste, and signals throughout the body. Blood can be classified as a tissue because it contains specialized cells that are suspended in a liquid medium called plasma. These cells consist of platelets, red blood cells, and leukocytes. Leukocytes include monocytes, neutrophils, basophils, eosinophils, and lymphocytes. In addition to cells, blood contains many different proteins. Each cell type in blood has a specific function. Red blood cells function mainly as a transporter, bringing oxygen to deoxygenated tissues and carrying $CO_2$ to the lungs to be expelled. Platelets function to propagate thrombus formation at the site of tissue damage. Leukocytes participate in both innate and adaptive immune responses.

### 1.1.1. The need for blood-contacting devices

Blood circulation driven by the cardiovascular system serves a variety of purposes, including transport of oxygen and nutrients required for all tissues to function. Damage to the cardiovascular system affects tissue function at the most basic levels and are thus associated with a multitude of different disease states. These states collectively termed cardiovascular disease the leading cause of death worldwide.[1,2,3] Cardiovascular diseases (coronary heart disease, congenital heart disease, rheumatic heart disease, pulmonary embolism, etc..) can require patient use of medical devices such as heart assists (helps circulate blood in the case of weaking heart or heart failure), replacement heart valves (replaces heart valves in the case of faulty valves which could be a result of developmental issues), extracorporeal membrane oxygenation machine (oxygenates and circulates blood during surgery), and stents (used to open occluded vessels in the case of plaque buildup).[4] These devices are designed to correct the malfunction causing the disease. However, the materials that these devices are made from do not interact favorably with blood.[5,6,7] The surfaces the biomaterials can initiate thrombosis and inflammation from interactions of blood components.[8,9] These materials can also allow the attachment of bacteria which can lead to infections.[10] There is an unmet need for development of materials designed to inhibit these unfavorable blood-material interactions. Design of materials with improved blood compatibility requires an understanding of the mechanisms leading to surface-induced thrombosis, inflammation, and infection.

### 1.1.2. Blood proteins and their roles

Blood can contain as many as 4500 different proteins and peptides that can participate in a vast array of biological processes.[5] The most abundant protein in blood is albumin. Other important blood proteins include fibrinogen, thrombin, von Willebrand factor (vWF), vitronectin, and the proteins of the complement system.[11] Fibrinogen, vWF, and vitronectin play important roles in coagulation and the complement system of proteins is associated with immune reactions. These proteins, among others, may adhere to biomaterials and lead to adverse biological reactions. For these reasons it is important for biomaterial researchers to understand how important blood proteins propagate coagulation and immune responses, and how different surface properties can influence protein-material interactions.

Fibrinogen is an abundant glycoprotein in blood (2 to 4 mg/mL) and is a key factor in regulating coagulation and inflammatory responses.[12,13] Fibrinogen is heterodimeric, with each dimer consisting of Aα, Bβ, and γ chains. Fibrinogen is a physiological marker of both coagulation and inflammation. Concentrations of fibrinogen can increase several fold whenever there is inflammation.[14]Coagulation and inflammation have been discussed as separate phenomena in the past, but they are now considered to be connected with similar mechanisms influencing their initiation.[12] While inflammation and coagulation are deeply connected, different properties of fibrinogen regulate each process separately. In coagulation, fibrinogen plays a role in platelet adhesion, and stabilizing the clot. When coagulation is activated, thrombin cleaves two short peptides, fibrinopeptide B and A from fibrinogen.[15] These two peptides then interact with each other to form fibrin, which contributes to the formation of a clot.[16] Fibrinogen also facilitates

platelet aggregation through interactions between platelet integrins and fibrinogen's γ chain C terminus.[17] Once the clot is fully formed, the fibrinolytic system regulates the break-down of the clot by the dissolution of fibrin.[12] Fibrinogen activates a variety of proinflammatory cells/responses through ligand-receptor interactions that are distinct from those that mediate coagulation.[12] Since fibrinogen can implement many responses from multiple mechanisms, researchers have investigated ways to inhibit fibrinogen binding on the surfaces of biomaterials.[18] When fibrinogen is adsorbed onto surfaces the fibrinogen protein can denature, exposing regions of the protein that can recruit platelets and inflammatory cells.

Thrombin is an allosteric serine protease that play a crucial role in thrombosis formation and is $Na^+$-activated.[19] Thrombin evolved from the proteins of the compliment system which are protein predominantly associated with immune responses. Thrombin has strong procoagulant activity by converting fibrinogen to fibrin which is one of the main structural components of a thrombus.[19] Thrombin also has anticoagulation activity in the presence of the cofactor thrombomodulin by the cleavage of the anticoagulant protein C.[19]

### 1.1.3 Protein interactions with biomaterials

Protein adsorption is often considered the first step in coagulation and inflammation at the surfaces of biomedical materials. Protein adsorption and denaturation creates a surface that has biological signals that blood cells can act upon. Protein adsorption and desorption onto surfaces is dictated by the physical and chemical properties of the proteins, the solutions they are suspended in, and the surface properties of the materials they are exposed to. Proteins may interact with material surfaces through

electrostatic interactions, van der Waals forces, hydrogen bonds, and hydrophobic dehydration. Irreversible protein adsorption onto surfaces is usually modeled as a series of steps that decreases the energy (G) of a system by a decrease in enthalpy (H) or an increase in entropy (S) at a constant T ($\Delta G = \Delta H - T\Delta S$).[5] Both the chemistry and the topography of surfaces can be changed to decrease protein adsorption and denaturation. Generally, Whitesides and coworkers to decrease protein adsorption onto surfaces by increasing the hydrophilicity of surfaces.[20] Hydrophilic surfaces are characterized by contact angles that are < 90° and have higher surface energy. Hydrophilicity decreases protein adsorption because hydrophilic surfaces tend to bind water strongly and for proteins to adsorb onto surfaces these water molecules would have to be displaced.

### 1.1.4. Platelets

Platelets, also called thrombocytes, are disc-shaped cell fragments that circulate through the cardiovascular system at a concentration of approximately 250,000 cells/uL.[21] The main function of thrombocytes is to help propagate the formation of a thrombus at the site of injury, initiating hemostasis, and preventing further blood loss. Platelets exist in a non-adhesive quiescent state and are concentrated in a fluid layer adjacent to the vessel wall. Due to their proximity to the vessel wall, they can immediately respond to a change in the endothelial lining, forming a clot in less than five minutes.[5,22]

In healthy vessel conditions, platelets maintain their quiescent state through multiple negative regulators presented by endothelial cells.[22] Intact endothelial cells release nitric oxide and prostacyclin (prostaglandin $I_2$, $PGI_2$) which in turn result in the phosphorylation of proteins essential to platelet activation, inhibiting the proteins' actions. These molecules' effects on platelets are reversable, and both have short half-lives.

Therefore, endothelial cells must continuously produce these signals. These signals decrease at the site of injury which results in pro-activation signals overriding the negative regulators.[22] Nitric oxide and prostacyclin are not the only negative regulators of platelet adhesion and activation. There are several checkpoints that platelets must pass before becoming activated, which prevent unwanted coagulation in healthy vessels and limit the size and intensity of clotting at the site of an injury. The first set of checkpoints are classified as receptor stimulation, which include platelet endothelial cell adhesion molecule (PECAM-1) and megakaryocyte and platelet inhibitory receptor G6B-B receptors located on platelets among other platelet/endothelial receptors.[22] The second checkpoint includes signaling pathways that control levels of platelet cytosolic calcium $Ca^{2+}$. Non-activated platelets have a low level of cytosolic $Ca^{2+}$, with values close to 50 nM, and when stimulated to activate $Ca^{2+}$, concentrations can increase to µM concentrations in a matter of milliseconds.[22] Increased $Ca^{2+}$ concentrations within the platelet cytosol help evoke cytoskeleton remodeling, integrin activation, granule secretion, and prostaglandin thromboxane $A_2$ ($TxA_2$ – stimulates platelet aggregation) generation.[22,23] The third and fourth signaling checkpoints for platelet activation consist of RAP1 (Ras-proximate-1) activation and the level of integrin outside-in signaling. Increasing RAP1 activation is associated with platelet adhesiveness and is dependent on $Ca^{2+}$-regulated signals.[22,24,25] Outside-in signaling consists of ligand binding to activated integrins which induces a cascade of signaling events. The signaling cascades in this final checkpoint contributes to platelet spreading and ultimately clot retraction and stabilization.[22,26] When each step in the platelets checkpoint system is passed, they become fully activated and contribute to the formation of a thrombus.

When tissue damage arises, tissue factor (TF) is expressed on the surface of the damaged or inflamed cells.[11,23] Additionally, collagen fibers may become exposed at the site of tissue damage, and there is less NO and $PGI_2$ production in that area. TF expression leads to tight binding of FVII which is then activated to FVIIa by several coagulation factors. These interactions result in small amounts of thrombin production.[27-29] At the same time platelets interact with and adhere to the exposed extracellular matrix components, and their activation is no longer inhibited by NO and $IPG_2$. The thrombin produced by the TF-expressing cells causes platelets to start to activate, leading to morphological and functional changes of the cell.[11,24,27,30,31] During activation platelets, their morphology changes from a discoid shape to a spherical one with extrusion of pseudopods.[32,33] More specifically, a spherical shape is characteristic of a platelet that is adhering to a surface. After adhesion, platelets can conform to a “short dendritic” (dendrites are shorter than the cell body) or “long dendritic” (dendrites are longer than the cell body) morphology. Both long and short dendritic stages are indicative of early-stage activation. Later stage activation is characterized by platelet spreading and aggregation. Fully activated platelets are said to have a “fried egg” morphology where the platelets are fully spread and flattened. Once activated, platelets express functioning cofactor V and VIII. Large-scale thrombin formation then takes place on the surface of the platelets, propagating thrombus formation.[31] The large-scale thrombin formation allows for the formation of a fibrin clot, which is laid onto platelets stabilizing the forming platelet plug. This, in turn, forms the clot that stops bleeding at the site of injury.[33] To help determine a material’s ability to inhibit coagulation many researchers have decided to evaluate platelet adhesion and activation.

### 1.1.5. Erythrocytes

Red blood cells (RBCs), erythrocytes are the main cell component of blood, and their main function is transporting O2 to tissues and CO2 and other wastes away to the lungs. The concentration of red blood cells in blood is dependent on sex, where males have a concentration of $4.35\times10^6$ to $5.65\times10^6$ cells/μL and females have $3.92\times10^6$ to $5.13\times10^6$ cells/μL. Erythrocytes have no nucleus, are biconcave discoid in shape, are extremely flexible, and contain the protein hemoglobin which is essential for erythrocytes' transport function.

Erythrocytes do not readily attach to biomaterials, but erythrocytes can lyse (hemolysis) due to shear stresses, interactions of RBCs with leachables, chemicals, electrical forces, and metal ions.[34–36] Hemolysis evaluations are the most common method to determine hemocompatibility of biomaterials.[37] When RBCs lyse they release their intracellular components into the circulating blood stream which may lead to hemoglobinemia, and in severe cases anemia.[38] Hemolysis due to implants has been correlated with complications that have been associated with mortality.[39] Thus researchers must design blood contacting devices/materials in ways that mitigate hemolysis.

### 1.1.6. Leukocytes and foreign body reactions

White blood cells (WBCs), or leukocytes are found at concentrations of 4500 to 11000 cells/μL. There are 3 different classifications of leukocytes which are granulocytes (neutrophils, eosinophils, and basophils), monocytes, and lymphocytes (T-, B-, and natural killer (NK) cells), which play parts in both the innate and acquired immune

systems. Neutrophils are the most numerous leukocyte type found in the blood (60-70%), followed by lymphocytes (25-20%), monocytes (3-8%), eosinophils (2-4%), and basophils (<1%). Each leukocyte cell type has different functions, but neutrophils and monocytes are most associated with their interactions with blood contacting biomaterials.[40]

All leukocytes respond to inflammation, and they migrate to the site of inflammation by first adhering to endothelial cells. This process of leukocyte recruitment is well documented.[41,42] First leukocytes rolling is initiated by the interactions between L-selectin present on most leukocytes and L-selectin and P-selectin expressed by inflamed endothelial cells (activated platelets can also express P-selectin).[41,43,44] Adhesion and rolling are also influenced by integrin interactions such as vascular cell-adhesion molecule 1 (VCAM1) with $\alpha_4\beta_1$-integrin on leukocytes and E-selectin/Intracellular adhesion molecule 1 (ICAM1) and $\beta_2$-integrins present on leukocytes.[45–47] The next step in this process is leukocyte arrest and activation. This is triggered by chemokines and mediated by the binding of leukocyte integrins to immunoglobulin superfamily members.[41] The leukocytes then migrate to the site of inflammation by either transcellular or paracellular migration. When activated leukocytes may crawl along vessel walls looking for the best site of transmigration.[41] During transmigration leukocytes have to pass through three barriers: endothelial cells, endothelial-cell basement membrane, and pericytes.[41] The paracellular migration pathway occurs when leukocytes slip between junctions of inflamed endothelial cells. It was previously believed that leukocytes migrate only using the paracellular route, but some studies have indicated that cells can use a transcellular route in the central nervous system and in vitro models[48–51]

Neutrophils and monocytes are more commonly evaluated for their responses to biomaterials as other leukocytes. Neutrophils are phagocytic cells that respond to the site of host-produced or bacteria-induced inflammation. Neutrophils are often the first cells to respond to the site of inflammation and function to destroy microbes using a variety of different antimicrobial mechanisms such as phagocytosis and development of phagosomes, excretion of substances capable of killing microbes/cells (such as: myeloperoxidase, defensins, lysozyme, bactericidal/permeability-increasing protein (BPI), etc.) from storage units specific to granulocytes (granules), and the use of reactive oxygen species.[52] Recruitment of other immune cells to sites of inflammation and infection by secretion of cytokines and chemokines i.e. IL-8, IL-1β, TNF-α, etc.) is another function of neutrophils.[52] Monocytes also are phagocytes and respond quickly to sites of infection and inflammation.[53] Monocytes can differentiate into macrophages or dendritic cells and are key components of the innate immune system.[53,54] Macrophages can adopt pro-inflammatory (M1), anti-inflammatory (M2), or mixed phenotypes, which are characterized primarily by their cytokine expression profiles.[55,54]

### 1.1.7. Leukocyte interactions with biomaterials

Neutrophils, monocytes, and macrophages can attach to biomaterials and cause an inflammatory response. These cells can attach to materials due to the presence of blood proteins on a surface or be recruited to the surface by the presence of activated platelets expressing p-selectin.[55,56] When in contact with biomaterials these phagocytic cells may try to engulf the foreign material. Since the materials are far too large for a single cell to engulf, more cells are recruited to help ingest the material.[57,58] These cells may also engage in a state of “frustrated phagocytosis” in which multinucleated foreign

body giant cells from, which are characteristic of chronic inflammation.[58,57] These cells along with other inflammatory cells can coat devices and deposit a fibrous capsule around the device inhibiting its intended purpose.[8,58]

### 1.2. Coagulation pathways

Hemostasis and thrombosis is a naturally occurring process in which a clot forms at the site of tissue damage to limit the loss of blood. The way this process should be discussed and characterized has been debated and has evolved throughout the years. Originally, blood clotting has been described as a biochemical cascade in which each clotting factor existed as a proenzyme which could be activated to a functional enzyme. This view was later modified after it was discovered that some coagulation factors were cofactors and not enzymes. This cascade was then split into extrinsic and intrinsic pathways which were sometimes said to converge at the “common pathway”. These pathways are briefly outlined in **Figure 1.1**. These pathways were then replaced by the cell based/TF models. *In vitro*, blood coagulation is still referred to as being broken up into intrinsic and extrinsic pathways.[40,59,60,9] Evaluating how biomaterials influence these pathways to cause unfavorable interactions has been a focus of material scientists and engineers, when designing new cardiovascular materials. Most studies tend to focus on the intrinsic pathway. This pathway occurs through the activation of FXII to FXIIa upon the presence of protein adsorption and then the activation of attached platelets.[9,61,62,59,60] The extrinsic pathway is started in response to the production of tissue factor (TF) which is expressed by damaged tissue. This process can also be initiated by inflammatory cells which have been activated by biomaterials to express TF.[40] Both intrinsic and extrinsic

pathways feed into the common pathway in which thrombin converts fibrinogen into fibrin. Fibrin then is polymerized making the matrix of the thrombus.[40]

Although materials are still evaluated on the basis of “intrinsic” or “extrinsic” pathways, coagulation has not been observed to independently operate through a separate intrinsic pathway or extrinsic pathway in vivo. For example, deficiencies in factor VIII or IX (components of the intrinsic pathway) result in serious bleeding disorders despite the extrinsic pathway still being intact.[63–65] The same is true for deficiencies of components of the extrinsic pathway. Deficiencies in factor VII lead to bleeding risks even though the intrinsic pathway is still intact.[63–65] Additionally, the role of FXII in the initiation of the intrinsic pathway is being debated due to deficiencies in this factor causing no clinical bleeding tendencies.[63,66,67] These findings suggest that the intrinsic and extrinsic “pathways” are not separately occurring phenomenon, and a better description of coagulation is needed.

A cell-based or TF based model of coagulation has been proposed which consists of different phases: initiation, amplification, and propagation (**Figure 1.2**).[63] The premise of these models is that coagulation is dependent on two cell types: TF-presenting cells and platelets.[63,65,67] These TF-presenting cells are typically not found in vasculature with the exception of monocytes.[63] The initiation phase of coagulation is started by the activation of TF-bearing cells, in which FVIIa rapidly binds. The TF-FVIIa complex amplifies the initial response by converting more FVII to FVIIa, and then activates FIX and FX.[63] This then leads to a small amount of thrombin production. The amplification stage is initiated by the activation of platelets from the thrombin production via the TF-bearing cells during initiation. The amplification phase is characterized by three

characteristic changes in platelets: platelet activation associated with a morphology change in the platelets, changes in the platelet membrane surface to its pro-coagulation form, and the release of granular contents from platelets, which contain additional coagulation factors.[63] At the same time the thrombin being produced by the TF-bearing cells is cleaving von Willebrand factor from FVIII, which allows it to mediate platelet adhesion and activation.[63] The propagation stage is initiated by the recruitment of additional platelets to the site of the TF-bearing cells.[63] The propagation phase occurs on platelet surfaces where ligand expression allows for platelet aggregation.[63] These aggregated platelets produce large amounts of FXa which results in a burst of thrombin production via the cleavage of thrombin.[63] This large amount of thrombin production then allows fibrinogen to convert to fibrin which spontaneously polymerize into fibrin strands creating a fibrin matrix.[63]

At the site of blood-contacting biomaterials thrombus formation is a complicated process. The initiation of thrombus formation begins by protein adsorption onto the surface of the material. Protein adsorption is not always problematic if the proteins can desorb from the material.[5] It is when the proteins denature and are unable to desorb that thrombus formation is most likely initiated. The adsorbed proteins can then interact with other blood components and initiate thrombus formation. Blood contacting materials can initiate coagulation through tissue damage associated with implantation, via protein adsorption, platelet adhesion and activation, or due to interactions between TF-bearing cells and the surface.

Inflammation and coagulation are interconnected in the foreign body response which results in failure of a biomaterial.[55,68] Activated platelets produce FVII, FXI, and PF4

which can recruit and cause a pro-inflammatory response in neutrophils or monocytes. These cells can also present TF and thus initiate the coagulation process on a surface or at the site of injury.

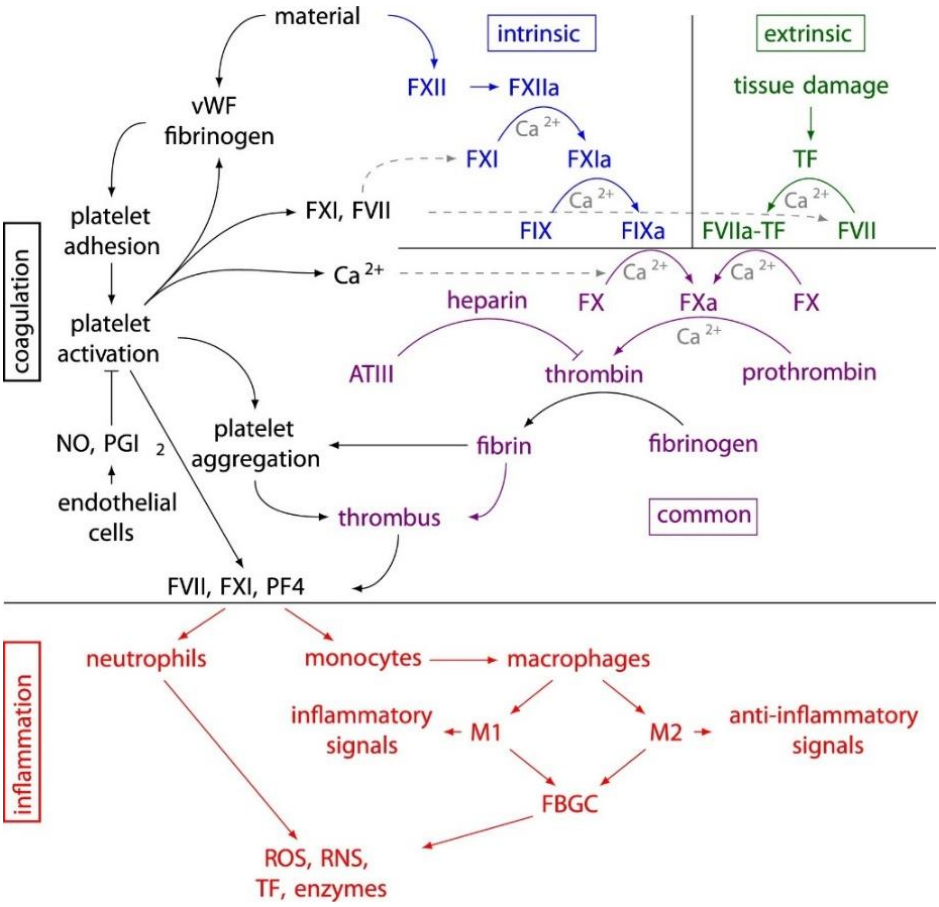


**Figure 1.1.** Schematic of relationships between coagulation and inflammatory pathways, with intrinsic, extrinsic, and common pathways labeled. Reprinted from Materials Science and Engineering: R: Reports, 138, Hedayati, M.H., Neufeld M.J., et. Al., The quest for blood-compatible materials: Recent advances and future technologies. 118-152, copywrite 2019, with permission from Elsevier.[40]

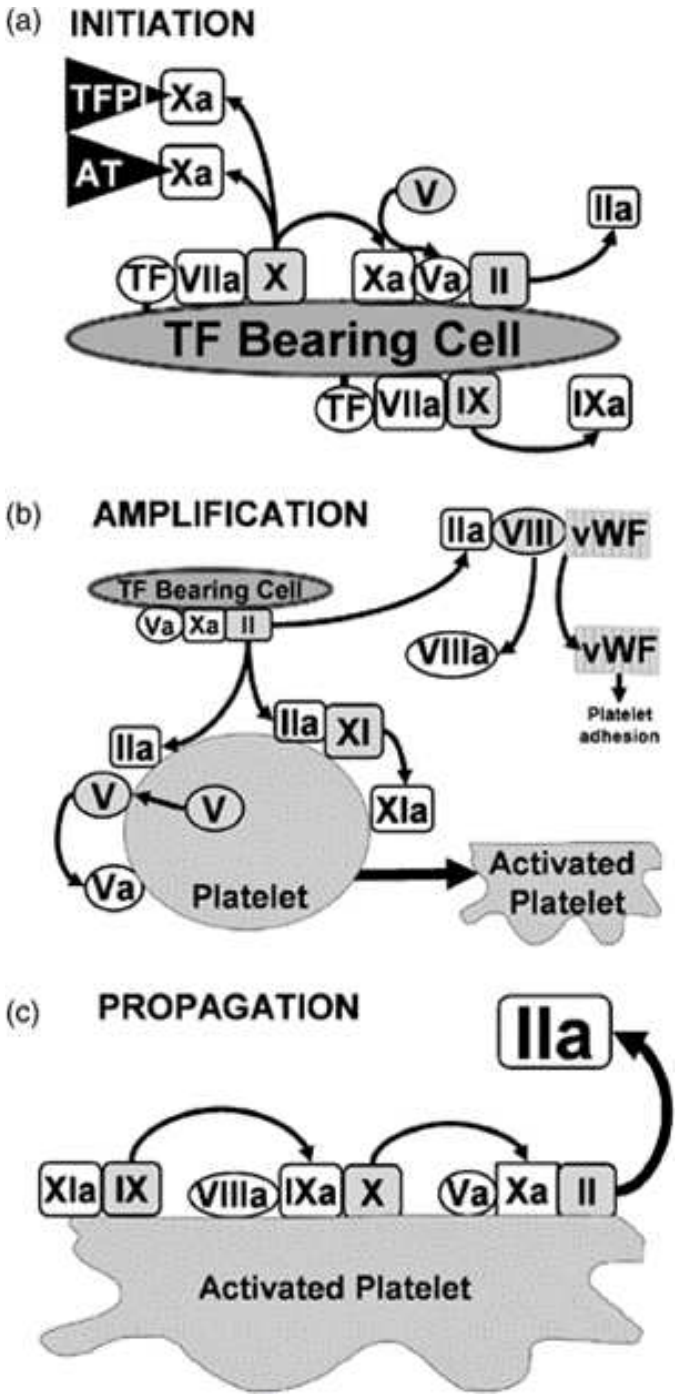


**Figure 1.2**. Schematic of coagulation cascade based on the cell-based model approach. Reprinted from Journal of Veterinary Emergency and Critical Care, 19, 1, Smith A.S., The cell-based model of coagulation. 3-10, copyright 2009 by permission of Wiley.[69]

### 1.3. The vascular endothelial glycocalyx

The only interface that interacts with blood and maintains normal function, is the vascular endothelial glycocalyx. The vascular endothelial glycocalyx is the inner luminal lining of blood vessels which consists of predominantly negatively charged macromolecules that are endothelium or plasma-derived. This layer consists of proteoglycans (PGs), glycoproteins (GPs), and glycosaminoglycans (GAGs), and soluble components which are arranged in a meshwork that is constantly being rearranged by enzymatic degradation, shear forces, endothelial cell activity, and adsorption and desorption of soluble molecules.[70]

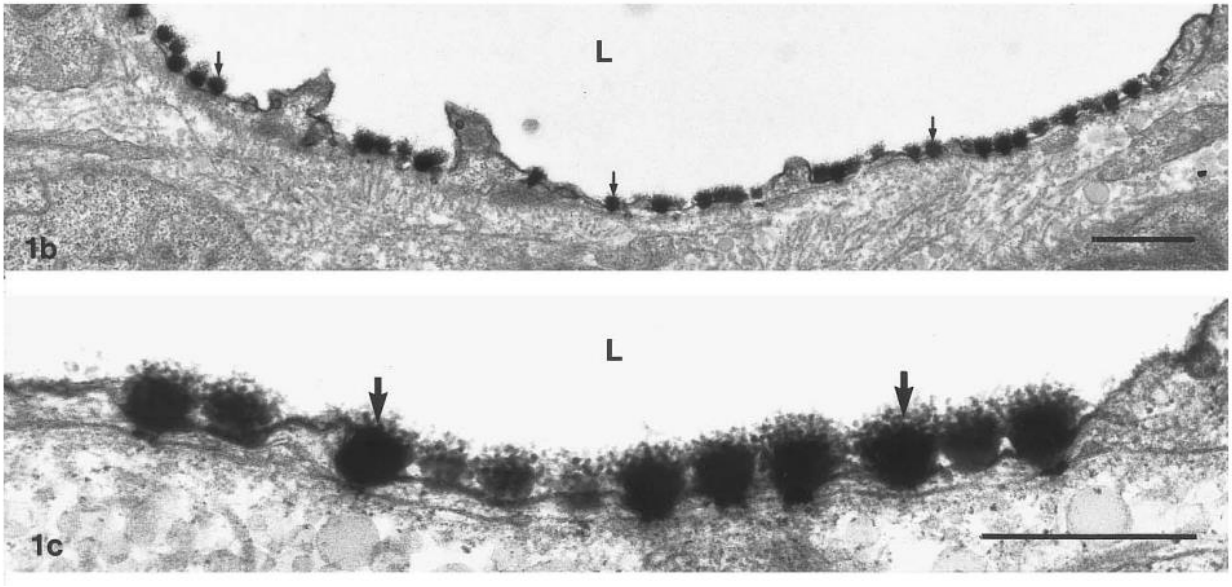


**Figure 1.3**. Electron micrograph images of a fenestrated capillary where "L" denotes the luminal side of the vessel. The bar in 1b is 1.0 µm and the bar in 1c is 0.5 µm. These micrographs were reproduced from Microvascular Research, 53, Jørgen Rostgaard and Klaus Qvortrup, Electron Microscopic Demonstrations of Filamentous. Molecular Sieve Plugs in Capillary Fenestrae, 1-13, Copyright (1997), with permission from Elsevier.[71]

### 1.3.1. Proteoglycans

PGs are the backbone of the glycocalyx.[72] PGs are macromolecular glycoconjugates and can be anchored to cells (such as syndecans or glypicans) or secreted by the cells (such as mimecan, and perlecan). These macromolecules can be found in most tissues in the human body and consist of a protein core to which GAGs can be linked. Different types of PGs can differ in their protein core, protein chain length, the GAGs bound, and the number of GAGs bound.[73] There is variability in the conformation within PG types. Differences in the number and type of GAGs attached to the protein core may change under different stimuli.[74,75] This wide variability in structure corresponds to the wide variety of functions of PGs in the glycocalyx as well as most other tissues. For example, PGs are known to contribute to mechanical properties of tissues, are organizers of other macromolecules, participate in a wide variety of signaling pathways, and cell differentiation. Additionally, misfunction associated with PGs is associated with a variety of diseases and disorders.

### 1.3.2. Glycosaminoglycans

GAGs (mucopolysaccharides) are negatively charged polysaccharides that are composed of repeating disaccharide units that are present in mammalian tissues. The most common GAG in the glycocalyx is heparan sulfate. Heparan sulfate is so abundant in the glycocalyx that proteoglycans presenting this glycosaminoglycan are considered to make up about 50-90% of the surface. [72] The second most abundant glycosaminoglycan is chondroitin sulfate, followed by dermatan sulfate, keratan sulfate, and hyaluronan (in

no order). Hyaluronan (HA) is unique to the other GAGs in that it is not covalently bound as proteoglycan sidechains. HA is attached to its assembly proteins instead. Glycosaminoglycans can be synthesized and modified resulting in thousands of different variations of these molecules which corresponds to the complexity of biological processes that they can help respond to or modulate, making them multifunctional polysaccharides.

### 1.3.3. Glycoproteins

Glycoproteins (GPs) are proteins that have carbohydrate groups attached to the polypeptide chain. GPs can also act as a "backbone" and are more classified due to their function. Some different families of these molecules include selectins, integrins, and immunoglobulins. These molecules play important roles as cell adhesion molecules, and influence coagulation, fibrinolysis, and hemostasis.[72]

### 1.3.4. Glycocalyx structure and function

The endothelial glycocalyx is not a static surface, so determining the structure of a healthy glycocalyx has been a challenge. Rostgaard *et al.* were able to capture images of the endothelial glycocalyx in a nephron artery by transmission electron microscopy (TEM) (**Figure 1.3**).[71,76] These images depict a surface that consists of clusters of macromolecules that are 100 to 200 nm in diameter. The thickness of the glycocalyx is reported to range from 200 to 4000 nm.[72] Depending on the imaging method used and the type of blood vessel, the structure and thickness of this layer changes. Even though the structure of this layer is difficult to define, it can be seen as a layer that is a meshwork of negatively charged molecules.

The luminal layer of blood vessels functions as an interface between the blood and the underlying tissue. The glycocalyx can help modulate hormone responses, inhibit platelet and leukocyte binding, initiate coagulation, regulate coagulation factors, quench free radicals, and contribute to a variety of other processes.[72] It also acts as a mechanotransducer, in which the changing forces due to the flow of blood are transmitted to the underlying tissue. This layer also acts as a molecular sieve. The dense meshwork of macromolecules keeps some circulating proteins, and cells from encountering the surface of the endothelium. Changes in density or net charge of this layer moderates what can encounter the surface of endothelial cells and what may not. Disturbances in this layer can cause inflammation, edema, capillary leak, platelet aggregation, hypercoagulability, and loss of vascular responsiveness.[77,78] A disrupted glycocalyx is often associated with disease states such as in hyperglycemia and atherosclerosis.[78–80] Additionally abnormalities/damage in the vascular endothelial glycocalyx can result in higher risk of severe disease symptoms. For example, the vascular glycocalyx has been proposed as a therapeutic target for the treatment of systemic COVID-19.[81] The endothelial layer can also release signaling molecules when prompted.[76] One such molecule is nitric oxide, which is released from the endothelium by the action of nitric oxide synthase. The release rates of NO are thought to be on the order of $10^{-10}$mol/cm$^2$/min from a healthy endothelium.[82]

### 1.3.5. Nitric oxide (NO)

NO is a small molecule hormone that has a short half-life that plays a variety of key roles in the cardiovascular system as well as in other biological systems. NO was first identified as an important component of the cardiovascular system because of its role in

vasodilation.[83–85] It has also been shown to have antiplatelet properties, and to contribute to angiogenesis in the cardiovascular system.[86–88] NO also plays a role in neurotransmission, inflammation, wound healing, and apoptosis, and it can act as an antibacterial agent.[86,88–93] In the Immune system nitric oxide is used by macrophages and other immune cells to kill potential pathogens, has an anti-tumor capacity by initiating cell cycle arrest and initiating apoptosis. NO can also have an anti-inflammatory effect by apoptosis of T cells, downregulation of macrophage proinflammatory cytokines, and downregulation of leukocyte adhesion molecules and chemokines.[94] The function of NO depends in part on the concentration. For example, lower concentrations can elicit responses that protect cells, were as higher concentrations can cause cell damage (1-100 nM vs. 400 – 1000 nm).[95] NO can act on cells and biomolecules either directly or indirectly through the production of peroxynitrite, nitrate, nitrite, and dinitrogen trioxide.[96] The half-life of NO is variable due to its high reactivity. For example, in extravascular tissue NO half-life can range from 0.09s to 2s and the half-life of NO in whole blood is much smaller ($1.8 \times 10^{-3}$ s) due to the presence of heme groups which NO reacts highly with.[96,97]

### 1.4. Hospital associated infections and bacteria

Along with all other implantable devices, blood-contacting ones pose a risk of infection.[10,98,99] Current sterile practices have reduced the instance of surgery-induced and medical device-induced infections, but these infections still persist.[100] The annual incidence of heath care associated infections in the united states is approximately 1.7 million, and patients in intensive care units (ICUs), burn units, organ transplant recipients, and neonates are particularly vulnerable to these infections.[98,101,102] The rate of infection

for some patient populations has improved in recent years.[103] The most common types of hospital-borne infections are: central line-associated bloodstream infections, catheter associated urinary tract infections, surgical site infections, and ventilator associated pneumonia.[98] Catheter-associated urinary tract infections are the most common, but central line-associated bloodstream infections are the most deadly, with a mortality rate of 12-25%.[104,105] The most common microorganism responsible for these infections is bacteria, and the most common types of bacteria responsible for these infections are *Staphylococcus aureus*, *Streptococcus* species, *Enterococcus* species (gram-positive), *Escherichia coli*, *Proteus mirabilis*, *Enterobacter* species, *Pseudomonas aeruginosa*, *Acinetobacter baumanii*, and *Burkholderia cepacian* (gram-negative).[106]

Bacteria can be commonly classified as gram-negative or gram-positive depending on their interactions with gram stain, crystal violet-iodine complex and a safranin counter stain. Gram-positive bacteria have thick peptidoglycan cell walls that stain indigo, and gram-negative bacteria have a thin peptidoglycan cell wall surrounded by an outer membrane of phospholipids, lipopolysaccharides, and proteins that does not retain the complex stain and counter stain giving a pink coloration. The two classes of bacteria can have different resistances to antibiotic treatments and responses in host immune systems.[107–109] Gram-negative bacteria are more resistant to antibiotics due to their outer membrane. For antibiotics to reach their desired targets they must pass this outer member and changes in structure or chemical composition may inhibit the antibiotics to access their targets.

*Pseudomonas aeruginosa* is an aerobic, rod-shaped, gram-negative bacterium that can be non-pathogenic in intestinal linings and can be an opportunistic pathogen for

immunocompromised and critically ill patients. *P. aeruginosa* can become resistant to antibiotic treatments by modifying membrane permeability, over-expression of efflux pumps, acquiring resistance genes, and by gene mutations that make the bacterium more difficult to treat. *P. aeruginosa* along with some other species of bacteria can also form biofilms on medical materials making them more resistant to antibacterial agents, and contributes to their spreading.[110] A biofilm is an excretion of extracellular polymeric substances (EPS) consisting of exopolysaccharides, proteins, extracellular DNA (eDNA), and humic acids and lipids that surrounds and protects a community of bacteria from outside threats such as environmental factors, immune responses, and antibiotics.[111] Some of the most effective treatments for P. aeruginosa infections are Colistin in conjunction with anti-pseudomonas agents like imipenem, piperacillin, aztreonam, ceftazidime, or ciprofloxacin, and Fosfomycin therapy in conjunction with aminoglycosides, cephalosporins, and penicilins.[108,112]

*Staphylococcus aureus* is a gram-positive, cocci-shaped (round) bacteria that typically exist in clusters, exists non-pathogenically on the skin and in mucous membranes, and is a common pathogen in both clinical and community settings.[113] S. *aureus* is one of the most common infectious bacteria and causes a wide variety of infections in different tissue types. *S. aureus* can cause skin infections, soft tissue infections, blood stream infections, pneumonia, meningitis, endocarditis, toxic shock syndrome, osteomyelitis, septic arthritis, prosthetic device infections, urinary tract infections, and gastroenteritis.[113,114] Antibiotic resistant strains of *S. aureus* have been problematic, including the most well-known strain, MRSA (methicillin-resistant *Staphylococcus aureus*).[98,113,114] *S. aureus* also form biofilms making them more difficult

to treat and more difficult for the immune system to combat.[110,111,113] Treatment of infections caused by *S. aureus* is dependent on strain and infection type. Penicillin is still used to treat non-antibiotic resistant strains and vancomycin is used to treat MRSA strains, and sometimes fluid-replacement therapies are necessary to treat *S. aureus* infections.[113,115]

The prescription of systemic antibiotics to treat these and other infections has caused the adaption of antibiotic resistant strains.[116,117] Historically antibiotics have been over-prescribed by physicians in developed countries, and in developing countries patients can buy antibiotics over the counter.[98] Overuse of antibiotics in human medicine, veterinary medicine, and agriculture, as well as inappropriate administration of these antibiotics (inappropriate doses, self-medication, prolonged use, and lack or standardization) are the main reasons why antibiotic-resistant strains have been able to develop.[98] To help reduce the emergence of antibiotic resistant bacteria strains, infections should be minimized by better hygiene and sanitation, increased vaccinations, and better diagnostic methods to target and treat specific microbes.[98] To help decrease the rate of infections, there is a need for materials that inhibit bacterial growth and attachment, in a way that bacteria will not have a means to adapt to.

### 1.5. Biomedical material longevity

Depending on the function of biomaterials used in medicine some may need to function for days, or months, or years; other biomaterials are designed to degrade over time, permitting their replacement by healthy cells and tissues. The longevity of these materials needs to be characterized to ensure that functionality of the material is consistent with the span of usage. Many different factors may influence the longevity of

the material, including cell material interactions, mechanical forces, solution composition (pH, ionic strength, and availability of suspended gases), temperature changes, and interactions with biomolecules such as enzymes.[118–123] Blood-contacting materials must withstand fluid forces, and interactions with blood cells and proteins.[5,9,124] Most blood-contacting materials used are able to maintain their functions with the use of anticoagulants. Any improvements to these surfaces made to eliminate the use of systemic anticoagulants also needs to remain functional for the life of the material or device. For example, drug eluting stents have improved the rates of in-stent restenosis but have indices to fail later by late stent thrombosis, which is a catastrophic complication that may lead myocardial infarction or sudden cardiac death.[125–127] Additionally, polyethylene oxide-based materials have shown promise in inhibiting unfavorable blood-material interactions but are unable to do so long term.[4]

Materials designed for blood contacting applications will be subject to forces exerted on them by the flow of blood. Blood is a complex fluid that is non-Newtonian (shear thinning), but behaves as a Newtonian fluid at shear rates greater or equal to 100 $s^{-1}$.[128] Vascular wall shear rates can range from 10 $s^{-1}$ in large veins to about 2000 $s^{-1}$ in small arteries, and up to 40,000 $s^{-1}$ in severe atherosclerotic arteries.[129,130] This corresponds to shear stress values of 0.35 to 70 dynes/$cm^2$ for healthy vasculature.[131] The geometry of a blood vessel or a blood-contacting device will also determine the forces exerted on blood contacting materials.[124] For example, a stent may experience a pressure of 12.6 dynes/$cm^2$, whereas a hemodialysis membrane surface sees a much higher pressure of 63 dynes/$cm^2$. Additionally, devices such as blood bags see little to no

shear stress over the duration of their use.[124] Materials must be evaluated for their specific application to determine viability.

Material interactions with the surrounding biology will also influence the longevity of the devices for blood-contacting applications. Materials that are made with biopolymers that can be found naturally in the human body or materials that resemble naturally occurring biomolecules have to evaluate their longevity against naturally occurring enzymes.[120,132,133] Some groups are taking advantage of these properties, by designing enzyme-responsive materials that release an active agent when acted on by enzymes.[134–137]

### 1.6. Current and past approaches

The use of blood-contacting surfaces and materials that help inhibit coagulation can date back to medieval times when people were first experimenting with the use of blood and other bodily fluids in medicine.[138] Some of the earliest published documentations of this date back to over a hundred years ago, reporting that coating glass tubes with paraffin wax lengthens blood coagulation times compared to untreated glass controls.[139] More modern approaches to blood compatibility research can be dated back to about 60 years ago.[6] Despite many decades of investigation, there are still no truly blood-compatible materials available. Some current strategies that researchers have investigated are designing biologically “inert” surfaces (surface passivation), incorporation of bioactive components, the release of anti-coagulant agents, addition of thrombolytic agents, bioinspired surfaces, and endotheliazition of surfaces.

### 1.6.1. Inert surfaces

Inert/passive materials are designed to inhibit the adsorption of proteins onto their surfaces. Some approaches that have been taken to construct these surfaces are combining current materials with a hydrophilic polymer (such as: polyethylene oxide (PEO), polyethylene glycol (PEG), polyvinylpyrrolidone (PVP), poly(hydroxyethyl methacrylate) (PHEM), or dextran) or the addition of zwitterionic polymers such as poly(2-methacryloyloxyethyl phosphorylcholine) (PMPC), poly(carboxybetaine acrylamide) (PCBAA), poly(carboxybetaine methacrylate) (PCBMA), or poly(sulfobetaine methacrylate) (PSMA).[140–147] Surface passivation tends to work best when surfaces are net neutral (won't attract oppositely charged proteins), and are hydrophilic (water barrier inhibits proteins through steric repulsion) , and, in the case of grafted surface polymers, high molecular weight grafts.[148] High molecular weight grafted polymers work best due to the conformation that they adopt.[148] Low molecular weight grafts tend to coil onto themselves and stay near the surface of the substrate in which they are grafted to form a mushroom conformation. High molecular weight grafts tend to stretch away from the substrate and are "brush phase" grafts.[4,148] These brush phase grafts tend to be better at inhibiting protein adsorption. These qualitative rules have been used as a justification of surface design for multiple different surface types. Although well designed brush s surfaces can inhibit the accumulation of adsorbed proteins, they are still not blood compatible.[149,150] Even PEO (Medtronic) surfaces that have made it to the market have shown to not be reliable long term because the oxygen species in the material are subject to oxidation.[4] Recently work from Le et al, expanded on the general qualitative rules and took a quantitative approach to designing bioinert surfaces using quantitative structure-

property relationship techniques.[151] This work was able to use machine learning algorithms to quantitatively evaluate chemical properties of potential surfaces with their ability to inhibit protein adsorption, and called on the field to use more standardized methods for evaluating protein adsorption so that data can be used to establish quantitative models to surface design.[151]

### 1.6.2. Bioactive materials

The incorporation of bioactive components to surfaces has been one of the most extensively researched ways to improve blood-compatibility of surfaces. The most researched bioactive component for the application of blood contacting surfaces is heparin.[152,153] Heparin was first evaluated by Grott et, al. in the 1960s as graphite benzalkonium heparin (GBH).[154] Heparin has been widely used as an anticoagulant because it resembles naturally occurring heparan sulfate. Heparin actively inhibits thrombosis due to its interactions with antithrombin.[155] Using heparin as a bioactive agent is also beneficial because it acts as a classically recycling catalyst.[4] Due to these benefits and the extensive research into materials modified with heparin, there have been several commercialized heparinized materials such as CBAS® (Carmeda AB), Duraflo II (Baxter Corp.), and Astute® (BioInteractions Ltd).[156] Other bioactive agents that have been used other than heparin are hirudin, which inhibits thrombin directly, and antiplatelet agents such as dipyridamole, prostaglandins, and apyrase.[157–160] These bioactive agents and their modified forms have all shown promise in inhibiting coagulation at the surfaces of biomaterials. There are still some issues with these materials. Heparin-containing biomaterials can interact with many blood proteins which leads to unintended side effects, such as heparin induced thrombocytopenia (low platelet counts) (HIT).[161–163]

Additionally, hirudin's interaction between antithrombin is irreversible and its antithrombosis activity only occurs initially.[164] These materials are being enhanced to alleviate some of these issues. For example, heparin has been covalently complexed with antithrombin and nitric oxide release to improve its efficiency, and hirudin derivatives such as bivalirudin have been developed to allow the thrombin interactions with these molecules to be reversable.[165–167]

### 1.6.3. Drug release

Drug-eluting materials are also an approach that has been investigated in modern blood-contacting materials. These materials are usually designed to release anti-thrombogenic agents such as heparin or aspirin by degradation of the polymer coating that is incasing the agents.[168,169] For example, degradable polyurethane has been designed to release dipyridamole (DPA) slowly.[170] Drug-eluting materials have decreased platelet adhesion and improved endothelialization on the surfaces.[171] Nanotube arrays functionalized with polydopamine (PDA) were also used to control the release of the bioactive agent bivalirudin (BVLD), which resulted in reduced clot sizes.[172] More recent studies have taken a more "on-demand" approach to drug release. These materials are designed to interact with the circulating biological components and release the anti-thrombogenic agent only when needed. Maitiz *et al.* designed hydrogels that were crosslinked with heparin using peptide linkers, which are selectively cleaved by activated blood coagulation factors.[173]

Despite the success of these materials *in vitro*, they may have some limitations *in vivo*. The flow of blood may carry the drugs away from the site of the material, making the drug's activity no longer localized to the surface of the device. It is better to design

drug-releasing surfaces with agents that have short half-lives and can act locally when released. NO is a molecule that can act locally and inhibit some prothrombogenic interactions. NO is a small molecule hormone that has many functions throughout the body. It acts as a vasodilator, anti-platelet agent, bactericidal agent, and can inhibit leukocyte recruitment.[174–177,90] Nitric oxide release can be achieved from biomaterials by decomposition of *S*-nitrosothiols and *N*-diazeniumdiolates bound to surfaces.[178] To extend the release of NO long-term, researchers have developed the catalytic generation of NO. This is done by adding components in the material that induce the release of NO from RSNO factors found in the circulating blood.[86,179] The Meyerhoff group first proposed the development of these materials by using selenide-based and telluride-based materials.[180] These materials and other approaches to this, such as the addition of copper species, have been limited by their ability to function long-term and by the toxicity of their degradation byproducts.[5] Another approach to long-term NO release is the addition of metal organic frameworks (MOFs) containing catalytic metal centers as a means of NO generation.[181-183] These materials are still relatively new and their potential degradation, and cytotoxicity have not been explored extensively.[5]

### 1.6.4. Thrombolytic agents

Thrombolytic agent incorporation to surfaces takes a different approach to blood compatibility. These surfaces aim to destroy a thrombus once it has already formed rather than preventing the formation of a clot. The thrombolytic approach to surfaces exploits the body's natural fibrinolytic system, which destroys hemostatic plugs once they are no longer needed.[184,185] These approaches have been implemented by mimicking the physiological fibrinolytic mechanism in the surface design, and by release of tissue-type

plasminogen activator or t-PA (a factor that stimulates plasminogen to active plasmin which degrades fibrin) into the blood.[186] Researchers have done this by using ε-lysine to capture plasminogen onto the surfaces of materials or by t-PA release via biodegradable polymers.[187-189]

### 1.6.5. Bioinspired surfaces

Researchers have developed bioinspired, antifouling surfaces that inhibit the adherence of blood components. Super hydrophobic and lubricant-infused surfaces have been designed to mimic lotus leaves and pitcher plants.[190,191] Materials have been modeled after these plant surfaces because of the lotus leaves' natural self-cleaning capabilities, and the pitcher plant's ability to inhibit the attachment of insects.[192] Superhydrophobic surfaces and lubricated surfaces were able to show decreased protein adsorption and platelet adhesion and activation but were limited by their durability and longevity.[193-195] Other groups have taken inspiration from the luminal lining of blood vessels called the endothelial glycocalyx.[196-198] The vascular endothelial glycocalyx is the only material that is cable of inhibiting thrombus formation when in long-term contact with blood.[72] Researchers hope that by mimicking some key features of this surface blood compatibility can be achieved. In the Kipper lab, surfaces like this have been designed and have shown reduction in protein adsorption and fibrin polymerization.[199] Other approaches that have modeled surfaces after the glycocalyx have been able to decrease protein adsorption, and platelet adhesion, and were able to promote endothelization on material surfaces.[196-198] Surfaces designed to mimic biology are showing to be a promising area in blood contacting devices, but have only been characterized by their short-term interactions with blood components thus far.

### 1.6.6. Endothelization

The idea of coating surfaces with vascular endothelial cells to improve blood compatibility has been ongoing since the 1980s.[200,201] Several approaches to this have been investigated: cells can be seeded onto materials *in vitro* before implantation, surfaces can be modified to promote migration of endothelial cells onto a device *in vivo*, and surfaces have also been designed to capture endothelial progenitor cells from the circulation.[4] There are problems that have limited the practicality of this approach. Despite researchers being successful in generating endothelialized surfaces, these studies have been done in static conditions. When the coated surfaces meet flowing blood, the cells are sheared off. Another hurdle that researchers have faced in this field is the time to culture these cells to confluency may not be compatible with clinical needs.[202,203]

## 1.7. Goal and aims

The overall goal of this work is to design surfaces that mimic the vascular endothelial glycocalyx topography and chemistry to improve the blood compatibility of surfaces. The goal of this work will be accomplished through 3 different aims:

**Aim 1:** Incorporating nitric oxide with polyelectrolyte complex nanoparticle (PCN) surfaces and evaluating their cell-surface interactions to determine potential blood compatibility.

**Aim 2:** Establishing structure function relationships between enzymes and proteoglycan mimics when absorbed onto polyelectrolyte multilayers (PEM) surfaces and suspended in solution.

**Aim 3:** Desinging more durable PEM surfaces and evaluating the modified PEMs along with graft copolymer (GC), and PCN surfaces on their whole blood interactions to determine if design strategies to improve durability hinder blood-material interactions.

### 1.7.1. Rationale to surface design and aims:

The surfaces purposed in these studies are designed to mimic the vascular endothelial glycocalyx topography, chemistry, and in some cases, nitric oxide release. The surfaces are designed in this way because the glycocalyx is the only truly blood compatible material. By mimicking key structural, chemical, and dynamic components, blood compatibility may be achieved. The materials synthesized for this study will be composed of GAGs found in the glycocalyx, which will be arranged in a way that resembles the dense meshwork of charges found on the endothelial surface. Hyaluronan, heparin, chondroitin sulfate, and a modified version of chitosan designed to release nitric oxide will be used to make these materials. On their own, these GAGs have been shown to reduce some unfavorable biological responses, with heparin being most widely used in blood-contacting materials. It has been long shown that heparin inhibits coagulation.[204-206] Chondroitin sulfate and hyaluronic acid are both naturally occurring glycosaminoglycans and components of the glycocalyx.[72] Hyaluronic acid-modified materials have been shown to inhibit thrombus formation, reduce platelet adhesion, and mediate immune responses.[207,208] Chondroitin sulfate has been shown to inhibit platelet attachment and promote endothelization.[209] Chitosan is not a naturally occurring GAG in the human body, but has been shown to promote endothelialization, wound healing, and to inhibit platelet adhesion.[210,211]

To improve the effectiveness of GAG surfaces, they are complexed together in a way that mimics the structure of macromolecules in the glycocalyx. This can be achieved in two ways: polyelectrolyte complex nanoparticle (PCN) formation by electrostatic interactions between polyanions and polycations, and by synthesizing proteoglycan mimetic graft copolymers (GC), which are composed of a hyaluronan backbone with GAGs (heparin and chondroitin sulfate) covalently grafted as side chains. The mimics are adsorbed onto the surface using polyelectrolyte multilayers (PEM) as a substrate. PEM surfaces are alternating layers of polycations and polyanions which are electrostatically adsorbed onto the surface of a substrate to hide the underlying surface chemistry.

The PEM surfaces are also a means in which NO release can be incorporated into the surfaces. A modified version of chitosan, chitosan thioglycolic acid, can be added to these surfaces which can be nitrosated to release nitric oxide. Using these multifunctional glycocalyx-mimetic surfaces we aim to improve cell-surface interactions to inhibit thrombus formation for long term blood compatibility.

Each aim in this work is designed to test the materials to determine whether they can accomplish the goal of the study. **Aim 1** focuses on cellular interactions between PCN, nitric oxide-releasing surfaces. The materials are evaluated by how platelets, leukocytes, macrophages, and gram positive and negative bacteria behave in contact with the surfaces. These cells are chosen because they play important roles in coagulation, foreign body reactions, and infection. **Aim 2** tests the durability of our proteoglycan mimics by exposing materials to enzymes when absorbed onto surface or in solution. Both GCs and PCNs are tested against hyaluronidases, chondroitinase ABC,

and lysozyme because of their specificity to the GAGs used in the mimics and their clinical relevance. In Aim 2 we achieve relationships between the different strategies in which we constructed our PG mimics and how this influenced their interactions with the enzymes tested. **Aim 3** determines whether the PEMs can withstand shear forces, what changes can be made to the surfaces to improve its mechanical durability, and how these changes influence the surfaces' interactions with whole blood. Additionally, all surfaces will be tested against their ability to inhibit coagulation when in contact with whole blood. In Aim 3 we develop new PEM surfaces that are more durable and compare their blood compatibility to surfaces that were designed to interact with the surrounding biology favorably. From the work in this dissertation, we show that by mimicking key features of the endothelial glycocalyx we can achieve surfaces that interact with the surrounding biology better than untreated controls. This work also will lead to future work in which the materials that preformed the best in all three aims can be further improved and tested for specific applications.

## Citations


1. Xu, J., Kochanek, K., Murphy, S. & Tejada-Vera, B. National vital statistics report. *Natl. Cent. Health Stat.* **58**, (2010).

2. Rosamond, W., Flegal, K., Furie, K. & et al. Heart disease and stroke statistics - 2008 update: a report from the American Heart Association Statistics Committee and Stroke Statistics Subcommittee. *Circulation* **117**, 25–146 (2008).

3. Scarborough, P., Wickramasinghe, K., Bhatnagar, P. & Rayner, M. Trends in coronary heart disease 1961-2011. *Lond. Br. Heart Found.* (2011).

4. Liu, X. *et al.* Blood compatible materials: state of the art. *J. Mater. Chem. B* **2**, 5718–5738 (2014).

5. Hedayati, M., Neufeld, M. J., Reynolds, M. M. & Kipper, M. J. The quest for blood-compatible materials: Recent advances and future technologies. *Mater. Sci. Eng. R Rep.* **138**, 118–152 (2019).

6. Ratner, B. D. The catastrophe revisited: Blood compatibility in the 21st Century. *Biomaterials* **28**, 5144–5147 (2007).

7. Ratner, B. D. The blood compatibility catastrophe. *J. Biomed. Mater. Res.* **27**, 283–287 (1993).

8. Anderson, J. M., Rodriguez, A. & Chang, D. T. Foreign body reaction to biomaterials. *Semin. Immunol.* **20**, 86–100 (2008).

9. Reviakine, I. *et al.* Stirred, shaken, or stagnant: What goes on at the blood–biomaterial interface. *Blood Rev.* **31**, 11–21 (2017).

10. Gristina, A. G., Naylor, P. & Myrvik, Q. Infections from biomaterials and implants: a race for the surface. *Med. Prog. Technol.* **14**, 205–224 (1988).

11. Xu, L.-C., Bauer, J. W. & Siedlecki, C. A. Proteins, platelets, and blood coagulation at biomaterial interfaces. *Colloids Surf. B Biointerfaces* **124**, 49–68 (2014).

12. Davalos, D. & Akassoglou, K. Fibrinogen as a key regulator of inflammation in disease. *Semin. Immunopathol.* **34**, 43–62 (2012).

13. Riedel, T. *et al.* Fibrinopeptides A and B release in the process of surface fibrin formation. *Blood* **117**, 1700–1706 (2011).

14. Adams, R. A., Passino, M., Sachs, B. D., Nuriel, T. & Akassoglou, K. Fibrin mechanisms and functions in nervous system pathology. *Mol. Interv.* **4**, 163–176 (2004).

15. Blombäck, B. FIBRINOGEN AND FIBRIN-PROTEINS WITH COMPLEX ROLES IN HEMOSTASIS AND THROMBOSIS. *Thromb. Res.* **83**, 1–75 (1996).

16. Yang, Z., Mochalkin, I. & Doolittle, R. F. A model of fibrin formation based on crystal structures of fibrinogen and fibrin fragments complexed with synthetic peptides. *Proc. Natl. Acad. Sci.* **97**, 14156–14161 (2000).

17. Holmbäck, K., Danton, M. J., Suh, T. T., Daugherty, C. C. & Degen, J. L. Impaired platelet aggregation and sustained bleeding in mice lacking the fibrinogen motif bound by integrin alpha IIb beta 3. *EMBO J.* **15**, 5760–5771 (1996).

18. Horbett, T. A. Fibrinogen adsorption to biomaterials. *J. Biomed. Mater. Res. A* **106**, 2777–2788 (2018).

19. Di Cera, E. Thrombin. *Mol. Aspects Med.* **29**, 203–254 (2008).

20. Ostuni, E., Chapman, R. G., Holmlin, R. E., Takayama, S. & Whitesides, G. M. A Survey of Structure−Property Relationships of Surfaces that Resist the Adsorption of Protein. *Langmuir* **17**, 5605–5620 (2001).

21. Rao, G. H. R. & Chandy, T. Role of platelets in blood-biomaterial interactions. *Bull. Mater. Sci.* **22**, 633–639 (1999).

22. Stefanini, L. & Bergmeier, W. Negative regulators of platelet activation and adhesion. *J. Thromb. Haemost.* **16**, 220–230 (2018).

23. Davì, G. & Patrono, C. Platelet Activation and Atherothrombosis. *N. Engl. J. Med.* **357**, 2482–2494 (2007).

24. Burkhart, J. M. *et al.* The first comprehensive and quantitative analysis of human platelet protein composition allows the comparative analysis of structural and functional pathways. *Blood* **120**, e73–e82 (2012).

25. Stolla, M. *et al.* The kinetics of αIIbβ3 activation determines the size and stability of thrombi in mice: implications for antiplatelet therapy. *Blood* **117**, 1005–1013 (2011).

26. Durrant, T. N., van den Bosch, M. T. & Hers, I. Integrin αIIbβ3 outside-in signaling. *Blood* **130**, 1607–1619 (2017).

27. Hoffman, M. Remodeling the Blood Coagulation Cascade. *J. Thromb. Thrombolysis* **16**, 17–20 (2003).

28. Mackman Nigel, Tilley Rachel E., & Key Nigel S. Role of the Extrinsic Pathway of Blood Coagulation in Hemostasis and Thrombosis. *Arterioscler. Thromb. Vasc. Biol.* **27**, 1687–1693 (2007).

29. Roberts, H. R., Hoffman, M. & Monroe, D. M. A Cell-Based Model of Thrombin Generation. *Semin. Thromb. Hemost.* **32**, 32–38 (2006).

30. Grunkemeier, J. M., Tsai, W. B., McFarland, C. D. & Horbett, T. A. The effect of adsorbed fibrinogen, fibronectin, von Willebrand factor and vitronectin on the procoagulant state of adherent platelets. *Biomaterials* **21**, 2243–2252 (2000).

31. Smith, S. A. The cell-based model of coagulation. *J. Vet. Emerg. Crit. Care* **19**, 3–10 (2009).

32. Kamath, S., Blann, A. D. & Lip, G. Y. H. Platelet activation: assessment and quantification. *Eur. Heart J.* **22**, 1561–1571 (2001).

33. Heemskerk, J., Bevers, E. & Lindhout, T. Platelet Activation and Blood Coagulation. *Thromb. Haemost.* **88**, 186–193 (2002).

34. Sohrabi, S. & Liu, Y. A Cellular Model of Shear-Induced Hemolysis: A Cellular Model of Shear-Induced Hemolysis. *Artif. Organs* **41**, E80–E91 (2017).

35. Niemoeller, O. M., Kiedaisch, V., Dreischer, P., Wieder, T. & Lang, F. Stimulation of eryptosis by aluminium ions. *Toxicol. Appl. Pharmacol.* **217**, 168–175 (2006).

36. Kempe, D. S. *et al.* Stimulation of erythrocyte phosphatidylserine exposure by lead ions. *Am. J. Physiol.-Cell Physiol.* **288**, C396–C402 (2005).

37. Henkelman, S., Rakhorst, G., Blanton, J. & van Oeveren, W. Standardization of incubation conditions for hemolysis testing of biomaterials. *Mater. Sci. Eng. C* **29**, 1650–1654 (2009).

38. Maraj, R., Jacobs, L. E., Ioli, A. & Kotler, M. N. Evaluation of hemolysis in patients with prosthetic heart valves. *Clin. Cardiol.* **21**, 387–392 (1998).

39. Omar, H. R. *et al.* Plasma Free Hemoglobin Is an Independent Predictor of Mortality among Patients on Extracorporeal Membrane Oxygenation Support. *PLOS ONE* **10**, e0124034 (2015).

40. Gorbet, M. B. & Sefton, M. V. Biomaterial-associated thrombosis: roles of coagulation factors, complement, platelets and leukocytes. *Biomaterials* **25**, 5681–5703 (2004).

41. Ley, K., Laudanna, C., Cybulsky, M. I. & Nourshargh, S. Getting to the site of inflammation: the leukocyte adhesion cascade updated. *Nat. Rev. Immunol.* **7**, 678–689 (2007).

42. Ley, K. History of Inflammation Research. in *Physiology of Inflammation* (ed. Ley, K.) 1–10 (Springer New York, 2001). doi:10.1007/978-1-4614-7512-5_1.

43. Kansas, G. Selectins and their ligands: current concepts and controversies. *Blood* **88**, 3259–3287 (1996).

44. McEver, R. P. & Cummings, R. D. Perspectives series: cell adhesion in vascular biology. Role of PSGL-1 binding to selectins in leukocyte recruitment. *J. Clin. Invest.* **100**, 485–491 (1997).

45. Berlin, C. *et al.* α4 integrins mediate lymphocyte attachment and rolling under physiologic flow. *Cell* **80**, 413–422 (1995).

46. Vajkoczy, P., Laschinger, M. & Engelhardt, B. α4-integrin-VCAM-1 binding mediates G protein–independent capture of encephalitogenic T cell blasts to CNS white matter microvessels. *J. Clin. Invest.* **108**, 557–565 (2001).

47. Salas, A. *et al.* Rolling Adhesion through an Extended Conformation of Integrin αLβ2 and Relation to α I and β I-like Domain Interaction. *Immunity* **20**, 393–406 (2004).

48. Feng, D., Nagy, J. A., Pyne, K., Dvorak, H. F. & Dvorak, A. M. Neutrophils Emigrate from Venules by a Transendothelial Cell Pathway in Response to FMLP. *J. Exp. Med.* **187**, 903–915 (1998).

49. Engelhardt, B. & Wolburg, H. Mini-review: Transendothelial migration of leukocytes: through the front door or around the side of the house? *Eur. J. Immunol.* **34**, 2955–2963 (2004).

50. Millán, J. *et al.* Lymphocyte transcellular migration occurs through recruitment of endothelial ICAM-1 to caveola- and F-actin-rich domains. *Nat. Cell Biol.* **8**, 113–123 (2006).

51. Nieminen, M. *et al.* Vimentin function in lymphocyte adhesion and transcellular migration. *Nat. Cell Biol.* **8**, 156–162 (2006).

52. Amulic, B., Cazalet, C., Hayes, G. L., Metzler, K. D. & Zychlinsky, A. Neutrophil Function: From Mechanisms to Disease. *Annu. Rev. Immunol.* **30**, 459–489 (2012).

53. Espinoza, V. E. & Emmady, P. D. Histology, Monocytes. in *StatPearls* (StatPearls Publishing, 2021).

54. Ginhoux, F. & Jung, S. Monocytes and macrophages: developmental pathways and tissue homeostasis. *Nat. Rev. Immunol.* **14**, 392–404 (2014).

55. Klopfleisch, R. & Jung, F. The pathology of the foreign body reaction against biomaterials. *J. Biomed. Mater. Res. A* **105**, 927–940 (2017).

56. Sperling, C., Maitz, M. F. & Werner, C. 4 - Test methods for hemocompatibility of biomaterials. in *Hemocompatibility of Biomaterials for Clinical Applications* (ed. Siedlecki, C. A.) 77–104 (Woodhead Publishing, 2018). doi:10.1016/B978-0-08-100497-5.00005-7.

57. Anderson, J. M. Chapter 39 - Biocompatibility and Bioresponse to Biomaterials. in *Principles of Regenerative Medicine (Third Edition)* (eds. Atala, A., Lanza, R., Mikos, A. G. & Nerem, R.) 675–694 (Academic Press, 2019). doi:10.1016/B978-0-12-809880-6.00039-4.

58. Sheikh, Z., Brooks, P. J., Barzilay, O., Fine, N. & Glogauer, M. Macrophages, Foreign Body Giant Cells and Their Response to Implantable Biomaterials. *Materials* **8**, 5671–5701 (2015).

59. Colman, R. W. Chapter 3 Mechanisms of thrombus formation and dissolution. *Cardiovasc. Pathol.* **2**, 23–31 (1993).

60. Furie, B. & Furie, B. C. Mechanisms of Thrombus Formation. *N. Engl. J. Med.* **359**, 938–949 (2008).

61. Ekdahl, K. N. *et al.* Dangerous liaisons: complement, coagulation, and kallikrein/kinin cross-talk act as a linchpin in the events leading to thromboinflammation. *Immunol. Rev.* **274**, 245–269 (2016).

62. Reynolds, M. M. & Annich, G. M. The artificial endothelium. *Organogenesis* **7**, 42–49 (2011).

63. Hoffman, M. & Monroe, D. M. A cell-based model of hemostasis. *Thromb. Haemost.* **85**, 958–965 (2001).

64. Gailani, D. & Broze, G. Factor XI activation in a revised model of blood coagulation. *Science* **253**, 909–912 (1991).

65. Hoffman, M. Remodeling the Blood Coagulation Cascade. *J. Thromb. Thrombolysis* **16**, 17–20 (2003).

66. Mackman, N. New Targets for Atherothrombosis. *Arterioscler. Thromb. Vasc. Biol.* **34**, 1607–1608 (2014).

67. Vojacek, J. F. Should We Replace the Terms Intrinsic and Extrinsic Coagulation Pathways With Tissue Factor Pathway? *Clin. Appl. Thromb.* **23**, 922–927 (2017).

68. Ekdahl, K. N., Huang, S., Nilsson, B. & Teramura, Y. Complement inhibition in biomaterial- and biosurface-induced thromboinflammation. *Semin. Immunol.* **28**, 268–277 (2016).

69. Smith, S. A. The cell-based model of coagulation. *J. Vet. Emerg. Crit. Care* **19**, 3–10 (2009).

70. Lipowsky, H. H. Microvascular Rheology and Hemodynamics. *Microcirculation* **12**, 5–15 (2005).

71. Rostgaard, J. & Qvortrup, K. Electron Microscopic Demonstrations of Filamentous Molecular Sieve Plugs in Capillary Fenestrae. *Microvasc. Res.* **53**, 1–13 (1997).

72. Reitsma, S., Slaaf, D. W., Vink, H., van Zandvoort, M. A. M. J. & oude Egbrink, M. G. A. The endothelial glycocalyx: composition, functions, and visualization. *Pflüg. Arch. - Eur. J. Physiol.* **454**, 345–359 (2007).

73. Kjellén, L. & Lindahl, U. Proteoglycans: Structures and Interactions. *Annu. Rev. Biochem.* **60**, 443–475 (1991).

74. Rapraeger, A. Transforming growth factor (type beta) promotes the addition of chondroitin sulfate chains to the cell surface proteoglycan (syndecan) of mouse mammary epithelia. *J. Cell Biol.* **109**, 2509–2518 (1989).

75. Mulivor, A. W. & Lipowsky, H. H. Inflammation- and ischemia-induced shedding of venular glycocalyx. *Am. J. Physiol.-Heart Circ. Physiol.* **286**, H1672–H1680 (2004).

76. Dane, M. J. C. *et al.* A microscopic view on the renal endothelial glycocalyx. *Am. J. Physiol. Renal Physiol.* **308**, NaN-NaN (2015).

77. Becker, B. F., Chappell, D., Bruegger, D., Annecke, T. & Jacob, M. Therapeutic strategies targeting the endothelial glycocalyx: acute deficits, but great potential. *Cardiovasc. Res.* **87**, 300–310 (2010).

78. Alphonsus, C. S. & Rodseth, R. N. The endothelial glycocalyx: a review of the vascular barrier. *Anaesthesia* **69**, 777–784 (2014).

79. Nieuwdorp, M. *et al.* Endothelial Glycocalyx Damage Coincides With Microalbuminuria in Type 1 Diabetes. *Diabetes* **55**, 1127–1132 (2006).

80. Vink, H., Constantinescu, A. A. & Spaan, J. A. E. Oxidized Lipoproteins Degrade the Endothelial Surface Layer: Implications for Platelet-Endothelial Cell Adhesion. *Circulation* **101**, 1500–1502 (2000).

81. Okada, H., Yoshida, S., Hara, A., Ogura, S. & Tomita, H. Vascular endothelial injury exacerbates coronavirus disease 2019: The role of endothelial glycocalyx protection. *Microcirculation* **28**, (2021).

82. Strijdom, H., Chamane, N. & Lochner, A. Nitric oxide in the cardiovascular system: a simple molecule with complex actions. *Cardiovasc. J. Afr.* **20**, 303–310 (2009).

83. Katsuki, S., Arnold, W., Mittal, C. & Murad, F. Stimulation of guanylate cyclase by sodium nitroprusside, nitroglycerin and nitric oxide in various tissue preparations and comparison to the effects of sodium azide and hydroxylamine. *J. Cyclic Nucleotide Res.* **3**, 23–35 (1977).

84. Arnold, W. P., Mittal, C. K., Katsuki, S. & Murad, F. Nitric oxide activates guanylate cyclase and increases guanosine 3':5'-cyclic monophosphate levels in various tissue preparations. *Proc. Natl. Acad. Sci.* **74**, 3203–3207 (1977).

85. Ignarro, L. J., Buga, G. M., Wood, K. S., Byrns, R. E. & Chaudhuri, G. Endothelium-derived relaxing factor produced and released from artery and vein is nitric oxide. *Proc. Natl. Acad. Sci.* **84**, 9265–9269 (1987).

86. Giustarini, D., Milzani, A., Colombo, R., Dalle-Donne, I. & Rossi, R. Nitric oxide and S-nitrosothiols in human blood. *Clin. Chim. Acta* **330**, 85–98 (2003).

87. Riddell, D. R. & Owen, J. S. Nitric Oxide and Platelet Aggregation. in *Vitamins & Hormones* (ed. Litwack, G.) vol. 57 25–48 (Academic Press, 1997).

88. Ziche, M. & Morbidelli, L. Nitric Oxide and Angiogenesis. *J. Neurooncol.* **50**, 139–148 (2000).

89. Ahonen, M. J. R., Dorrier, J. M. & Schoenfisch, M. H. Antibiofilm Efficacy of Nitric Oxide-Releasing Alginates against Cystic Fibrosis Bacterial Pathogens. *ACS Infect. Dis.* **5**, 1327–1335 (2019).

90. Neufeld, B. H. & Reynolds, M. M. Critical nitric oxide concentration for Pseudomonas aeruginosa biofilm reduction on polyurethane substrates. *Biointerphases* **11**, 031012 (2016).

91. Bogdan, C. Nitric oxide synthase in innate and adaptive immunity: an update. *Trends Immunol.* **36**, 161–178 (2015).

92. Kalsner, S. *Nitric Oxide and Free Radicals in Peripheral Neurotransmission*. (Springer Science & Business Media, 2000).

93. Moncada, S. & Erusalimsky, J. D. Does nitric oxide modulate mitochondrial energy generation and apoptosis? *Nat. Rev. Mol. Cell Biol.* **3**, 214–220 (2002).

94. Bogdan, C. Nitric oxide and the immune response. *Nat. Immunol.* **2**, 907–916 (2001).

95. Coneski, P. N. & Schoenfisch, M. H. Nitric oxide release: Part III. Measurement and reporting. *Chem. Soc. Rev.* **41**, 3753 (2012).

96. Toledo, J. C. & Augusto, O. Connecting the Chemical and Biological Properties of Nitric Oxide. *Chem. Res. Toxicol.* **25**, 975–989 (2012).

97. Liu, X., Yan, Q., Baskerville, K. L. & Zweier, J. L. Estimation of Nitric Oxide Concentration in Blood for Different Rates of Generation. *J. Biol. Chem.* **282**, 8831–8836 (2007).

98. Khan, H. A., Baig, F. K. & Mehboob, R. Nosocomial infections: Epidemiology, prevention, control and surveillance. *Asian Pac. J. Trop. Biomed.* **7**, 478–482 (2017).

99. Stickler, D. & McLean, R. Biomaterials Associated Infections: The Scale of the Problem. *Cells Mater.* **5**, (1995).

100. Su, L., Li, Y., Liu, Y., An, Y. & Shi, L. Recent Advances and Future Prospects on Adaptive Biomaterials for Antimicrobial Applications. *Macromol. Biosci.* **0**, 1900289.

101. Klevens, R. M. *et al.* Estimating Health Care-Associated Infections and Deaths in U.S. Hospitals, 2002. *Public Health Rep.* **122**, 160–166 (2007).

102. Welsh, C. A., Flanagan, M. E., Hoke, S. C., Doebbeling, B. N. & Herwaldt, L. Reducing health care-associated infections (HAIs): Lessons learned from a national collaborative of regional HAI programs. *Am. J. Infect. Control* **40**, 29–34 (2012).

103. Patrick, S. W. *et al.* Health Care-Associated Infections Among Critically Ill Children in the US, 2007-2012. *PEDIATRICS* **134**, 705–712 (2014).

104. Vital Signs: Central Line–Associated Blood Stream Infections—United States, 2001, 2008, and 2009. *Ann. Emerg. Med.* **58**, 447–450 (2011).

105. Warren, J. W. Catheter-associated urinary tract infections. *Int. J. Antimicrob. Agents* **17**, 299–303 (2001).

106. Sikora, A. & Zahra, F. Nosocomial Infections. in *StatPearls* (StatPearls Publishing, 2021).

107. Tietze, K. *et al.* Differences in innate immune responses upon stimulation with gram-positive and gram-negative bacteria. *J. Periodontal Res.* **41**, 447–454 (2006).

108. Breijyeh, Z., Jubeh, B. & Karaman, R. Resistance of Gram-Negative Bacteria to Current Antibacterial Agents and Approaches to Resolve It. *Molecules* **25**, 1340 (2020).

109. Feezor, R. J. *et al.* Molecular Characterization of the Acute Inflammatory Response to Infections with Gram-Negative versus Gram-Positive Bacteria. *Infect. Immun.* **71**, 5803–5813 (2003).

110. del Pozo, J. L. & Patel, R. The Challenge of Treating Biofilm-associated Bacterial Infections. *Clin. Pharmacol. Ther.* **82**, 204–209 (2007).

111. Chew, S. C. & Yang, L. Biofilms. in *Encyclopedia of Food and Health* 407–415 (Elsevier, 2016). doi:10.1016/B978-0-12-384947-2.00069-6.

112. Pachori, P., Gothalwal, R. & Gandhi, P. Emergence of antibiotic resistance Pseudomonas aeruginosa in intensive care unit; a critical review. *Genes Dis.* **6**, 109–119 (2019).

113. Taylor, T. A. & Unakal, C. G. Staphylococcus Aureus. in *StatPearls* (StatPearls Publishing, 2021).

114. Sydnor, E. R. M. & Perl, T. M. Hospital Epidemiology and Infection Control in Acute-Care Settings. *Clin. Microbiol. Rev.* **24**, 141–173 (2011).

115. Boucher, H. W. & Corey, G. R. Epidemiology of Methicillin-Resistant *Staphylococcus aureus*. *Clin. Infect. Dis.* **46**, S344–S349 (2008).

116. Andersson, D. I. Persistence of antibiotic resistant bacteria. *Curr. Opin. Microbiol.* **6**, 452–456 (2003).

117. Walsh, C. Antibiotics: actions, origins, resistance. *Antibiot. Actions Orig. Resist.* (2003).

118. Bodmer, D., Kissel, T. & Traechslin, E. Factors influencing the release of peptides and proteins from biodegradable parenteral depot systems. *J. Controlled Release* **21**, 129–137 (1992).

119. Hänzi, A. C., Gerber, I., Schinhammer, M., Löffler, J. F. & Uggowitzer, P. J. On the in vitro and in vivo degradation performance and biological response of new biodegradable Mg–Y–Zn alloys☆. *Acta Biomater.* **6**, 1824–1833 (2010).

120. Briquez, P. S., Lorentz, K. M., Larsson, H. M., Frey, P. & Hubbell, J. A. Human Kunitz-type protease inhibitor engineered for enhanced matrix retention extends longevity of fibrin biomaterials. *Biomaterials* **135**, 1–9 (2017).

121. Geetha, M., Singh, A. K., Asokamani, R. & Gogia, A. K. Ti based biomaterials, the ultimate choice for orthopaedic implants – A review. *Prog. Mater. Sci.* **54**, 397–425 (2009).

122. Rahyussalim, A. J., Marsetio, A. F., Saleh, I., Kurniawati, T. & Whulanza, Y. The Needs of Current Implant Technology in Orthopaedic Prosthesis Biomaterials Application to Reduce Prosthesis Failure Rate. *J. Nanomater.* **2016**, 1–9 (2016).

123. Goonoo, N., Bhaw-Luximon, A. & Jhurry, D. Biodegradable polymer blends: miscibility, physicochemical properties and biological response of scaffolds: Biodegradable polymer blends. *Polym. Int.* **64**, 1289–1302 (2015).

124. Spijker, H. On the influence of flow conditions and wettability on blood material interactions. *Biomaterials* **24**, 4717–4727 (2003).

125. Joner Michael *et al.* Pathology of Drug-Eluting Stents in Humans. *J. Am. Coll. Cardiol.* **48**, 193–202 (2006).

126. Lüscher, T. F. *et al.* Drug-Eluting Stent and Coronary Thrombosis: Biological Mechanisms and Clinical Implications. *Circulation* **115**, 1051–1058 (2007).

127. Daemen, J. *et al.* Early and late coronary stent thrombosis of sirolimus-eluting and paclitaxel-eluting stents in routine clinical practice: data from a large two-institutional cohort study. *The Lancet* **369**, 667–678 (2007).

128. Fournier, Ronald L. *Basic Transport Pheomena in Biomedical Engineering*. (Talor & Francis, 2017).

129. Strony, J., Beaudoin, A., Brands, D. & Adelman, B. Analysis of shear stress and hemodynamic factors in a model of coronary artery stenosis and thrombosis. *Am. J. Physiol.-Heart Circ. Physiol.* **265**, H1787–H1796 (1993).

130. Ranucci, M., Laddomada, T., Ranucci, M. & Baryshnikova, E. Blood viscosity during coagulation at different shear rates. *Physiol. Rep.* **2**, e12065 (2014).

131. Sakariassen, K. S., Orning, L. & Turitto, V. T. The impact of blood shear rate on arterial thrombus formation. *Future Sci. OA* **1**, fso.15.28 (2015).

132. Zhang, Q. *et al.* Preservation of the Structure of Enzymatically-Degraded Bovine Vitreous Using Synthetic Proteoglycan Mimics. *Invest. Ophthalmol. Vis. Sci.* **55**, 8153–8162 (2014).

133. Yourtee, D. M. *et al.* The stability of methacrylate biomaterials when enzyme challenged: Kinetic and systematic evaluations. *J. Biomed. Mater. Res.* **57**, 522–531 (2001).

134. Ulijn, R. V. Enzyme-responsive materials: a new class of smart biomaterials. *J. Mater. Chem.* **16**, 2217 (2006).

135. Ghadiali, J. E. & Stevens, M. M. Enzyme-Responsive Nanoparticle Systems. *Adv. Mater.* **20**, 4359–4363 (2008).

136. de la Rica, R., Aili, D. & Stevens, M. M. Enzyme-responsive nanoparticles for drug release and diagnostics. *Adv. Drug Deliv. Rev.* **64**, 967–978 (2012).

137. Hu, J., Zhang, G. & Liu, S. Enzyme-responsive polymeric assemblies, nanoparticles and hydrogels. *Chem. Soc. Rev.* **41**, 5933 (2012).

138. Barsoum, N. & Kleeman, C. Now and Then, the History of Parenteral Fluid Administration. *Am. J. Nephrol.* **22**, 284–289 (2002).

139. Tait, J. & Gunn, J. D. The Blood of Astacus Fluviatilis: A Study in Crustacean Blood, with Special Reference to Coagulation and Phagocytosis. *Q. J. Exp. Physiol.* **12**, 35–80 (1918).

140. Hayama, M. *et al.* Nanoscopic behavior of polyvinylpyrrolidone particles on polysulfone/polyvinylpyrrolidone film. *Biomaterials* **25**, 1019–1028 (2004).

141. Jin, Z., Feng, W., Zhu, S., Sheardown, H. & Brash, J. L. Protein-resistant polyurethane by sequential grafting of poly(2-hydroxyethyl methacrylate) and poly(oligo(ethylene glycol) methacrylate) via surface-initiated ATRP. *J. Biomed. Mater. Res. A* **95A**, 1223–1232 (2010).

142. Kumar, S., Tong, X., L. Dory, Y., Lepage, M. & Zhao, Y. A CO 2 -switchable polymer brush for reversible capture and release of proteins. *Chem. Commun.* **49**, 90–92 (2013).

143. Frazier, R. A. *et al.* Characterization of protein-resistant dextran monolayers. *Biomaterials* **21**, 957–966 (2000).

144. Zhang, Z. *et al.* Nonfouling Behavior of Polycarboxybetaine-Grafted Surfaces: Structural and Environmental Effects. *Biomacromolecules* **9**, 2686–2692 (2008).

145. Yang, W., Xue, H., Li, W., Zhang, J. & Jiang, S. Pursuing “Zero” Protein Adsorption of Poly(carboxybetaine) from Undiluted Blood Serum and Plasma. *Langmuir* **25**, 11911–11916 (2009).

146. Futamura, K., Matsuno, R., Konno, T., Takai, M. & Ishihara, K. Rapid Development of Hydrophilicity and Protein Adsorption Resistance by Polymer Surfaces Bearing Phosphorylcholine and Naphthalene Groups. *Langmuir* **24**, 10340–10344 (2008).

147. Jiang, S. & Cao, Z. Ultralow-Fouling, Functionalizable, and Hydrolyzable Zwitterionic Materials and Their Derivatives for Biological Applications. *Adv. Mater.* **22**, 920–932 (2010).

148. Surman, F. *et al.* Polymer Brushes Interfacing Blood as a Route Toward High Performance Blood Contacting Devices. *Macromol. Biosci.* **15**, 636–646 (2015).

149. Harding, J. L. & Reynolds, M. M. Combating medical device fouling. *Trends Biotechnol.* **32**, 140–146 (2014).

150. Jaffer, I. H., Fredenburgh, J. C., Hirsh, J. & Weitz, J. I. Medical device-induced thrombosis: what causes it and how can we prevent it? *J. Thromb. Haemost.* **13**, S72–S81 (2015).

151. Le, T. C., Penna, M., Winkler, D. A. & Yarovsky, I. Quantitative design rules for protein-resistant surface coatings using machine learning. *Sci. Rep.* **9**, 265 (2019).

152. Murugesan, S., Xie, J. & Linhardt, R. J. Immobilization of Heparin: Approaches and Applications. *Curr. Top. Med. Chem.* **8**, 80–100 (2008).

153. Chen, H., Yuan, L., Song, W., Wu, Z. & Li, D. Biocompatible polymer materials: Role of protein–surface interactions. *Prog. Polym. Sci.* **33**, 1059–1087 (2008).

154. Gott, V. L., Whiffen, J. D. & Dutton, R. C. Heparin Bonding on Colloidal Graphite Surfaces. *Science* **142**, 1297–1298 (1963).

155. Sanchez, J., Elgue, G., Riesenfeld, J. & Olsson, P. Studies of Adsorption, Activation, and Inhibition of Factor XII on Immobilized Heparin. *Thromb. Res.* **89**, 41–50 (1998).

156. Larm, O., Larsson, R. & Olsson, P. A New Non-Thrombogenic Surface Prepared by Selective Covalent Binding of Heparin Via a Modified Reducing Terminal Residue. *Biomater. Med. Devices Artif. Organs* **11**, 161–173 (1983).

157. Agnelli, G., Renga, C., Weitz, J. I., Nenci, G. G. & Hirsh, J. Sustained antithrombotic activity of hirudin after its plasma clearance: comparison with heparin. *Blood* **80**, 960–965 (1992).

158. Maraganore, J. M., Bourdon, P., Jablonski, J., Ramachandran, K. L. & Fenton, J. W. Design and characterization of hirulogs: a novel class of bivalent peptide inhibitors of thrombin. *Biochemistry* **29**, 7095–7101 (1990).

159. Performance of a polyurethane vascular prosthesis carrying a dipyridamole (Persantin®) coating on its lumenal surface - Aldenhoff - 2001 - Journal of Biomedical Materials Research - Wiley Online Library. https://onlinelibrary.wiley.com/doi/abs/10.1002/1097-4636(200102)54:2%3C224::AID-JBM9%3E3.0.CO;2-E.

160. Chandy, T., Das, G. S., Wilson, R. F. & Rao, G. H. R. Use of plasma glow for surface-engineering biomolecules to enhance bloodcompatibility of Dacron and PTFE vascular prosthesis. *Biomaterials* **21**, 699–712 (2000).

161. Krauel, K., Hackbarth, C., Furll, B. & Greinacher, A. Heparin-induced thrombocytopenia: in vitro studies on the interaction of dabigatran, rivaroxaban, and low-sulfated heparin, with platelet factor 4 and anti-PF4/heparin antibodies. *Blood* **119**, 1248–1255 (2012).

162. Laster, J. & Silver, D. Heparin-coated catheters and heparin-induced thrombocytopenia. *J. Vasc. Surg.* **7**, 667–672 (1988).

163. Gao, C. *et al.* Heparin promotes platelet responsiveness by potentiating αIIbβ3-mediated outside-in signaling. *Blood* **117**, 4946–4952 (2011).

164. Stone, S. R. & Hofsteenge, J. Kinetics of the inhibition of thrombin by hirudin. *Biochemistry* **25**, 4622–4628 (1986).

165. Chan, A. *et al.* Covalent Antithrombin-Heparin Complexes with High Anticoagulant Activity INTRAVENOUS, SUBCUTANEOUS, AND INTRATRACHEAL ADMINISTRATION. *J. Biol. Chem.* **272**, 22111–22117 (1997).

166. Zhou, Z. & Meyerhoff, M. E. Preparation and characterization of polymeric coatings with combined nitric oxide release and immobilized active heparin. *Biomaterials* **26**, 6506–6517 (2005).

167. Gladwell, T. D. Bivalirudin: A direct thrombin inhibitor. *Clin. Ther.* **24**, 38–58 (2002).

168. Luong-Van, E. *et al.* Controlled release of heparin from poly(ε-caprolactone) electrospun fibers. *Biomaterials* **27**, 2042–2050 (2006).

169. Del Gaudio, C. *et al.* Aspirin-loaded electrospun poly(ε-caprolactone) tubular scaffolds: potential small-diameter vascular grafts for thrombosis prevention. *J. Mater. Sci. Mater. Med.* **24**, 523–532 (2013).

170. Stahl, A. M. & Yang, Y. P. Tunable Elastomers with an Antithrombotic Component for Cardiovascular Applications. *Adv. Healthc. Mater.* **7**, 1800222 (2018).

171. Xu, C. *et al.* Enhancing anti-thrombogenicity of biodegradable polyurethanes through drug molecule incorporation. *J. Mater. Chem. B* **6**, 7288–7297 (2018).

172. Yang, Y. *et al.* Polydopamine Modified TiO2 Nanotube Arrays for Long-Term Controlled Elution of Bivalirudin and Improved Hemocompatibility. *ACS Appl. Mater. Interfaces* **10**, 7649–7660 (2018).

173. Maitz, M. F. *et al.* Adaptive release of heparin from anticoagulant hydrogels triggered by different blood coagulation factors. *Biomaterials* **135**, 53–61 (2017).

174. Riccio, D. A. & Schoenfisch, M. H. Nitric oxide release: Part I. Macromolecular scaffolds. *Chem. Soc. Rev.* **41**, 3731–3741 (2012).

175. Simon-Walker, R. *et al.* Glycocalyx-Inspired Nitric Oxide-Releasing Surfaces Reduce Platelet Adhesion and Activation on Titanium. *ACS Biomater. Sci. Eng.* **3**, 68–77 (2017).

176. Jen, M. C., Serrano, M. C., Lith, R. van & Ameer, G. A. Polymer-Based Nitric Oxide Therapies: Recent Insights for Biomedical Applications. *Adv. Funct. Mater.* **22**, 239–260 (2012).

177. Frost, M. C., Reynolds, M. M. & Meyerhoff, M. E. Polymers incorporating nitric oxide releasing/generating substances for improved biocompatibility of blood-contacting medical devices. *Biomaterials* **26**, 1685–1693 (2005).

178. Hrabie, J. A. & Keefer, L. K. Chemistry of the Nitric Oxide-Releasing Diazeniumdiolate ("Nitrosohydroxylamine") Functional Group and Its Oxygen-Substituted Derivatives. *Chem. Rev.* **102**, 1135–1154 (2002).

179. Hou, Y., Guo, Z., Li, J. & Wang, P. G. Seleno Compounds and Glutathione Peroxidase Catalyzed Decomposition ofS-Nitrosothiols. *Biochem. Biophys. Res. Commun.* **228**, 88–93 (1996).

180. Hwang, S. & Meyerhoff, M. E. Polyurethane with tethered copper(II)–cyclen complex: Preparation, characterization and catalytic generation of nitric oxide from S-nitrosothiols. *Biomaterials* **29**, 2443–2452 (2008).

181. Harding, J. L. & Reynolds, M. M. Metal Organic Frameworks as Nitric Oxide Catalysts. *J. Am. Chem. Soc.* **134**, 3330–3333 (2012).

182. Harding, J. L., Metz, J. M. & Reynolds, M. M. A Tunable, Stable, and Bioactive MOF Catalyst for Generating a Localized Therapeutic from Endogenous Sources. *Adv. Funct. Mater.* **24**, 7503–7509 (2014).

183. Neufeld, B. H., Neufeld, M. J., Lutzke, A., Schweickart, S. M. & Reynolds, M. M. Metal–Organic Framework Material Inhibits Biofilm Formation of Pseudomonas aeruginosa. *Adv. Funct. Mater.* **27**, 1702255 (2017).

184. Lijnen, H. R. Elements of the Fibrinolytic System. *Ann. N. Y. Acad. Sci.* **936**, 226–236 (2001).

185. Gorog, D. A. Prognostic Value of Plasma Fibrinolysis Activation Markers in Cardiovascular Disease. *J. Am. Coll. Cardiol.* **55**, 2701–2709 (2010).

186. Li, D., Chen, H. & Brash, J. L. Mimicking the fibrinolytic system on material surfaces. *Colloids Surf. B Biointerfaces* **86**, 1–6 (2011).

187. McClung, W. G., Clapper, D. L., Hu, S.-P. & Brash, J. L. Adsorption of plasminogen from human plasma to lysine-containing surfaces. *J. Biomed. Mater. Res.* **49**, 409–414 (2000).

188. McClung, W. G., Babcock, D. E. & Brash, J. L. Fibrinolytic properties of lysine-derivatized polyethylene in contact with flowing whole blood (Chandler loop model). *J. Biomed. Mater. Res. A* **81A**, 644–651 (2007).

189. Park, Y.-J., Liang, J., Yang, Z. & Yang, V. C. Controlled release of clot-dissolving tissue-type plasminogen activator from a poly(l-glutamic acid) semi-interpenetrating polymer network hydrogel. *J. Controlled Release* **75**, 37–44 (2001).

190. Feng, L. *et al.* Super-Hydrophobic Surfaces: From Natural to Artificial. *Adv. Mater.* **14**, 1857–1860 (2002).

191. Wen, G., Guo, Z. & Liu, W. Biomimetic polymeric superhydrophobic surfaces and nanostructures: from fabrication to applications. *Nanoscale* **9**, 3338–3366 (2017).

192. Zhang, P., Lin, L., Zang, D., Guo, X. & Liu, M. Designing Bioinspired Anti-Biofouling Surfaces based on a Superwettability Strategy. *Small* **13**, 1503334 (2017).

193. Huang, Q. *et al.* Role of trapped air in the formation of cell-and-protein micropatterns on superhydrophobic/superhydrophilic microtemplated surfaces. *Biomaterials* **33**, 8213–8220 (2012).

194. Sun, T., Tan, H., Han, D., Fu, Q. & Jiang, L. No Platelet Can Adhere—Largely Improved Blood Compatibility on Nanostructured Superhydrophobic Surfaces. *Small* **1**, 959–963 (2005).

195. Yang, Y. *et al.* A novel electrochemical strategy for improving blood compatibility of titanium-based biomaterials. *Colloids Surf. B Biointerfaces* **79**, 309–313 (2010).

196. Sen Gupta, A. *et al.* Glycocalyx-mimetic dextran-modified poly(vinyl amine) surfactant coating reduces platelet adhesion on medical-grade polycarbonate surface. *Biomaterials* **27**, 3084–3095 (2006).

197. Zhou, G., Niepel, M. S., Saretia, S. & Groth, T. Reducing the inflammatory responses of biomaterials by surface modification with glycosaminoglycan multilayers. *J. Biomed. Mater. Res. A* **104**, 493–502 (2016).

198. Köwitsch, A., Niepel, M. S., Michanetzis, G. P. A., Missirlis, Y. F. & Groth, T. Effect of Immobilized Thiolated Glycosaminoglycans on Fibronectin Adsorption and Behavior of Fibroblasts. *Macromol. Biosci.* **16**, 381–394 (2016).

199. Hedayati, M., Reynolds, M. M., Krapf, D. & Kipper, M. J. Nanostructured Surfaces That Mimic the Vascular Endothelial Glycocalyx Reduce Blood Protein Adsorption and Prevent Fibrin Network Formation. *ACS Appl. Mater. Interfaces* **10**, 31892–31902 (2018).

200. Herring, M. *et al.* Endothelial seeding of Dacron and polytetrafluoroethylene grafts: The cellular events of healing. *Surgery* **96**, 745–755 (1984).

201. Köveker, G. B., Burkel, W. E., Graham, L. M., Wakefield, T. W. & Stanley, J. C. Endothelial cell seeding of expanded polytetrafluoroethylene vena cava conduits: Effects on luminal production of prostacyclin, platelet adherence, and fibrinogen accumulation. *J. Vasc. Surg.* **7**, 600–605 (1988).

202. Pawlowski, K., J. Endothelial cell seeding of polymeric vascular grafts. *Front. Biosci.* **9**, 1412 (2004).

203. Poole–Warren, L. A., Schindhelm, K., Graham, A. R., Slowiaczek, P. R. & Noble, K. R. Performance of small diameter synthetic vascular prostheses with confluent autologous endothelial cell linings. *J. Biomed. Mater. Res.* **30**, 221–229 (1996).

204. Pasche, B., Kodama, K., Larm, O., Olsson, P. & Swedenborg, J. Thrombin inactivation on surfaces with covalently bonded heparin. *Thromb. Res.* **44**, 739–748 (1986).

205. Lagergren, H., Olsson, P. & Swedenborg, J. Inhibited platelet adhesion: A non-thrombogenic characteristic of a heparin-coated surface. *Surgery* **75**, 643–650 (1974).

206. Larsson, R., Eriksson, J.-C., Lagergren, H. & Olsson, P. Platelet and plasma coagulation compatibility of heparinized and sulphated surfaces. *Thromb. Res.* **15**, 157–167 (1979).

207. Mizrahy, S. *et al.* Hyaluronan-coated nanoparticles: The influence of the molecular weight on CD44-hyaluronan interactions and on the immune response. *J. Controlled Release* **156**, 231–238 (2011).

208. Hyaluronan enhancement of expanded polytetrafluoroethylene cardiovascular grafts - Hieu T Bui, Aidan RW Friederich, Emily Li, David A Prawel, Susan P James, 2018. https://journals.sagepub.com/doi/full/10.1177/0885328218776807.

209. Thalla, P. K. *et al.* Chondroitin Sulfate Coatings Display Low Platelet but High Endothelial Cell Adhesive Properties Favorable for Vascular Implants. *Biomacromolecules* **15**, 2512–2520 (2014).

210. Li, Q.-L. *et al.* Endothelial Cell and Platelet Behavior on Titanium Modified with a Mutilayer of Polyelectrolytes. *J. Bioact. Compat. Polym.* **24**, 129–150 (2009).

211. Francis Suh, J.-K. & Matthew, H. W. T. Application of chitosan-based polysaccharide biomaterials in cartilage tissue engineering: a review. *Biomaterials* **21**, 2589–2598 (2000).

# CHAPTER 2: VASCULAR ENDOTHELIUM-MIMETIC SURFACES THAT MITIGATE MULTIPLE CELL-MATERIAL INTERACTIONS: TOWARD BLOOD-COMPATIBLE MATERIALS[1]

## Overview

When flowing whole blood contacts medical device surfaces the most common blood-material interactions result in coagulation, inflammation, and infection. Many new blood-contacting biomaterials have been proposed based on strategies that address just one of these common modes of failure. This study proposes to mitigate unfavorable biological reactions that occur with blood-contacting medical devices by designing multifunctional surfaces, with features optimized to meet multiple performance criteria. These multifunctional surfaces incorporate the release of the small molecule hormone nitric oxide (NO) with surface chemistry and nanotopography that mimic features of the vascular endothelial glycocalyx. These multifunctional surfaces have features that interact with coagulation components, inflammatory cells, and bacterial cells. While a single surface feature alone is not sufficient to achieve multiple functions, the release of NO from our surfaces along with their modification to mimic the endothelial glycocalyx produce the most favorable blood-material interactions. This work demonstrates that new blood-compatible materials should be designed with multiple functions, to better address the multiple modes of failure of blood-contacting medical devices.

[1]This work was published in *Advanced Healthcare Materials* and is reproduced with minor modifications with permission [1]. J. Vlcek was responsible for experimental design, data collection, and data analysis for all sections excluding the NO detection. A.C. Melvin conducted NO release experiments and assisted in data analysis. M. Hedayati assisted in AFM image data collection, assisted with experimental design, and helped revise the manuscript. M.J. Kipper and M.M. Reynolds conceived the research, advised work, and edited manuscript.

## 2.1. Introduction

Despite modern advances in materials, thrombosis, foreign body responses, and infection persist as leading causes of cardiovascular device failure.[1–3] Long-term blood-contacting devices can only perform their intended functions with the assistance of systemic drugs that prevent unfavorable blood-material interactions.[3–6] While the use of systemic drugs allows the devices to function normally, their long-term use causes bleeding disorders and other side effects.[7] Thus, there is a need for materials that locally inhibit thrombosis, inflammation, and infection at the blood-surface interface. Advanced surfaces could reduce or obviate the need for long-term systemic anticoagulant, antiplatelet, and other therapies.

Two common design objectives for improving blood-material interactions are bioinert surfaces and bioactive surfaces. Bioinert surfaces reduce protein adhesion thereby reducing cell-surface interactions. In contrast, bioactive surfaces present biological signals. These include heparinized, bactericidal, and thrombolytic surfaces.[8–11] While offering promising short-term results, neither approach has led to development of a truly blood-compatible material, that can inhibit thrombosis, infection, and inflammation, for long-term applications.[3,8–12]

Our group along with others has taken inspiration form biology, by mimicking the inner surface of blood vessels. The vascular endothelium is the biological gold standard of a blood-compatible surface. Our group has demonstrated reduced protein adsorption, fibrin polymerization, and bacterial attachment by mimicking key features of the blood vessel endothelium.[13,14] This biomimetic strategy has successfully elucidated structure-function relationships linking individual surface features to individual surface activities.

Others have successfully designed materials with singular functionality that address individual blood-material interactions.[13–16] When multifunctional chemistries or surface features are designed, most studies using them do not take a wholistic approach to evaluating blood compatibility. For example many groups have used poly(ethylene glycol) and glycosaminoglycans (GAGs) common to the glycocalyx such as heparin (HEP), chondroitin sulfate (CS), and hyaluronic acid (HA), by conjugating them to substrate surfaces.[13,14,17–21] While these are multifunctional chemistries, studies using them are generally focused on only one important cell-material interaction. Advancements have been made in preparation of dual-feature surfaces.[11,16,22–24] Blood compatibility, however, requires that materials/surfaces interact with multiple biological processes to prevent thrombosis, infection and inflammation; therefore, a knowledge gap exists between multifunctional materials and their effects on multiple cell types.

In the present work, we aim to inhibit unfavorable cellular interactions by designing a multifunctional surface (i.e., the surface can function when exposed to various cell types) that is made to mimic multiple features (both static and dynamic) of the vascular endothelium, and to evaluate these new surfaces against the unfavorable interactions of multiple cell types (**Figure 2.1**). In this study, we combine GAGs, nanotopography, and nitric oxide (NO) release to prepare new blood-contacting surfaces with multiple synergistic functions. Previously, we have developed GAG-based surfaces that also mimic the nanoscale structure and macromolecular assembly of the proteoglycans in the vascular endothelial glycocalyx using polyelectrolyte complex nanoparticles (PCNs).[25,26] The use of PCNs overcomes the electrostatic repulsion that otherwise prevents the dense clustering of GAGs, which is characteristic of the endothelial glycocalyx.[24] In the current

work, we extend this innovation to mimic an important dynamic property of the endothelium by incorporating an *S*-nitrosothiol chemistry, for the sustained release of NO. We hypothesize that the synergistic effects of glycocalyx-mimetic chemistry, nanostructure, and hormone delivery can be optimized to reduce bacterial infection, blood coagulation, and inflammatory responses. These hypotheses are tested by evaluating cell-material interactions, using human platelets, monocytes, macrophages, and both Gram-positive and Gram-negative bacteria (*Pseudomonas aeruginosa* and *Staphylococcus aureus*).

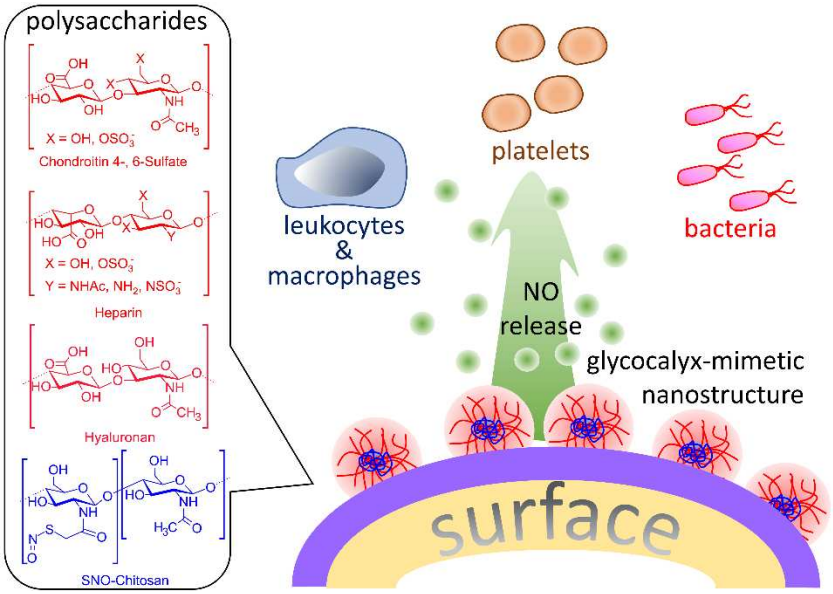


**Figure 2.1.** Schematic of the features of the multifunctional surface and the multiple cell types investigated in this work.

## 2.2. Materials and Methods

### 2.2.1. Materials

Chitosan was purchased from MP Biomedicals. Chondroitin sulfate sodium (CS) salt (from shark cartilage, 6% sulfur, 6-sulfate/4-sulfate = 1.24, $M_w$ = 84.3 kDa), hyaluronic acid (HA) sodium salt ($M_w = 1.5 \times 10^3$ kDa), thioglycolic acid, *N*-(3-(dimethyamino)propyl)-*N'*-ethylcarbodimide hydrochloride (EDC), tris(2-carboxyethyl) phosphine, tert butyl nitrite, 3% gluteraldahide, (grade -), sodium cacodylate, sucrose, phorbol 12-myristate 13-acetate (PMA) and lipopolysaccharide (LPS) were all purchased from Sigma-Aldrich. Heparin sodium (HEP) (from porcine intestinal mucosa, 12.5% sulfur) was purchased from Celsus Laboratories. Glass-bottom petri dishes were purchased from Willco Wells and 8 mm diameter circular cover glasses were purchased from Thomas Scientific. Chromogenic LAL endotoxin assay kit was supplied by GenScript. Phosphate buffer saline (PBS) was purchased from Gibco. Lysogeny broth (LB) and 5000 MWCO snakeskin dialysis tubing was purchased from Thermo Fisher. Calcein AM, rhodamine phalloidin, and DAPI stains were purchased from Thermo Fisher (life technologies). All cell types not taken from donors were purchased form American Type Culture Collection (ATCC). TNF-α enzyme-linked immunosorbent assay (ELISA) kit and supplemental materials were purchased from R & D Systems. Lymphoprep isolation kit was purchased form Stemcell. A Millipore water purification unit was used to obtain 18.2 MΩ cm water, used for making all aqueous solutions.

### 2.2.2. Synthesis of Chitosan Thioglycolic Acid

To achieve NO release from surfaces we modified CHI to incorporate S-nitrosothiol chemistries. This approach was used since it is an established way to release NO without the incorporation of metals, using a surface composed entirely of polysaccharides. First thioglycolic acid is conjugated to CHI using EDC coupling resulting in the product of CHI-TGA. We can then use this product to construct our polyelectrolyte multilayer (PEM) and polyelectrolyte complex nanoparticle (PCN) surfaces. After the surfaces are constructed, they can be further nitrosated by submerging the samples in a solution of tert-butyl nitrite. During this step a nitroso group is added to the thiol of the CHI-TGA.

Chitosan thioglycolic acid (CHI-TGA) was synthesized as previously described.[16,28] Briefly, 0.5 g of chitosan was dissolved in 0.05 L of DI water and 0.0005 L of glacial acetic acid at room temperature. Thioglycolic acid (0.000754 L) was added to the suspension and stirred for 5 minutes. *N*-(3-(dimethyamino) propyl)-*N'*-ethylcarbodimide hydrochloride (1.9 g) was then added. The mixture was protected from light using aluminum foil and allowed to stir for at least 12 h. The solution was then transferred to dialysis tubing and dialyzed against 2 L of DI water adjusted to pH 4-5 using acetic acid, for at least 12 h, with 4 or 5 dialysate changes. The solution was then transferred out of the dialysis tubing, covered with aluminum foil and 0.050 g of tris(2-carboxyethyl) phosphine was added to the solution and stirred for 1 h. The solution was then transferred to dialysis tubing and dialyzed against the same solution as described above. The solution was dialyzed for 7 d with daily dialysate changes. After dialysis, the CHI-TGA was lyophilized until dry.

### 2.2.3. Preparation of PCN and PEM

Polyelectrolyte complex nanoparticles (PCNs) were prepared as previously described.[25,27] Briefly, CHI-TGA, HEP, and CS solutions were prepared at concentrations of 1, 1.5, and 2.8 mg/mL in an acetate buffer solution (0.2 M sodium acetate and acetic acid at pH 5.0), by stirring for 2 h at room temperature. Solutions were filtered using 0.22 µm PDVF syringe filters. The PCN solutions were prepared by adding 36 ml CS or 24 ml HEP solutions to 6 ml CHI-TGA solutions while stirring. After 3 hours of stirring all solutions were allowed to settle overnight.

Polyelectrolyte multilayers (PEMs) were prepared as previously described.[27,29] Hyaluronan (HA) (0.5 mg/mL) and CHI-TGA (1 mg/mL) solutions were prepared in an acetate buffer (0.2 M sodium acetate and acetic acid at pH 5.0), by stirring the for 2 h at room temperature. Solutions were filtered through 22.0 µm PDVF syringe filters. PEMs were constructed using CHI-TGA as the polycation and HA as the polyanion. Glass surfaces were first cleaned and oxidized with oxygen plasma for 7 min. The surfaces were then immediately rinsed with an aqueous acetic acid rinse (pH 4.0; DI water) for 3 min while on a shaker at a low RPM. The rinse was aspirated from the surfaces. Then the layer-by-layer assembly of the PEM was conducted by alternatively exposing the surfaces to polyelectrolyte and rinse solutions in the following sequence: CHI-TGA (5 min), rinse (3 min), HA (5 min), rinse (3 min). This was repeated until there were 19 layers. The PCNs were then adsorbed onto select PEM surfaces. The PCNs were adsorbed onto the surface for a 5-minute interval followed by a rinse, after which the PCN solution was added 2 more times each followed by a rinse. After adding PCN the samples were then dried under nitrogen and stored at (3 – 5 °C) or were immediately nitrosated. For

nitrosation, samples were soaked overnight in *tert*-butyl nitrite. They were then rinsed with methanol followed by diethyl ether and dried under vacuum. Surfaces without PCNs are referred as PEM. Surfaces with PCN are referred to as “PCN-CS” and “PCN-HEP”, depending upon the PCN chemistry. After nitrosation, these are referred to as “PCN-CS-NO” and “PCN-HEP-NO”, respectively.

### 2.2.4. PCN Characterization by DLS

A Zetasizer Nano ZS (Malvern) was used to measure the hydrodynamic diameter and zeta potential of PCN using a 633 nm laser. Measurements were performed at an angle of 175°, at 25 °C, in phosphate buffered saline solution. Three measurements were made on each of the PCN-containing samples.

### 2.2.5. Surface Characterization by XPS

Surface chemistry was analyzed using X-ray photoelectron spectroscopy (XPS) using a Physical Electronics 5800 Spectrometer (Chanhassen, MN). Spectra were obtained with a monochromatic Al K-α X-ray source ($h\nu$ = 1486.6 eV). A hemispherical analyzer, and multichannel detector. High-resolution spectra were obtained using 23.5 eV analyzer pass energy with 0.1 eV steps and an X-ray spot of 800 um. All spectra were taken at a photoelectron takeoff angle of 45°. Spectral curve fitting was done using Origin software (version 9.6). All spectra were shifted according to the aliphatic carbon peak at 284.8 eV.

### 2.2.6. Surface Characterization by AFM

Atomic force microscopy was performed on the surfaces prepared on glass-bottom petri dishes (Ted Pella #14036), using a Bruker Bioscope Resolve atomic force

microscope. All surfaces were submerged in DI water at room temperature for AFM imaging. The ScanAsyst mode was used, with a triangular silicon tip on a nitride lever with a nominal tip radius of 2 nm, a spring constant of 0.12 N/m, and a gold-coated reflective back side (SNL-10 B, Bruker). The peak force set point was set near 2 nN and was optimized using NanoScope software. The scan rate was set to 0.7 Hz with a tapping frequency of 2 kHz. Representative images were taken at 5 μ × 5 μm areas on each sample. Image analysis was preformed using NanoScope Analysis version 1.8.

### 2.2.7. Nitric Oxide Release Quantification

In preparation for NO detection samples were dried completely and stored at 2-8$^{o}$C prior to nitrosation. Each replicate was analyzed immediately after nitrosation to ensure that the full amount of NO was captured. The replicates consisted of 2 glass pucks (15 mm diameter) coated with either PEMs or PCNs. Nitric oxide release was recorded in real time in parts per billion (ppb) using Sievers Nitric Oxide Analyzers (NOA 280i, GE Analytical, Boulder, CO) with nitrogen bubbling (anaerobic). Detection of NO was conducted under near physiological conditions (samples submerged in 2.5 mL of PBS, pH 7.4, at 37$^{o}$C) with a recording interval of 1s and shielded from light. The reaction was continued until the NO release was below the limit of detection. Moles NO was calculated using instrument-specific calibration constant (moles/ppb*sec).

### 2.2.8. Sample sterilization

Samples were sterilized immediately before each study. Each sample was sterilized with a 70% ethanol solution for 15 minutes. The samples were then washed 3x with sterile PBS before use.

### 2.2.9. Endotoxin Assay

Endotoxin presence on glass bottom petri dish surfaces coated with PEM, PCN CS, PCN HEP, PEM NO, PCN CS NO, PCN HEP NO was evaluated using a LAL endotoxin assay kit. Before use the samples were sterilized using the same procedure mentioned previously with the addition of DI washing steps. The samples were then submerged with 2 mL endotoxin free water for 2 hours at room temperature on a shaker. The supernatant was collected, and the concentration of endotoxin was determined using manufacturer's protocol. The maximum sensitivity of the kit used is 0.01 EU/mL.

### 2.2.10. Bacterial culturing and attachment

Bacterial studies were performed as previously described.[30] Briefly, *Pseudomonas aeruginosa* (ATCC 15442) and *Staphylococcus aureus* (ATCC 29213) were thawed at room temperature after being frozen in a 1:1 glycerol solution. Cultures were then centrifuged at 5938 g for 10 min. After centrifugation the supernatant was disposed of and the pellet was resuspended in warm LB broth. The bacterial cultures were incubated in liquid culture at 37 °C on a shaker at 945 g. After at least 24 h of incubation, optical density measurements were taken, and samples were seeded at O. D. 600nm ~ 0.35. At this density bacteria are all in the logarithmic growth phase. After 6 and 24 h, samples were fixed for scanning electron microscopy (SEM; JEOL JSM-6500F). The samples were fixed in the primary fixative [3% glutaraldehyde, 0.1 M sodium cacodylate, and 0.1 M sucrose] for 0.75 h at room temperature. The samples were then washed with a buffer [0.1 M sodium cacodylate, and 0.1 M sucrose] for 10 min. The samples were then dried with increasing concentrations of ethanol solutions (35%, 50%, 75%, and 100%) for 10 min each. To prepare samples for imaging samples were coated with 10 nm of gold and

grounded with copper tape. Samples were imaged at 15 kV at 1000 × magnification for cell counting (5 images per sample) and 3500 × for evaluating cell morphology (1 image per sample). Bacterial coverage was quantified by determining the percent area of bacteria per sample using ImageJ software.

### 2.2.11. Donor Blood Collection

The protocol for blood isolation from healthy individuals who had refrained from taking thromboxane inhibitors for at least 2 weeks was approved by the Colorado State University Institutional Review Board (#14-70B). Blood was drawn via venous phlebotomy, by a trained phlebotomist. Blood was collected into EDTA-coated vacuum tubes (BD).

### 2.2.12. Platelet rich Plasma Isolation and Analysis

Blood was separated by centrifugation at 150×*g* – 180×*g* for 15 min. Platelet rich plasma was collected by pipetting off the top layer containing the plasma and the buffy coat. The remaining layer of red blood cells was removed and discarded. The plasma was pooled and allowed to rest for 10 min at room temperature prior to seeding. For adhesion and activation studies PEM, PCN-CS, PCN-HEP, PCN-CS-NO, and PCN-HEP-NO samples were placed into a 48-well plate and incubated with 200 µL of pooled platelet rich plasma on a horizontal shaker plate at 100 rpm for 2 h at 37 °C and 5 % $CO_2$.

To determine the number of platelets attached, calcien AM was used to stain cytoplasm of live platelets. Briefly, after 2 h of incubation the samples were washed with PBS to remove any unattached cells. Calcien-AM (0.5 mL of 5-uM solution) in PBS was added to the samples. The samples were incubated for 30 min at room temperature in

the staining solution. The solution was then aspirated, and samples were rinsed with PBS. Samples were imaged immediately after staining using a Zeiss Axiovision fluorescence microscope. Five images were taken on each of the three biological replicates ($n = 3$) and the study was repeated twice with 2 different donors. All images were processed using ImageJ software to quantify the number of platelets attached.

Scanning electron microscopy (SEM; JEOL JSM-6500F) was used to qualitatively assess platelet attachment and adhesion. The samples were fixed using the same method described above. Samples were coated with 10 nm of gold and grounded using carbon tape for imaging. Samples were imaged at 15 kV and 3 representative images were taken per group.

### 2.2.13. Mononucleated cell isolation

Collected blood was isolated using Lymphoprep isolation kit. Briefly, donor blood was diluted 1:1 with PBS and then slowly added on top of a layer of Lymphoprep that was added to a 15-ml conical tube. Tubes were then centrifuged for 20 min at 800×*g*. The mononucleated cell layer was then pipetted off into a solution of PBS that was then centrifuged again at 250×*g* for 10 min. The cells were then collected and seeded at a density of $2\times10^6$ cells $mL^{-1}$ directly onto samples in 48-well plates. These cells were cultured in RPMI-1640 media supplemented with 1% penicillin and streptomycin (pen/strep) and 5% fetal bovine serum (FBS).

Leukocyte attachment and aggregation were visualized using DAPI (nuclei) staining and rhodamine phalloidin (actin) staining. After 1 or 4 d of incubation the samples were rinsed with PBS to remove unattached cells. Samples were then fixed with 3.67%

formaldehyde solution with PBS for 15 min. After fixation the samples were rinsed 3 times and then cells were permeabilized with triton 1× solution for 3 min. Samples were stained with 70 nM rhodamine phalloidin solution for 25 min and then counterstained with 1.49 mM DAPI solution for an additional 5 min. Samples were then rinsed and stored in PBS until they were imaged with a Zeiss Axiovision fluorescence microscope.

### 2.2.14. THP-1 Cell Culturing and Differentiation

THP-1 cells (human peripheral blood monocytes, ATCC TIB-202) were cultured in RPMI-1640 media supplemented with 1% pen/strep and 5% FBS. Cells were split every 4 d and kept at a density of about $5\times10^5$ cells/mL. Cells were differentiated into macrophages as previously described.[31] In brief, cells were seeded in onto test and control samples in a 48-well plate at a density of $1\times10^5$ cells/mL. Growth media was supplemented with 25 ng/mL PMA. Cells were cultured on samples in this media for 48 h. After 48 h of differentiation onto sample surfaces media was collected and stored at -80 °C and supplemented with protease inhibitor until further evaluation. For cells on control samples, media was discarded after 48 h and replaced with LPS containing media for 1 to 3 h. This media was then replaced with normal differentiation media in which the cells were cultured in for an additional 24 h after which media was collected for control samples to evaluate the cells response to LPS.

### 2.2.15. TNF- α expression

Media collected from differentiated THP-1 cells that were seeded on samples was tested for TNF- α production using an ELISA. The assay was performed according to manufacturer's instructions. Briefly, a 96 well plate was coated with a capture antibody

overnight. The plate was then washed and blocked with bovine serum albumin (BSA) for 1 h. After an additional washing step, media samples and standards were added to the plate for 2 h. Once the plate was aspirated and washed, a detection antibody was added to the plate and incubated for 2 h, streptavidin-HRP for 20 min, and a substrate solution was added for 20 min with a wash between each step. A stop solution was added to the solution and the adsorption was immediately read at 540 and 570 nm.

### 2.2.16. Statistical Analysis

Peak fitting analysis was conducted on XPS data sets using Origin software (version 9.6) after spectra was shifted to the aliphatic carbon. Normality tests were performed on these data sets using R (version 3.6.1). To meet normality assumption all data sets except for XPS data and TNF-α data were log transformed. Two-way ANOVAs and One-way ANOVAs with post hoc Tukey tests were run on log transformed and original data sets (except XPS data) using R (version 3.6.1).

## 2.3. Results and Discussion

### 2.3.1. Preparation of Six Endothelium-Mimetic Surfaces

We designed and prepared six different endothelium-mimetic surfaces, using different combinations of functional features: GAG chemistry, glycocalyx mimetic nanostructure and NO-release. The six surface types are denoted PEM, PCN-CS, PCN-HEP, PEM-NO, PCN-CS-NO, and PCN-HEP-NO. PEM surfaces are coated with polyelectrolyte multilayers of hyaluronan (HA) and a thioglycolic acid-modified chitosan (CHI-TGA). PCN-CS and PCN-HEP surfaces are PEM surfaces further modified by adsorption of negatively charged polyelectrolyte complex nanoparticles (PCNs), rich in

either chondroitin sulfate (CS) or heparin (HEP). We have previously shown that these PCNs formed from chitosan (CHI) and GAGs (CS or HEP) mimic key features (nanostructure and composition) of the vascular endothelial glycocalyx, and can inhibit protein adsorption and fibrin fiber polymerization and adsorption to surfaces.[25,26,32] Finally, the PEM, PCN-CS and PCN-HEP were each modified with a NO-releasing *S*-nitrosothiol group, through the TGA on the CHI-TGA to produce PEM-NO, PCN-CS-NO, and PCN-HEP-NO surfaces.

### 2.3.2. Surface chemistry and nanotopography

X-ray photoelectron spectroscopy (XPS) was used to confirm the surface chemistries. **Figure 2.2** shows high-resolution spectra of PEM and PCN CS NO surfaces. All surfaces have S2p peaks present, indicating successful incorporation of the CHI-TGA (in PEM and PEM-NO) and from the adsorption of the sulfate-containing polysaccharides (HEP and CS). All the nitrosated samples contain a peak at 408 eV in the N1s envelope, that is absent in the non-nitrosated samples. This confirms successful nitrosation.

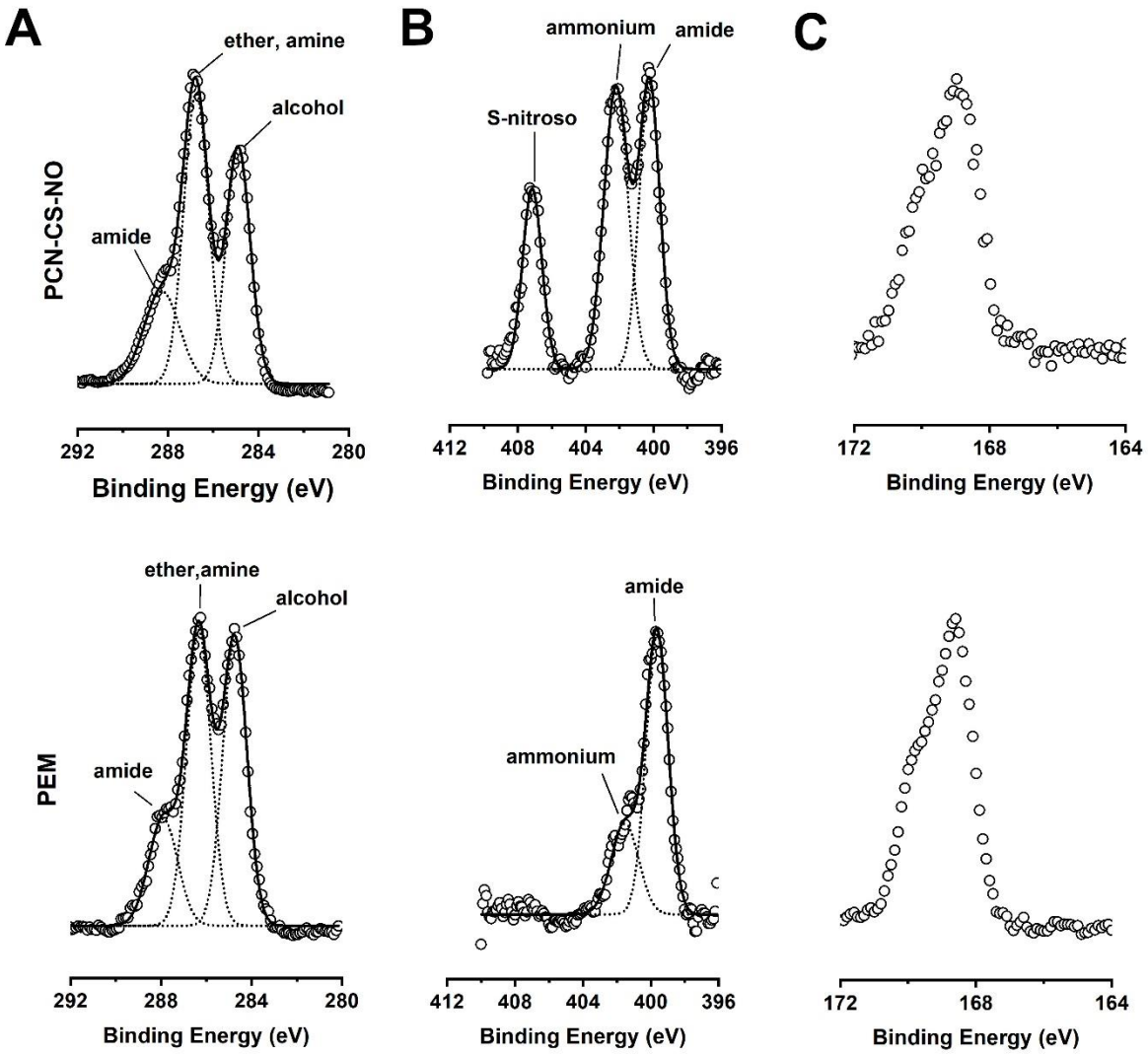


**Figure 2.2**. High resolution XPS spectra of (A) C1s (B) N1s, and (C) S2p envelopes for PCN-CS-NO (top row) and PEM (bottom row) samples. Data are circles, individual peaks are dotted lines, and sums of individual peaks from the curve fit are solid lines.

All of the surfaces were prepared by a layer-by-layer assembly process to form 19-layer PEMs, containing CHI-TGA (as the polycation), and HA (as the polyanion). These 19-layer PEMs completely cover the underlying glass substrate, which is confirmed by the loss of peaks associated with silica in the XPS (supporting information **Figure 2.S1**).

Surfaces with nanoscale texture and features mimicking the organization of GAGs in the vascular endothelial glycocalyx were prepared by adsorbing CS-containing and

HEP-containing PCNs to the PEMs, as we have previously reported.[25,26] Negatively charged polyelectrolyte complex nanoparticles were prepared using glycosaminoglycans (CS and HEP) as the polyanions and CHI-TGA as the polycation, using techniques we have previously described.[33–35] DLS and zeta potential measurements confirm the formation of negatively charged PCNs (supporting information **Table 2.S1**). The negative zeta potential confirms that negatively charged PCNs are formed.

The PCNs were adsorbed onto the surface of the PEMs and subsequently nitrosated. The presence of PCNs on both the non-nitrosated (PCN CS and PCN HEP) and nitrosated (PCN CS-NO and PCN HEP-NO) surfaces is confirmed by atomic force microscopy (AFM) (**Figure 2.3**) **(Table 2.S2)**. On the PCN-containing samples, the adsorbed PCN are clearly visible as individual domains, several hundred nanometers in diameter and approximately 100 to 200 nm in height with roughness values ($R_q$) significantly higher than PEM surfaces (Table 2.S2). The surface characterization via XPS and AFM confirms successful preparation of glycocalyx mimics containing HEP and CS nanoparticles and NO donor chemistry (**Figure 2.2** and **2.3**). The additional *S*-nitrosation of the PCN-CS-NO and PCN-HEP-NO samples did not greatly alter the surface topography of our samples as seem by AFM images and roughness values (**Figure 2.3**) (Table 2.S2). Nitrosation did result in slight smoothing of the surfaces, but nanoparticles were not dispersed from the surface and the same trend in roughness values was kept between PEM and PCN samples (PCN $R_q$ > PEM $R_q$).

### 2.3.3. Nitric oxide release profile

Nitric oxide release profiles are characterized at 37ºC in pH 7.4 PBS for each NO-releasing surface using a Sievers Nitric Oxide Analyzers (NOA 280i, GE Analytical,

Boulder, CO). The NO release profile is described by a quick, initial burst of NO followed by a steady NO release level for up to 18 h. The characterization of the profile aligns with other NO release materials that have been reported in the literature. **Figure 2.4** shows a representation of the release profile out to 2 h. All samples followed the same NO release trend with some slight differences between initial burst values (**Figure 2.S2**). On average the PEM-NO samples tended to have a greater accumulative release of NO, but there were no significant differences between different sample types (Figure 2.S2). Additionally, given that NO is a radical and has a short half-life, NO does not accumulate in solution like other drug eluting substances. As a result, accumulative release is not representative of the NO dosing at any given time. The given amount of NO available to cells from these formulations are 0.47 ± 0.24, 0.19 ± 0.15, 0.36 ± 0.25 pmol/mm$^2$ during the burst period (1 min) and 0.10 ± 0.08, 0.02 ± 0.01, 0.01 ± 0.009 pmol/mm$^2$ (1 h) to 0.05 ± 0.02, 0.02 ± 0.01, 0.009 ± 0.008 pmol/mm$^2$ (2 h) during the steady state period for PEM-NO, PCN-CS-NO, and PCN-HEP-NO surfaces respectively.

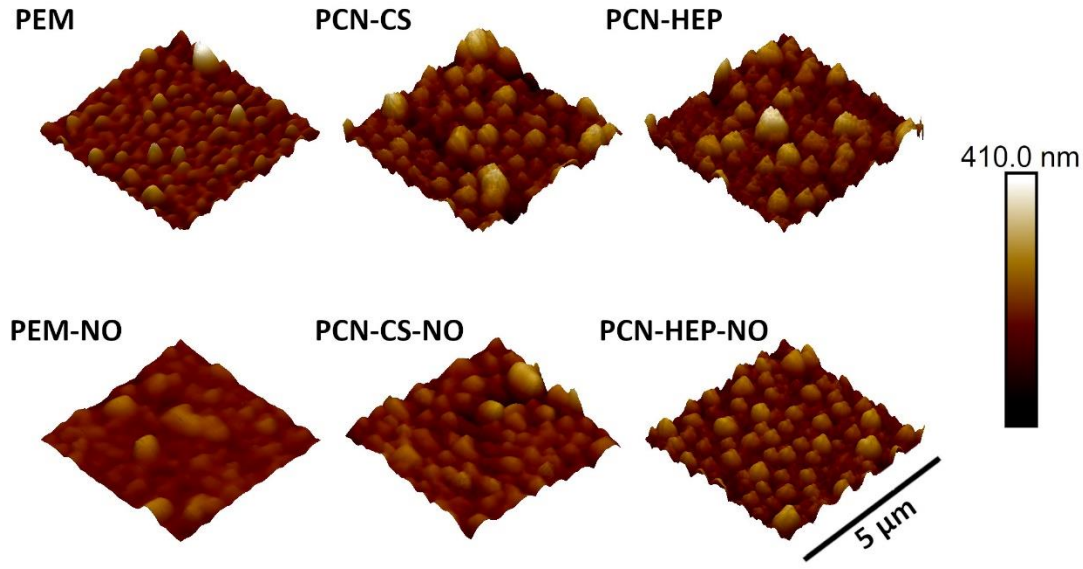


**Figure 2.3.** Atomic force microscopy images (5 µm × 5 µm) of PEM, PCN-CS, PCN-HEP, PEM-NO, PCN-CS-NO, and PCN-HEP-NO.

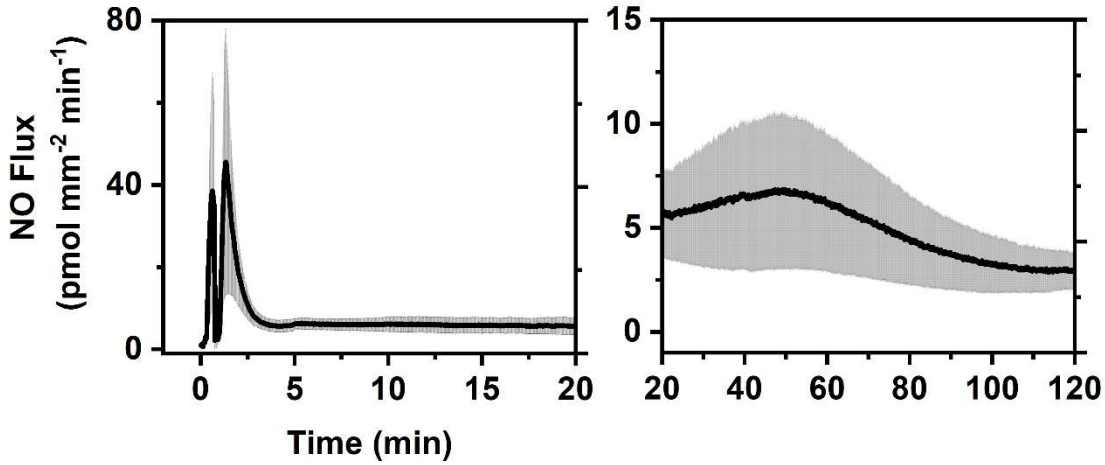


**Figure 2.4**. NO flux from 0 to 20 min (right) and 20 to 120 min (left) for PEM-NO samples (n=3) (mean ± standard deviation).

### 2.3.4. Platelet adhesion and activation

Both platelet adhesion and platelet activation were measured to demonstrate how the surface features affect platelet responses. Platelets were evaluated due to their importance in coagulation. Without platelets arterial thrombosis would not occur in response to foreign bodies. **Figure 2.5A** shows the %-coverage of platelets on each

surface, normalized to the %-coverage on a control surface, after exposure to platelet-rich plasma from healthy human donors for 2 h. Untreated glass slides were used as a positive control for platelet adhesion and activation. Except for the PCN HEP, all the experimental samples have substantially reduced platelet adhesion compared to the control surface. A two-factor (surface type and +/- NO) ANOVA reveals that the addition of NO significantly reduces the number of platelets attached for all surface types (**Figure 2.5A)**.

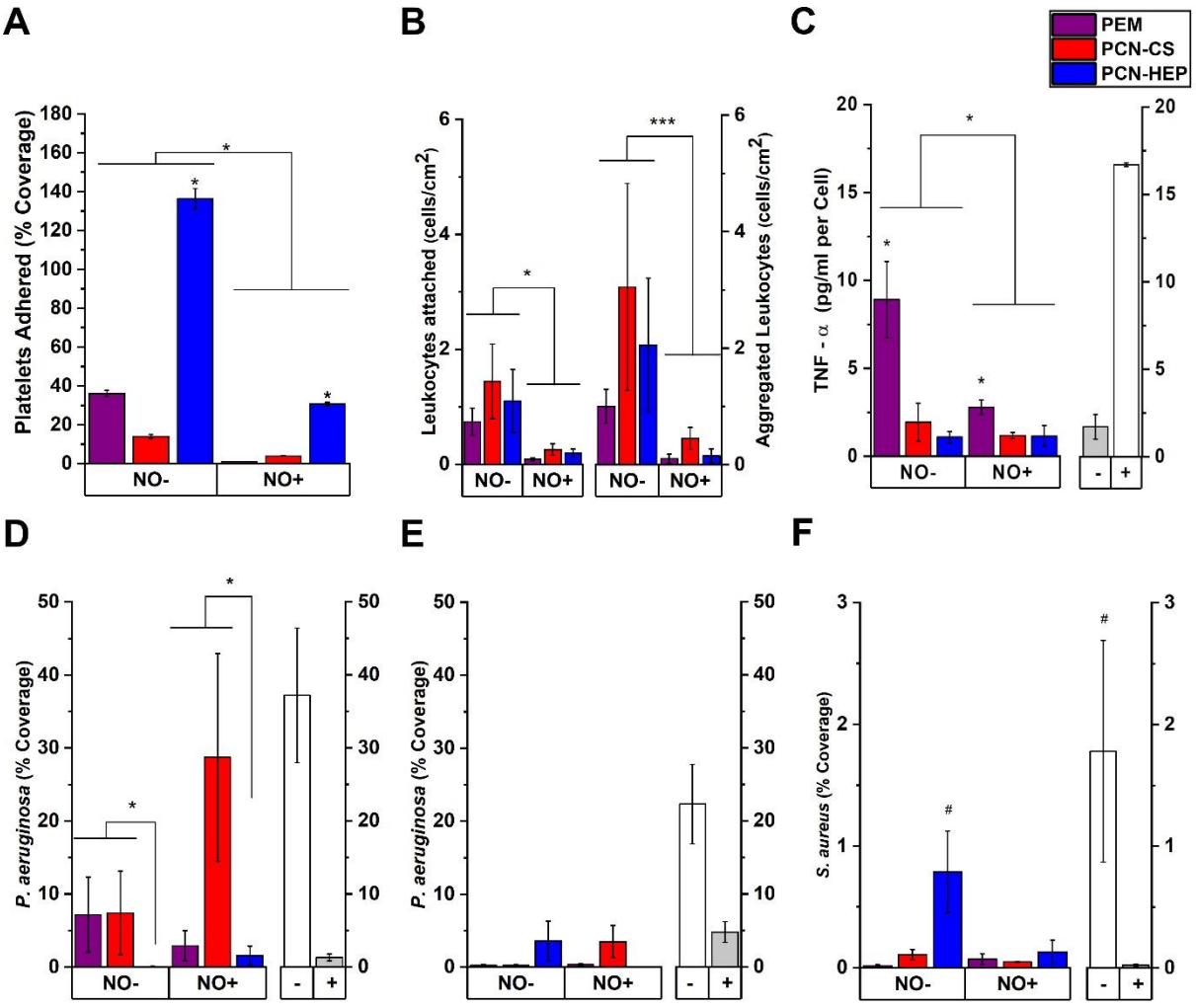


**Figure 2.5**. Surface cell interactions (*n* = 3 samples) (mean ± standard error) where (A) is %-coverage of platelets relative to the control surface. (B) is total number of leukocytes adhered to surfaces (left) and total number of cell aggregates (right) where aggregates

are defined as 3 or more nuclei where the rhodamine stain is overlapped, both of which are normalized to the control surface. (C) is TNF-α (pg/mL) produced per M0 macrophage seeded on samples. Controls are with (+) and without (-) LPS. (D) is percent coverage of *P. aeruginosa* after 6 h and 24 h (E), and (F) is percent coverage of *S. aureus* after 24 h. Controls for (D), (E), and (F) are with (+) and without (-) antibiotic on polystyrene surfaces. Two-factor ANOVA with post hoc Tukey test was conducted (on log-transformed data for (A), (B), (D), (E), and (F) and non-transformed data for (C)) where the factors are NO+/NO- and surface type. Comparisons between each separate sample were not made. Statistically significant differences are indicated by stars and brackets (* $p<0.5$, ** $p<0.05$, *** $p<0.005$). One-way ANOVA with post hoc Tukey test was also conducted to determine differences between samples and controls. For (E) and (F) all samples were grouped as performing the same as antibiotic treated controls except for PCN-HEP-NO samples in (F). The # shows that PCN-HEP-NO is grouped the same as tissue culture polystyrene controls.

Previous studies have shown CHI- and CS-containing materials show reduced platelet adhesion.[36,37] Other groups have also demonstrated NO has strong antiplatelet activity.[16,38–42] Statistical analysis revealed an additional synergistic effect of the combination of surface type and NO release resulting in a greater reduction of platelet coverage than either CS-PCN or NO alone. Our lab previously showed that CS and HEP PCN-terminated materials enable reversible protein adsorption and desorption and inhibit fibrin polymerization.[25] Since platelet responses to biomaterials are in part determined by irreversibly adsorbed and denatured serum proteins the PCN-CS and PCN-CS-NO surfaces inhibit platelet adhesion through multiple synergistic functions.[43]

Nitric oxide release also reduces platelet activation **(Figure 2.6)**. Platelet activation occurs through a series of shape changes identifiable in electron microscopy. When platelets adhere to a surface they initially change from a discoid to spherical shape. This is followed by the formation of finger-like dendrites. The “short dendritic” morphology has dendrites that are shorter than the diameter of the cell body, while the “long dendritic” morphology has dendrites longer than the cell body. The short and long dendritic morphologies are characteristic of platelets that are not yet fully activated. Late activation

is characterized by platelet spreading and the formation of lamellipodia. Fully activated platelets adopt a “fried egg” morphology, characterized by increased spreading and flattening, with intracellular components concentrated near the center of the cell body. The surfaces studied here clearly induce different levels of activation. Figure 2.6 shows representative examples of platelets on each surface type including the glass control. PEM and PEM-NO surfaces have some short- and long-dendritic platelets, whereas the PCN-CS and the PCN-CS-NO surfaces have very few platelets that are mostly not activated. In contrast the PCN-HEP surfaces show the most activated platelets, which are also exhibiting aggregation. The addition of NO to the PCN-HEP-NO surfaces has a strong anti-activation effect on platelets.

An LAL endotoxin assay was used to determine if the samples released any endotoxin into solution to determine if platelet activation was due to their presence. The assay found that the concentration of endotoxins released from the surfaces was below the limits of detection (**Figure 2.S2**). We do not propose that the bulk materials are endotoxin free, but that the surfaces are so thin that the amount of endotoxin released from the surface is so low that it would have a negligible effect on the platelets. The platelets activation due described above is due to the surface characteristics and not endotoxin presence.

The PCN-HEP surfaces promote attachment and activation of the platelets. This is an important observation, as HEP is used in both soluble and surface-adsorbed states as an anticoagulant.[14,44] Heparin inhibitions coagulation by binding to and activating antithrombin III, which inhibits multiple coagulation factors.[17,45,46] In contrast, HEP—particularly high molecular weight HEP—may also cause platelet aggregation.[47] This

matches what has been observed clinically with heparin-coated coronary stents being removed from the market after causing higher rates of restenosis than anticipated.[47] The effect of HEP on platelet attachment is diminished by the addition of NO. The effect of NO release on platelet activation is also clearly illustrated by comparing the PCN-HEP and PCN-HEP-NO samples; when added to the PCN HEP surface, the NO release dramatically reduces platelet adhesion and platelet activation as shown by the representative SEM images in Figure 2.6**.**

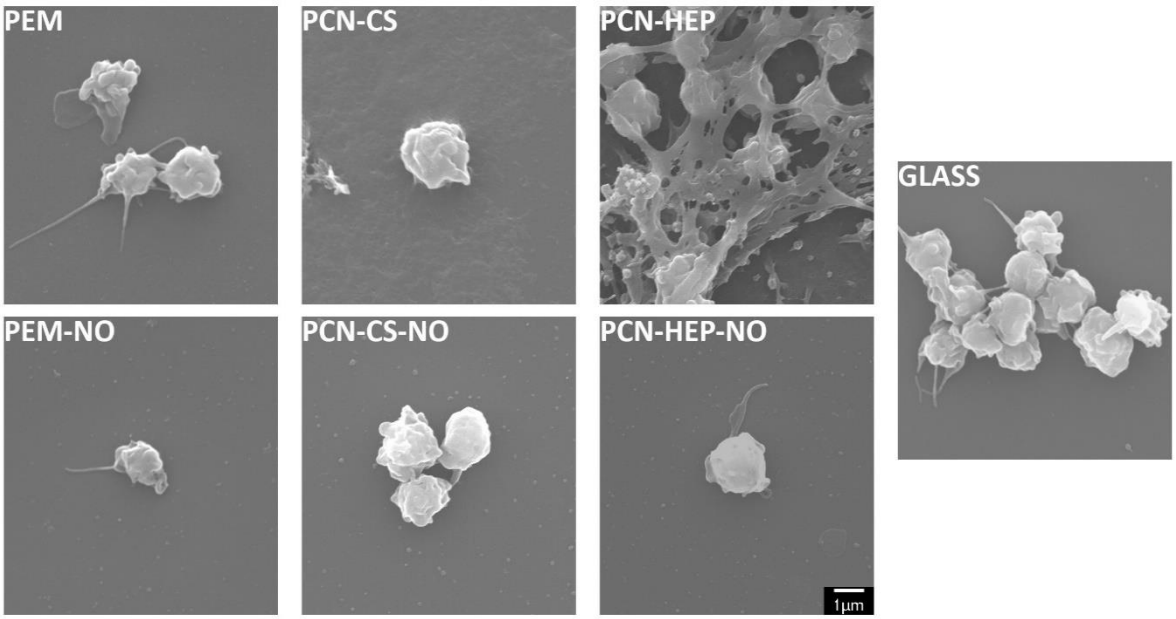


**Figure 2.6**. Representative SEM images of samples showing differing degrees of platelet activation. All samples had examples of platelets with some degree of activation. The glass control along with the PCN-HEP samples showed highly activated and aggregated platelets meaning thrombus formation is likely on these samples. For all experimental surfaces, addition of NO reduces the degree of platelet activation.

### 2.3.5. Leukocyte attachment, aggregation, and TNF-α release by Macrophages

Leukocyte attachment and aggregation was evaluated due to their role in inflammatory responses. Mononucleated cells were isolated from donor blood using a separation medium, after which the cells were seeded onto samples. The number of cells

attached and aggregated after 1 d of incubation is significantly reduced on NO-releasing samples (Figure 2.5B). The aggregation is characteristic of frustrated phagocytosis that may lead to foreign body giant cell formation and chronic inflammation. PCN-containing samples increased attachment and aggregation of these cells, though this effect is not statistically significant. After 4 d there are no differences in sample types for attachment or aggregation of cells (supporting information **Figure 2.S3**).

Since macrophages are the primary phagocytic cells in the body and can have both pro- and anti-inflammatory functions macrophage, responses to our materials were also evaluated. THP-1 monocytes were differentiated into M0 macrophages to further evaluate inflammatory responses to our surfaces. The media from these cells was used to determine the amount of extracellular TNF-α (Figure 2.5C). The LPS-treated cells (positive control for pro-inflammatory macrophage activation) have an increase in TNF-α. All sample types released less TNF-α than the negative control. (This difference is not indicated in the figure). Nitric oxide release and nanoparticle presence both reduce macrophage TNF-α production.

Taken together, the release of NO significantly reduces the inflammatory responses to our materials. Nitric oxide can reduce the immune response and inflammation *in vivo*.[48] Nitric oxide inhibits leukocyte recruitment and pro-inflammatory macrophage activity.[48] Macrophages have also been reported to respond to surface nanotopography.[49] The differences between the PCN-modified and PEM surfaces may also be due to the changes in surface chemistry. Chondroitin sulfate and HEP have some anti-inflammatory properties on their own.[50–52] Therefore, the multiple glycocalyx mimetic

features of these surfaces work together to reduce the inflammatory response of monocytes/macrophages.

### 2.3.6. Bacterial attachment

Blood contacting devices always pose a risk of infection. Both Gram-positive and Gram-negative bacteria can contribute to these infections, but may require different antibiotic treatments. Therefore, we evaluated antibacterial activity with respect to both Gram- positive (*Staphylococcus aureus*) and Gram-negative bacteria (*Pseudomonas aeruginosa*).

Statistical analysis revealed that growth of *P. aeruginosa* growth is affected by surface type, but not by NO release after 6 h (Figure 2.5D), with HEP PCNs significantly reducing the percent coverage of *P. aeruginosa* in the presence or absence of NO. However, after 24 h, there are no significant differences among the experimental sample types (Figure 2.5E and **Figure 2.7**), with all experimental surfaces exhibiting lower attachment than the glass control, and similar cell attachment to the antibiotic-treated control. Heparin surfaces have demonstrated antimicrobial activity against Gram-negative bacteria in previous studies, which is consistent with our findings after 6 hours.[50,53] Chitosan, chitosan derivatives, and CS have also been shown to inhibit bacterial attachment.[54–59] Exposure time is an important factor in the antimicrobial activity of some polysaccharides. For example, previous studies have shown the greatest reduction in bacterial attachment and activity on chondroitin sulfate surfaces after at least 8 h, which is consistent with the differences we observe between 6 and 24 h.[54]

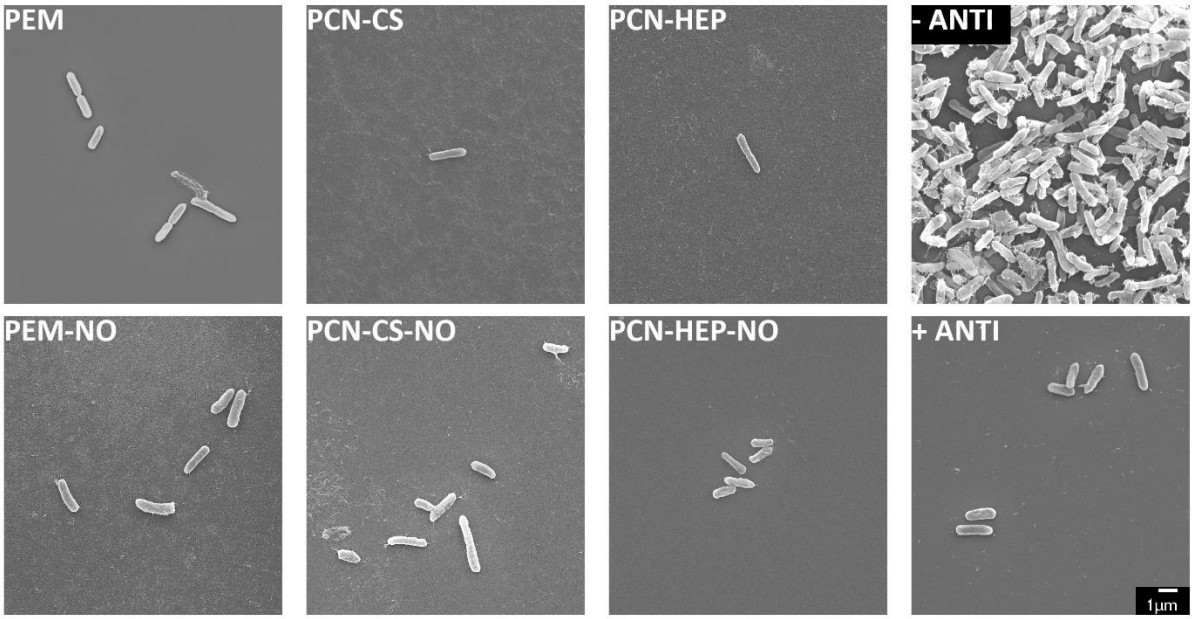


**Figure 2.7**. Representative SEM images of samples and controls showing *Pseudomonas aeruginosa* attachment. Images are examples of samples after 24 h of incubation at 37 °C.

The growth of *S. aureus* was not significantly different between any of the sample types at 6 h of incubation and there was very little bacterial growth at that time (supporting information **Figure 2.S4**). After 24 h, the percent coverage of bacteria decreased for all sample types, including controls. After 24 h the cell coverage was significantly greater on the TCPS samples than on all other sample types except for PCN-HEP (Figure 2.5F and **Figure 2.8**).

The bacterial coverage was greatest on tissue culture-treated and plain polystyrene pucks, which were used as negative controls for inhibiting *S. aureus* and *P. aeruginosa* growth, respectively. There was no significant reduction of bacterial attachment due to the release of NO. This is surprising as NO is a known endogenous antimicrobial signal.[48] In the presence of pathogens, macrophages will release large amounts of NO and other reactive oxygen species, which can damage the structural elements, replication machinery, nucleic acids, and metabolic enzymes of pathogens.[48]

Other work has also shown that NO-releasing materials have broad spectrum antimicrobial activity.[24,42,60–63] The minimal observed antimicrobial properties of our NO-releasing surfaces may be due to the amount of NO released. Previously published literature from our group has shown that 2.73 nM NO is required to produce a 90% reduction in bacterial biofilm viability.[60] Our surfaces were able to exceed or match this value during the initial burst release and during steady state release for some samples. However, this was still not enough NO release to improve bactericidal properties of the surfaces beyond the improvements seen due to changes in surface chemistry. To further improve the antimicrobial activity of these surfaces NO release should be increased by adsorbing more layers of CHI-TGA, or by synthesizing a polyanion modified for NO release to incorporate more NO-donor moieties.

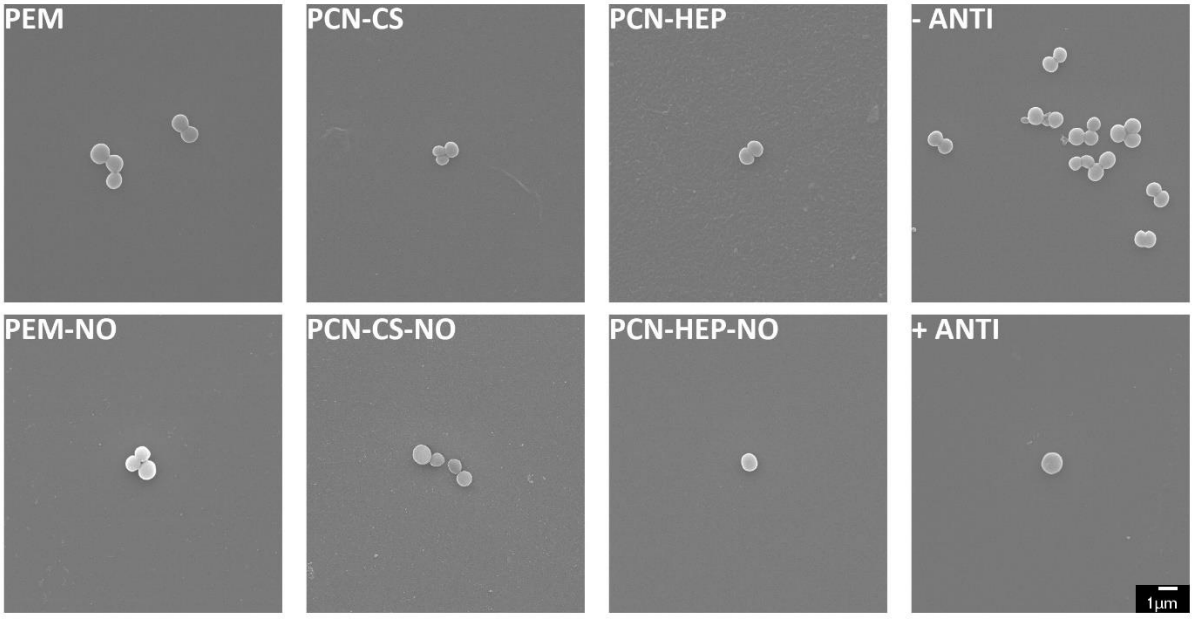


**Figure 2.8**. Representative SEM images of samples and controls showing *Staphylococcus aureus* attachment. Images are examples of samples after 24 h of incubation at 37 °C.

## 2.4. Conclusion:

Strategic biomimicry is an excellent design strategy for improving blood-compatibility of materials. The addition of NO donor chemistry and surface modification with endothelial glycocalyx-mimetic, GAG-containing nanostructures to surfaces can reduce unfavorable cellular reactions related to coagulation, inflammation, and infection. This work investigated platelet, leukocyte, macrophage, and bacterial cell responses to multifunctional surfaces, and showed for the first time that multiple synergistic surface features (chemistry, topography, and dynamic properties) can be combined to prepare multifunctional surfaces for enhancing key predictors of blood-compatibility. This work demonstrates the need for and feasibility of designing multifunctional surfaces. For example, while the HEP-containing nanoparticle samples were able to reduce TNF-α production they caused a high degree of adhesion and activation of platelets. No one material combination preformed the best in every scenario. However, CS-containing PCNs combined with NO release, substantially improves the antiplatelet activity, while also exhibiting favorable interactions with both leukocytes and bacteria. Due to its overall positive performance in the different experimental conditions PCN CS NO samples would be selected as the best material out of the ones tested for use in blood contacting materials. Despite PCN CS NO being the best candidate, other material combinations also showed promise. From these studies we were able to discover more about what is needed to design a successful blood contacting material. The novel surfaces discussed in this work are better suited to deal with the complexity of material-blood interactions than surfaces designed with only a single feature or function.

## Citations


1. Reviakine, I. *et al.* Stirred, shaken, or stagnant: What goes on at the blood–biomaterial interface. *Blood Rev.* **31**, 11–21 (2017).

2. Stickler, D. & McLean, R. Biomaterials Associated Infections: The Scale of the Problem. *Cells Mater.* **5**, (1995).

3. Anderson, J. M., Rodriguez, A. & Chang, D. T. Foreign body reaction to biomaterials. *Semin. Immunol.* **20**, 86–100 (2008).

4. Ratner, B. D. The blood compatibility catastrophe. *J. Biomed. Mater. Res.* **27**, 283–287 (1993).

5. Ratner, B. D. The catastrophe revisited: Blood compatibility in the 21st Century. *Biomaterials* **28**, 5144–5147 (2007).

6. Gristina, A. G., Naylor, P. & Myrvik, Q. Infections from biomaterials and implants: a race for the surface. *Med. Prog. Technol.* **14**, 205–224 (1988).

7. Jung, F. & Braune, S. Thrombogenicity and hemocompatibility of biomaterials. *Biointerphases* **11**, 029601 (2015).

8. Harding, J. L. & Reynolds, M. M. Combating medical device fouling. *Trends Biotechnol.* **32**, 140–146 (2014).

9. Anderson, J. M. Biological Responses to Materials. *Annu. Rev. Mater. Res.* **31**, 81–110 (2001).

10. Jaffer, I. H., Fredenburgh, J. C., Hirsh, J. & Weitz, J. I. Medical device-induced thrombosis: what causes it and how can we prevent it? *J. Thromb. Haemost.* **13**, S72–S81 (2015).

11. Zhan, W. *et al.* Bioinspired Blood Compatible Surface Having Combined Fibrinolytic and Vascular Endothelium-Like Properties via a Sequential Coimmobilization Strategy. *Adv. Funct. Mater.* **25**, 5206–5213 (2015).

12. Jackson, C. M. & Nemerson, Y. Blood Coagulation. *Annu. Rev. Biochem.* **49**, 765–811 (1980).

13. Maitz, M. F. *et al.* Adaptive release of heparin from anticoagulant hydrogels triggered by different blood coagulation factors. *Biomaterials* **135**, 53–61 (2017).

14. Larsson, R., Eriksson, J.-C., Lagergren, H. & Olsson, P. Platelet and plasma coagulation compatibility of heparinized and sulphated surfaces. *Thromb. Res.* **15**, 157–167 (1979).

15. Sen Gupta, A. *et al.* Glycocalyx-mimetic dextran-modified poly(vinyl amine) surfactant coating reduces platelet adhesion on medical-grade polycarbonate surface. *Biomaterials* **27**, 3084–3095 (2006).

16. Simon-Walker, R. *et al.* Glycocalyx-Inspired Nitric Oxide-Releasing Surfaces Reduce Platelet Adhesion and Activation on Titanium. *ACS Biomater. Sci. Eng.* **3**, 68–77 (2017).

17. Pasche, B., Kodama, K., Larm, O., Olsson, P. & Swedenborg, J. Thrombin inactivation on surfaces with covalently bonded heparin. *Thromb. Res.* **44**, 739–748 (1986).

18. Lagergren, H., Olsson, P. & Swedenborg, J. Inhibited platelet adhesion: A non-thrombogenic characteristic of a heparin-coated surface. *Surgery* **75**, 643–650 (1974).

19. Bui, H. T., Friederich, A. R., Li, E., Prawel, D. A. & James, S. P. Hyaluronan enhancement of expanded polytetrafluoroethylene cardiovascular grafts. *J. Biomater. Appl.* **33**, 52–63 (2018).

20. Pang, X. *et al.* Mimicking the endothelial glycocalyx through the supramolecular presentation of hyaluronan on patterned surfaces. *Faraday Discuss.* **219**, 168–182 (2019).

21. Lowe, S., O'Brien-Simpson, N. M. & Connal, L. A. Antibiofouling polymer interfaces: poly(ethylene glycol) and other promising candidates. *Polym. Chem.* **6**, 198–212 (2014).

22. Wu, B., Gerlitz, B., Grinnell, B. W. & Meyerhoff, M. E. Polymeric coatings that mimic the endothelium: Combining nitric oxide release with surface-bound active thrombomodulin and heparin. *Biomaterials* **28**, 4047–4055 (2007).

23. Zhou, Z. & Meyerhoff, M. E. Preparation and characterization of polymeric coatings with combined nitric oxide release and immobilized active heparin. *Biomaterials* **26**, 6506–6517 (2005).

24. Xu, L.-C., Meyerhoff, M. E. & Siedlecki, C. A. Blood coagulation response and bacterial adhesion to biomimetic polyurethane biomaterials prepared with surface texturing and nitric oxide release. *Acta Biomater.* **84**, 77–87 (2019).

25. Hedayati, M., Reynolds, M. M., Krapf, D. & Kipper, M. J. Nanostructured Surfaces That Mimic the Vascular Endothelial Glycocalyx Reduce Blood Protein Adsorption and Prevent Fibrin Network Formation. *ACS Appl. Mater. Interfaces* **10**, 31892–31902 (2018).

26. Hedayati, M. & Kipper, M. J. Atomic force microscopy of adsorbed proteoglycan mimetic nanoparticles: Toward new glycocalyx-mimetic model surfaces. *Carbohydr. Polym.* **190**, 346–355 (2018).

27. Hedayati, M. & Kipper, M. J. Atomic force microscopy of adsorbed proteoglycan mimetic nanoparticles: Toward new glycocalyx-mimetic model surfaces. *Carbohydr. Polym.* **190**, 346–355 (2018).

28. Lutzke, A., Pegalajar-Jurado, A., Neufeld, B. H. & Reynolds, M. M. Nitric oxide-releasing S-nitrosated derivatives of chitin and chitosan for biomedical applications. *J Mater Chem B* **2**, 7449–7458 (2014).

29. Boddohi, S., Killingsworth, C. E. & Kipper, M. J. Polyelectrolyte Multilayer Assembly as a Function of pH and Ionic Strength Using the Polysaccharides Chitosan and Heparin. *Biomacromolecules* **9**, 2021–2028 (2008).

30. Pegalajar-Jurado, A. *et al.* Nitric oxide-releasing polysaccharide derivative exhibits 8-log reduction against Escherichia coli, Acinetobacter baumannii and Staphylococcus aureus. *J. Controlled Release* **217**, 228–234 (2015).

31. Park, E. K. *et al.* Optimized THP-1 differentiation is required for the detection of responses to weak stimuli. *Inflamm. Res.* **56**, 45–50 (2007).

32. Hedayati, M., Marruecos, D. F., Krapf, D., Kaar, J. L. & Kipper, M. J. Protein adsorption measurements on low fouling and ultralow fouling surfaces: A critical comparison of surface characterization techniques. *Acta Biomater.* **102**, 169–180 (2020).

33. Volpato, F. Z. *et al.* Preservation of FGF-2 bioactivity using heparin-based nanoparticles, and their delivery from electrospun chitosan fibers. *Acta Biomater.* **8**, 1551–1559 (2012).

34. Place, L. W., Sekyi, M. & Kipper, M. J. Aggrecan-mimetic, glycosaminoglycan-containing nanoparticles for growth factor stabilization and delivery. *Biomacromolecules* **15**, 680–689 (2014).

35. Boddohi, S., Moore, N., Johnson, P. A. & Kipper, M. J. Polysaccharide-based polyelectrolyte complex nanoparticles from chitosan, heparin, and hyaluronan. *Biomacromolecules* **10**, 1402–1409 (2009).

36. Thalla, P. K. *et al.* Chondroitin Sulfate Coatings Display Low Platelet but High Endothelial Cell Adhesive Properties Favorable for Vascular Implants. *Biomacromolecules* **15**, 2512–2520 (2014).

37. Şenel, S. & McClure, S. J. Potential applications of chitosan in veterinary medicine. *Adv. Drug Deliv. Rev.* **56**, 1467–1480 (2004).

38. Riddell, D. R. & Owen, J. S. Nitric Oxide and Platelet Aggregation. in *Vitamins & Hormones* (ed. Litwack, G.) vol. 57 25–48 (Academic Press, 1997).

39. Frost, M. C., Reynolds, M. M. & Meyerhoff, M. E. Polymers incorporating nitric oxide releasing/generating substances for improved biocompatibility of blood-contacting medical devices. *Biomaterials* **26**, 1685–1693 (2005).

40. Riccio, D. A. & Schoenfisch, M. H. Nitric oxide release: Part I. Macromolecular scaffolds. *Chem. Soc. Rev.* **41**, 3731–3741 (2012).

41. Suchyta, D. J., Handa, H. & Meyerhoff, M. E. A Nitric Oxide-Releasing Heparin Conjugate for Delivery of a Combined Antiplatelet/Anticoagulant Agent. *Mol. Pharm.* **11**, 645–650 (2014).

42. Wo, Y., Brisbois, E. J., Bartlett, R. H. & Meyerhoff, M. E. Recent advances in thromboresistant and antimicrobial polymers for biomedical applications: just say yes to nitric oxide (NO). *Biomater. Sci.* **4**, 1161–1183 (2016).

43. Xu, L.-C., Bauer, J. W. & Siedlecki, C. A. Proteins, platelets, and blood coagulation at biomaterial interfaces. *Colloids Surf. B Biointerfaces* **124**, 49–68 (2014).

44. Laster, J. & Silver, D. Heparin-coated catheters and heparin-induced thrombocytopenia. *J. Vasc. Surg.* **7**, 667–672 (1988).

45. Larsson, R., Olsson, P. & Lindahl, U. Inhibition of thrombin on surfaces coated with immobilized heparin and heparin-like polysaccharides: A crucial non-thrombogenic principle. *Thromb. Res.* **19**, 43–54 (1980).

46. Olsson, P., Lagergren, H., Larsson, R. & Rådegran, K. Prevention of Platelet Adhesion and Aggregation by a Glutardialdehyde-Stabilized Heparin Surface. *Thromb. Haemost.* **37**, 274–282 (1977).

47. Krauel, K., Hackbarth, C., Furll, B. & Greinacher, A. Heparin-induced thrombocytopenia: in vitro studies on the interaction of dabigatran, rivaroxaban, and low-sulfated heparin, with platelet factor 4 and anti-PF4/heparin antibodies. *Blood* **119**, 1248–1255 (2012).

48. Bogdan, C. Nitric oxide synthase in innate and adaptive immunity: an update. *Trends Immunol.* **36**, 161–178 (2015).

49. S. Smith, B., Capellato, P., Kelley, S., Gonzalez-Juarrero, M. & C. Popat, K. Reduced in vitro immune response on titania nanotube arrays compared to titanium surface. *Biomater. Sci.* **1**, 322–332 (2013).

50. Fu, J., Ji, J., Yuan, W. & Shen, J. Construction of anti-adhesive and antibacterial multilayer films via layer-by-layer assembly of heparin and chitosan. *Biomaterials* **26**, 6684–6692 (2005).

51. Young, E. The anti-inflammatory effects of heparin and related compounds. *Thromb. Res.* **122**, 743–752 (2008).

52. Ronca, F., Palmieri, L., Panicucci, P. & Ronca, G. Anti-inflammatory activity of chondroitin sulfate. *Osteoarthritis Cartilage* **6**, 14–21 (1998).

53. Fu, J., Ji, J., Fan, D. & Shen, J. Construction of antibacterial multilayer films containing nanosilver via layer-by-layer assembly of heparin and chitosan-silver ions complex. *J. Biomed. Mater. Res. A* **79A**, 665–674 (2006).

54. Jou, C.-H., Lee, J.-S., Chou, W.-L., Yu, D.-G. & Yang, M.-C. Effect of immobilization with chondroitin-6-sulfate and grafting with chitosan on fibroblast and antibacterial activity of polyester fibers. *Polym. Adv. Technol.* **16**, 821–826 (2005).

55. Tsai, G.-J. & Su, W.-H. Antibacterial Activity of Shrimp Chitosan against Escherichia coli. *J. Food Prot.* **62**, 239–243 (1999).

56. Sudarshan, N. R., Hoover, D. G. & Knorr, D. Antibacterial action of chitosan. *Food Biotechnol.* **6**, 257–272 (1992).

57. Liu, X. F., Guan, Y. L., Yang, D. Z., Li, Z. & Yao, K. D. Antibacterial action of chitosan and carboxymethylated chitosan. *J. Appl. Polym. Sci.* **79**, 1324–1335 (2001).

58. Almodóvar, J. *et al.* Chitosan-heparin polyelectrolyte multilayers on cortical bone: Periosteum-mimetic, cytophilic, antibacterial coatings. *Biotechnol. Bioeng.* **110**, 609–618 (2013).

59. Martins, A. F. *et al.* Chitosan/iota-carrageenan and chitosan/pectin polyelectrolyte multilayer scaffolds with antiadhesive and bactericidal properties. *Appl. Surf. Sci.* **502**, 144282 (2020).

60. Neufeld, B. H. & Reynolds, M. M. Critical nitric oxide concentration for Pseudomonas aeruginosa biofilm reduction on polyurethane substrates. *Biointerphases* **11**, 031012 (2016).

61. Neufeld, B. H., Neufeld, M. J., Lutzke, A., Schweickart, S. M. & Reynolds, M. M. Metal-Organic Framework Material Inhibits Biofilm Formation of *Pseudomonas aeruginosa*. *Adv. Funct. Mater.* **27**, 1702255 (2017).

62. Doverspike, J. C. *et al.* Nitric oxide releasing two-part creams containing S-nitrosoglutathione and zinc oxide for potential topical antimicrobial applications. *Nitric Oxide* **90**, 1–9 (2019).

63. Wang, X. *et al.* Nitric oxide-releasing semi-crystalline thermoplastic polymers: preparation, characterization and application to devise anti-inflammatory and bactericidal implants. *Biomater. Sci.* **6**, 3189–3201 (2018).

# CHAPTER 3: ENZYMATIC DEGRADATION OF POLYSACCHARIDE-BASED, PROTEOGLYCAN-MEMETIC MATERIALS IN SOLUTION AND ON POLYELECTROLYTE MULTILAYER SURFACES[1]

## Overview

Proteoglycans (PGs) play many important roles in biology, contributing to the mechanical properties of tissues, helping to organize extracellular matrix components, and participating in signaling mechanisms related to mechanotransduction, cell differentiation, immune responses, and wound healing. Since PGs can play many roles, researchers have created materials that mimic their structure and chemistry for biomedical applications. Our lab has designed two different PG-mimics: polyelectrolyte complex nanoparticles (PCNs) and PG-memetic graft copolymers (GCs) both of which are prepared using naturally occurring glycosaminoglycans (GAGs), but which are held together using different bond types. Polyelectrolyte complex nanoparticles (PCN) are prepared by the electrostatic complexation of oppositely charged polyelectrolytes (using the GAG as the polyanion and chitosan as the polycation). Graft copolymers (GC) are prepared by covalently attaching GAG side chains to a modified hyaluronan core. This work furthers our knowledge of these materials by evaluating their enzymatic stability against hyaluronidases (I-S, IV-S, and II), chondroitinase ABC, and lysozyme when suspended in solution and adsorbed onto surfaces. Hyaluronan- (HA) and chondroitin sulfate- (CS) containing PG-mimics are degraded by the hyaluronidases.

[1]This work was published in *Biomacromolecules* and is reproduced in modified form here with permission [1]. J. Vlcek was responsible for designing experiments, collecting data, data analysis, and preparing the manuscript. M.J. Kipper and M.M. Reynolds conceived the research, advised work, and edited the manuscript.

PCN prepared with CS and GC prepared with HEP are the only CS and HA containing PG-mimics protected from chondroitinase ABC. None of the materials are measurably degraded by lysozyme. Adsorption to polysaccharide-based polyelectrolyte multilayer (PEM) surfaces protects PG-mimics from degradation, compared to when PG-mimics are combined with enzymes in solution; all surfaces are still intact after 21 d of enzyme exposure. The unmodified PEM surfaces results in the most cleavage of the polysaccharides, and the addition of the GCs to the surfaces results in the best protection against enzymatic cleavage. Generally, enzymatic degradation increases the roughness of the surfaces compared to controls, except when CS-containing PG mimics are on the surface. This work provides important information about the durability of PG-mimetic materials, essential for advancing their applications in cardiovascular materials, orthopedic materials, and growth factor delivery applications.

### 3.1. Introduction

Proteoglycans (PGs) are macromolecular glycoconjugates found in nearly every tissue in the body. They consist of a protein core with a varying number of glycosaminoglycan (GAG) side chains.[1–6] Proteoglycans can differ in their protein chain length, the types of GAGs that are bound, and the number of the bound GAGs.[1–7] This versatility of structure and composition enables a variety of important biochemical and biomechanical roles in the human body. For example, aggrecan, a PG with a high density of chondroitin sulfate (CS) side chains, imparts compressive strength to cartilage and lubricates articular cartilage surfaces by its high osmotic pressure and charge density.[8–13] Biglycan, a small leucine-rich PG with only two CS side chains, plays an important role in musculoskeletal development, and acts as a danger signal that initiates inflammatory

responses.[14,15] PGs also have crucial roles in tissue morphogenesis and healing, mechanotransduction, and regulating the structure of extracellular and pericellular matrices; PGs bind many important structural proteins, signaling proteins, and receptors, thereby stabilizing and regulating multiple signaling pathways, and organizing other macromolecular extra cellular matrix (ECM) components. [1–8,10–24]

Due to the variety of functions PGs have in biological systems, they are desirable components to include in biomaterials and therapeutics. The use of natural proteoglycans obtained from tissues for biomedical applications is often not practical, and while recombinant PGs have shown some promise, their applications are limited due to of the difficulty of scaling their production and controlling the GAG sequences.[25] Thus, researchers have created materials that can mimic the properties of PGs. These are referred to in the literature as proteoglycan mimics or neoproteoglycans. The applications of these materials span a broad range of uses, including cartilage therapeutics, ocular therapeutics, drug and growth factor delivery systems, blood contacting surfaces, and tissue engineering applications.[16,25–36]

Researchers have pursued several different approaches to mimicking PG structures and functions. Naturally occurring proteins, such as albumin, or synthetic proteins have been used as core structures to which GAGs can be conjugated.[32,33,37–39] While protein-GAG complexes can mimic the structure of PGs well, they can be associated with cytotoxicity and lack some functions of the core PG proteins they are designed to mimic.[40] Others have designed PG-mimics that simulate the architecture of PGs (a core molecule with GAG side chains) by using materials other than proteins.[26,36,41,42] Prudnikova *et al.* bound chondroitin sulfate onto a poly(acrylic acid)

core, generating molecules that mimic the 3D bottlebrush architecture of aggrecan. They also integrated these mimics into cartilage tissue by injection.[26] Nanoparticles that consist of an outer layer of GAGs may mimic the chemistry and approximate size of PGs, resulting in favorable material properties.[16,31,34,43–47] Polymer-GAG complexes may not have the same chemical composition as PGs, but they can still mimic some key functions of PGs in the ECM.[48–53] Regardless of the approach, all PG mimics should be designed to be biocompatible and effective for their specific application.

Little research has been done on the durability of PG mimics against enzymes. Zhang *et al.* evaluated CS-based PG-mimics ability to protect bovine vitreous from trypsin enzymatic degradation.[33] The durability of the PG-mimics against this enzyme was not directly evaluated.[33] Materials that are designed to be enzyme-responsive have been evaluated against enzymes, but few PG-mimics have been evaluated this way.[54–57] For the first time, this work aims to evaluate the enzymatic stability of PG-mimics designed in our lab against enzymes specific to the constituent polymers, to discover how the PG mimetic architecture affects their stability.

Our lab has previously designed and investigated different PG-mimics which were made using naturally occurring polysaccharides and GAGs. Polyelectrolyte complex nanoparticles (PCN) were made to mimic the relative size and charge of dense PG clusters.[43] Polyelectrolyte complex nanoparticles on surfaces can inhibit bacterial attachment, some immune responses, platelet adhesion, protein attachment and polymerization, and can stabilize and deliver growth factors.[16,34,44,58,59] We have referred to PCN materials as PG-mimics, glycocalyx-mimics, and aggrecan-mimics depending on their intended application.[16,34,43,44,60] These mimics are stabilized through simple

electrostatic interacts between polyanions and polycations, which makes them easy to synthesize, but which does not allow for tunability of specific properties. These particles also cannot be dried under vacuum or stored in solution for long periods of time. Our lab has also developed a family of PG-mimetic graft copolymers (GC) that has tunable graft density and is made from covalent attachments, making it more durable than the PCNs. The PG-memetic GC consist of a high molecular weight hyaluronic acid (HA) core, with heparin (HEP), chondroitin sulfate (CS), dextran, or dextran sulfate side chains.[36,61] These materials have tunable graft density, side chain identity, and molecular weight; they can improve mechanical properties of hydrogels, and can deliver growth factors to cells, in a context that mimics the biological presentation of growth factors by proteoglycans in the pericellular space.[29,36]

Both the PCN and GC PG mimics developed in our lab have favorable properties for a variety of applications. The present work is essential for the further development of applications of these materials. Here, we evaluate the enzymatic degradation of both the PCN and GC PG mimics for the first time. Understanding the enzymatic stability of these materials is essential for designing materials for intermediate to long-term use (weeks to years) as components of tissue engineering scaffolds, cell culture platforms, and drug delivery systems. Biodegradability via biologically relevant enzymes is important for tissue engineering applications and can influence cell material interactions and cytotoxicity. Recently, enzyme-responsive materials have been designed as responsive biomaterials.[54–57,62] These studies could help determine whether our materials could be modified to release therapeutics as enzyme-responsive materials. The enzymes used in this study are also used as therapeutics or in conjunction with therapeutics.

Hyaluronidase is commonly used clinically with fillers and has been used in conjunction with local anesthetics to help integration into the tissue.[63–67] Hyaluronidase has also been evaluated in conjunction with cancer treatments.[68] Chondroitinase ABC is being proposed as a therapeutic in spinal cord injuries as it helps break down excessive scar tissue.[69–72]

In this work, PG-mimetic materials were evaluated against enzymatic degradation using three hyaluronidases, chondroitinase, and lysozyme. Enzymatic degradation was performed in solution over 7 d using a reducing sugar detection assay. PG-mimics were also adsorbed onto the surfaces of PEMs and evaluated against enzymatic degradation for up to 21 d. The amount of reducing sugar ends in solution was evaluated for each time point and the change in surface topography was evaluated at d 0 and 21 using atomic force microscopy (AFM). Understanding the enzymatic durability of these materials will influence the design of PG-mimetic biomaterials for drug delivery, tissue engineering, and other therapeutic applications.

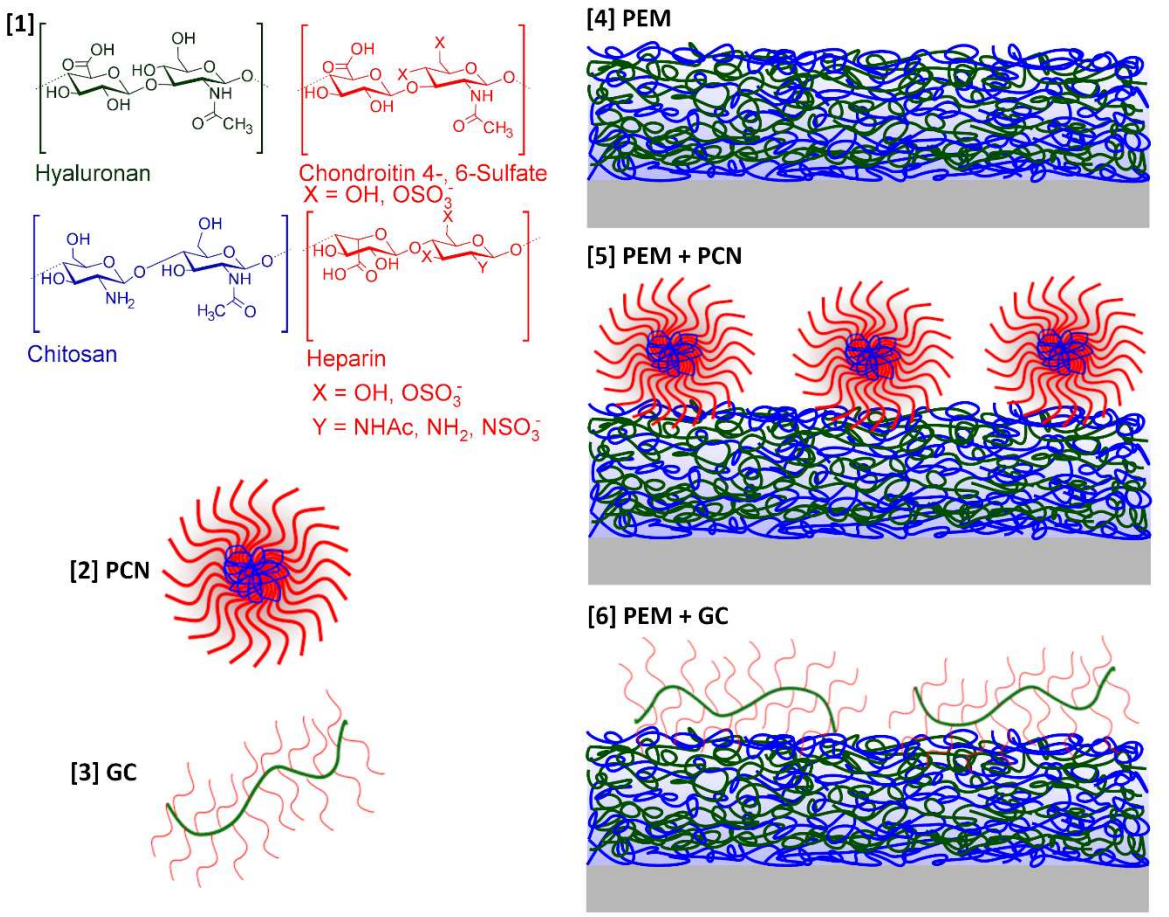


**Figure 3.1:** Schematic of materials used, and the chemistry of the polysaccharides. The figure is color coded with chitosan being blue, hyaluronan being green, and chondroitin sulfate or heparin being red. Figure 3.1.1 the chemistry of the polysaccharides used, the center shows the PCN (1.2) and GC (1.3), and the right shows the PEM structure (1.4), PCN + PEM structure (1.5), and GC + PEM structure (1.6).

## 3.2. Materials and Methods

### 3.2.1. Materials

Chitosan (CHI) was purchased from MP Biomedicals. Chondroitin sulfate sodium (CS) salt (from shark cartilage, 6% sulfur, 6-sulfate/4-sulfate = 1.24, Mw = 84.3 kDa), hyaluronan (HA) sodium salt (Mw = $1.5\times10^3$ kDa), cysteamine hydrochloride, tris(2-carboxyethyl) phosphine hydrochloride (TCEP), (2-(*N*-morpholino)ethanesulfonic acid

(MES), *N*,*N*-dimethylformamide (DMF), chondroitinase ABC (from *Proteus vulgaris*), hyaluronidase (I-S, IV-S, and II) (from bovine testes), and sodium acetate were all purchased from Sigma Aldrich. *N*-(3-dimethylaminopropyl)-*N'*-ethylcarbodiimide hydrochloride (EDC), *N*-hydroxysuccinimide (NHS), *N*- [β-maleimidopropionic acid] hydrazide trifluoroacetic acid salt (BMPH), and Zeta desalting columns (7k MWCO) were all supplied via Thermo Fisher. Sodium triacetoxyborohydride (STAB) and lysozyme (from chicken egg white) was purchased from Alfa Aesar. Acetic acid was purchased from Acros, and heparin sodium (HEP) (from porcine intestinal mucosa, 12.5% sulfur) was purchased from Celsus Laboratories.

### 3.2.2. Preparation of graft copolymer (GC) proteoglycan mimics

PG-mimetic graft copolymers are composed of an HA backbone with pendent functional groups that are reacted with the reducing end of GAGs (HEP or CS) to covalently graft side chains. Details of the copolymer synthesis are provided in previous work from our group.[36,61] Briefly, the synthesis is divided into three separate steps: HA backbone thiolation, backbone hydrazide activation, and coupling via reductive amination. During thiolation, HA (250 mg) was mixed with EDC (645 mg) and NHS (976 mg) in MES buffer (50 mL, pH 6.0) to activate the carboxylate functional group on the HA. After the pH of the solution was raised to 7.2, cysteamine hydrochloride (880 mg) was added to the reaction mixture and bound to the activated HA. The thiolated HA (HA-SH) product was then purified and lyophilized. The second step of the synthesis process starts by combining HA-SH (100 mg) with TCEP (114 mg) in PBS (50 mL, pH 8.0) to reduce any disulfide bonds that may have formed between thiol groups. Desalting columns were used to change the buffer (from PBS pH 8 to PBS pH 7.2). Then BMPH (80 mg) was

added to the solution, and the HA-BMPH intermediate was purified and lyophilized. To attach GAG side chains (in this work the GAGs CS and HEP are used), HA-BMPH (15 mg) and HEP (170 mg) or CS 1000 mg) were dissolved together in a DMF (10 mL) and acetic acid (0.35 mL) solution at a 1:1 molar ratio of each thiolated side chain on the HA backbone to CS or HEP. A reducing agent, STAB (1000 mg), was also dissolved in DMF (10 mL) in a separate round-bottom flask. Both vessels were purged with nitrogen and sealed. The HA-BMPH and GAG solution was slowly heated to 85 °C, then 350 uL of the reducing agent solution was added. The reducing agent solution was added 4 more times over the course of 8 hours. This reaction was allowed to proceed overnight, after which the DMF was pulled off using a Schlenk line with a solvent trap and the dried material was dissolved in de-ionized water. The product was then purified and lyophilized. The final product PG mimics were then stored at 4 °C.

### 3.2.3. Preparation of polyelectrolyte complex nanoparticle (PCN) PG mimics

Polyelectrolyte complex nanoparticles (PCN) were prepared as previously described.[16,43,44,60] Briefly, CHI (1mg/mL), HEP (1.5mg/mL), and CS (2.8 mg/mL) solutions were prepared in an acetate buffer solution (0.2 M sodium acetate and acetic acid at pH 5.0). Solutions were filtered using 0.22 μm PDVF syringe filters. The PCN solutions were prepared by adding 36 mL CS or 24 mL HEP solutions to 6 mL CHI solutions while stirring at 1000 rpm. Stirring speed was decreased to 700 rpm, and after 3 h of stirring all solutions settled overnight.

### 3.2.4. Preparation of PEMs and PG mimic (both GC and PCN) adsorption on surfaces

Each PG mimic (GC or PCN) was dissolved in acetate buffer solution (0.2 M sodium acetate and acetic acid at pH 5.0) for at least 3 h at 1 mg/mL. The solutions were then moved to conical tubes and allowed to settle overnight before use.

PEMs were prepared as previously described.[43,44] Briefly, chitosan (CHI) (1 mg/mL) and HA (0.5 mg/mL) solutions were prepared with acetate buffer (0.2 sodium acetate and acetic acid at pH 5.0). Solutions were stirred for at least 2 h at room temperature and were then filtered through 2.0 um PDVF syringe filters. Glass surfaces that were cleaned and then oxidized with oxygen plasma for 8 min (PlasmaTech model PE-25) were used as substrates for PEM deposition. The PEMs were constructed by alternating layers of a polyanion (HA) and polycation (CHI) with 3-min acetic acid rinse (pH 4.0; de-ionized water acidified with acetic acid) between adsorption steps (5 min). This procedure was repeated until a 15-layer, chitosan-terminated PEM, or a 14-layer hyaluronic acid-terminated PEM (PEM HA) was produced. After a 15-layer, chitosan-terminated PEM was deposited, a solution containing a PG mimic, HA-CS GC, HA-HEP GC, CHI-HEP PCN, or CHI-CS PCN) was adsorbed. The solution containing the PG mimic was added to the PEM for 4 min followed by a 3-min rinse. This was repeated three times and the samples were washed with a final 30 s de-ionized water rinse step.

### 3.2.5. PG-mimic characterization by NMR and DLS

Each synthesis step for the GC materials was analyzed by proton nuclear magnetic resonance on an Agilent (Varian) 400MR. Samples were dissolved in $D_2O$ at

concentrations of 2 to 5 mg/mL. Spectra were collected using >64 scans, with 5 s relaxation time, at 25 °C.

A Zetasizer Nano ZS (Malvern) was used to measure the hydrodynamic diameter and zeta potential of PG mimics using 633-nm laser. GC samples were dissolved in PBS at 5 mg/mL. PCN samples were suspended in sodium acetate buffer and collected right after preparation. Measurements were performed at 25 °C with a fixed angle of 90° for hydrodynamic diameter, and zeta potential. Three measurements were made on each sample, and this was repeated three times. Values are reported as average ± standard deviation.

### 3.2.6. Enzyme Degradation

PG-mimetic PCN and GC were tested against enzymatic degradation when adsorbed onto PEM surfaces and when suspended in solution. GCs, along with controls (unmodified polysaccharides), were prepared at concentrations of 5 mg/mL in PBS pH 5.3 for hyaluronidase experiments and in PBS pH 7.4 for lysozyme and chondroitinase ABC experiments. PCN solutions were kept in acetic acid buffer as they could not be resuspended in another solution. The concentration of PCN used was calculated from the dry mass of the remaining solution subtracted from the original mass of all the dry components. To compare values between GC and PCN samples all values were normalized by the mass of the material, and an additional study was conducted to determine how the enzymes preformed in the acetic acid buffer, compared to the recommended solutions. The PCN data was then normalized further to correct for the difference in enzyme efficiency in the acetic acid buffer.

Each sample was exposed to enzymes (lysozyme, chondroitinase ABC, hyaluronidase I-S, hyaluronidase IV-S, and hyaluronidase II) for 0.25, 1, 2, and 7 d when suspended in solution, and 7, 14, and 21 d when adsorbed onto surfaces. Hyaluronidases were diluted to the concentrations recommended by the supplier (Sigma, 15 units/mL) in a solution of 20 mM sodium phosphate, 77 mM sodium chloride, and 0.01% BSA at pH 7. Lysozyme solutions were diluted in PBS pH 7.4 at 15 units/mL to match the concentration of hyaluronidases and 150 units/mL to match relative concentrations of the enzyme in human plasma.[73] Chondroitinase ABC was dissolved in a 50 mM Tris (pH 8), 60 mM sodium acetate, and 0.02% BSA solution at a concentration of 0.75 units/mL. The enzyme solutions were combined in a 1:1 mixture with suspended samples or were added directly to surfaces. The samples were incubated at 37 °C. Samples were made prepared in five experimental replicates ($n$ = 5) for studies in solution. At each time point two measurements were taken for each sample (2 technical replicates). The technical replicates were averaged together to give the value of the experimental replicates and values for samples were reported as the average of experimental replicates ± the standard deviation of the experimental replicates. Surface studies were conducted on 50 mm diameter petri dishes. There was one control and one treated surface per sample type. For each time point solutions were collected and three measurements were made per sample; these values were averaged together and reported (as mean ± standard deviation). The entire experiments for hyaluronidase in solution studies were repeated at least twice for control samples. Lysozyme and surface studies were repeated twice for all samples, and the chondroitinase study was repeated only once because of the availability

of the enzyme. Experimental replicates had differences between samples, but the overall trend was preserved between replicates.

### 3.2.7. Reducing Sugar Assay

Reducing sugar ends are produced by the cleavage of glycosidic bonds between subunits of the GAGs by the enzymes. The degree of degradation of the samples was quantified as the amount of reducing sugar ends in solution using a para-hydroxybenzoic acid hydrazide (pHBH) assay. The pHBH reacts with hemiacetal groups in solution, opening the sugar ring forming an osazone, which has a yellow color. This assay has been described previously.[74] Briefly, a 2 M sodium hydroxide solution, and a 2% (w/v) para hydroxybenzoic acid hydrazide solution in 0.5 M hydrochloric acid were prepared. Once these solutions were fully dissolved, they were combined in a 1:1 ratio, making the detection solution. In a 96-well polymerase chain reaction (PCR) plate, 40 µl of sample was combined with 120 µl of the detection solution. The mixture was then heated at 65 °C for 15 min in a water bath, and subsequently cooled on ice. The solution was then transferred to a 96-well, clear-bottom plate. The absorbance in each well was measured using at 410 nm. Glucose equivalent values were calculated from the measured absorbances using a standard curve.

### 3.2.8. Atomic force microscopy (AFM)

Atomic force microscopy was used to evaluate the topography of PEM PG mimic surfaces. This method was also used to evaluate and topographical changes to the surfaces after incubation with the enzymes. Imaging was performed on the surfaces prepared on glass-bottom petri dishes (Ted Pella #14036), using a Bruker Bioscope

Resolve atomic force microscope. All surfaces were submerged in DI water at room temperature for AFM imaging. The ScanAsyst mode was used, with a triangular silicon tip on a nitride cantilever with a nominal tip radius of 2 nm, a spring constant of 0.12 N/m, and a gold-coated reflective back side (SNL-10 B, Bruker). Surface imaging was conducted in the peak force tapping mode, with the peak force set point near 2 nN (optimized using NanoScope software). The scan rate was set to 1 Hz with a peak force tapping frequency of 1-2 kHz. Representative images were taken at 5 μm × 5 μm areas on each sample. Six images were obtained per sample on 2 distinct areas (3 images per area). Image analysis was preformed using NanoScope Analysis version 1.8. The roughness values were for the 6 images ($n = 6$) were averaged together and values were reported (mean ± standard deviation). Representative images are reported.

### 3.2.9. Statistical analysis

Peak fitting analysis was conducted on NMR data sets using Igor software. Statistical analysis was performed on reducing sugar, and AFM roughness data sets using R (version 3.6.1). A repeated measures one-way ANOVAs with pairwise comparisons were performed on in solution enzyme studies were measurements were made from the same samples over different time points. Samples were compared over all time points instead of being compared at each time point separately. A one-way ANOVA with post hoc Tukey test was performed on data from surface studies (both reducing sugar data and Rq and Ra values).

## 3.3. Results

### 3.3.1. Enzymatic degradation in solution

Enzymatic stability of PG-mimics was evaluated against three different hyaluronidases, chondroitinase ABC, and lysozyme at two different concentrations. Hyaluronidase and chondroitinase ABC were chosen because of their specificity to the GAGs in the PG mimics, and because these enzymes have therapeutic uses or are used in conjunction with therapeutics.[63–72,75–78] Lysozyme is found in most bodily fluids, functions as a bactericidal agent, and is a part of the innate immune system.[73,79] Lysozyme studies were conducted at two different concentrations: 15 U/mL (to match concentrations of hyaluronidases) and 150 U/mL (within the range of lysozyme found in plasma).[73,79] Enzymatic degradation of PG mimics and control GAGs in solution was evaluated at four time points: 0.25, 1, 2, and 7 days.

The enzymatic susceptibility of the GAGs and PG mimics with respect to each enzyme evaluated is summarized in Table 3.1. The kinetics of degradation is shown in Figures 3.2 and 3.3.

**Table 3.1.** Enzymatic susceptibility of each GAG and PG mimic to each of the enzymes studied.

| | ***Hyaluronidases*** | | | ***Chondroitinase ABC*** | ***Lysozyme*** |
|---|---|---|---|---|---|
| ***GAG or PG mimic*** | ***IV-S*** | ***I-S*** | ***II*** | | |
| **GAGs** | | | | | |
| CS | ++ | ++ | ++ | +++ | − |
| HEP | − | − | − | − | − |
| HA | +++ | +++ | ++ | +++ | − |
| **PG mimics** | | | | | |
| GC CS | + | ++ | + | +++ | - |
| GC HEP | + | + | + | − | - |
| PCN CS | +++ | + | +++ | − | - |
| PCN HEP | − | − | − | − | _-_ |

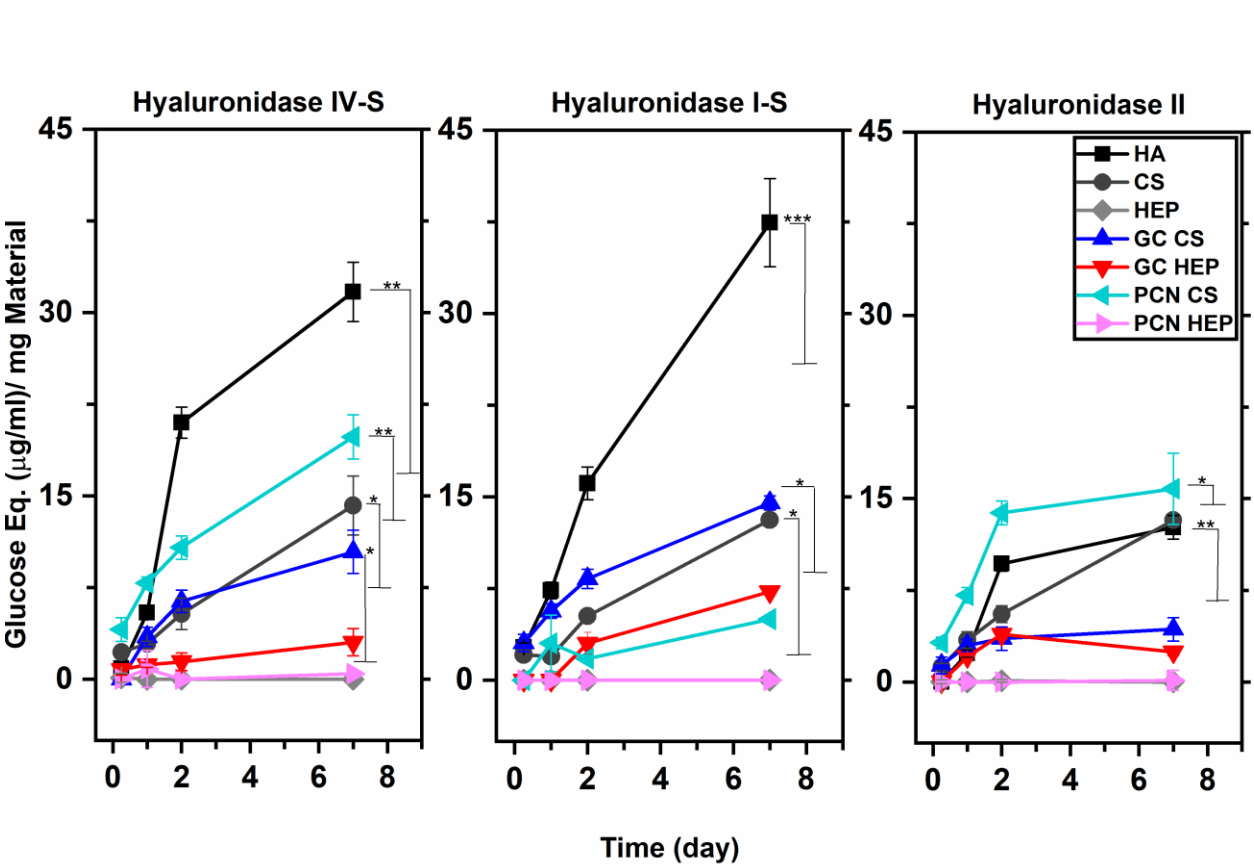


**Figure 3.2.** Relative enzymatic degradation of HA, CS, and HEP controls, and PG mimics when exposed to different hyaluronidases. Values are converted to glucose equivalent and normalized to mass of material in solution (mean ± standard deviation) ($n$ = 3 for CS and HEP, $n$ = 5 for all other samples). Data for PCN samples were further normalized to correct for the difference in the efficiency of each enzyme dissolved in acetic acid solution as compared to PBS. Greater glucose equivalent value corresponds to more reducing sugar ends in solutions, which means the material has been cleaved by the enzymes. A one-way repeated-measures ANOVA with a pairwise comparisons was conducted to determine differences between samples. Asterisks indicate the greatest significance value between one sample and all the samples below (* $p$<0.05, ** $p$<0.005, *** $p$<0.0005). For exact $p$-values between sample types, refer to the supplementary information.

Figure 3.2 depicts the enzymatic degradation of PG-mimics and controls in solution with hyaluronidase I-S, hyaluronidase II, and hyaluronidase IV-S. The relative degradation of HA between the hyaluronidases matches what is already known about their types. Hyaluronidases type I, and type IV have stronger enzymatic activity than

hyaluronidase type II.[65] Additionally, hyaluronidase type II only acts on long-chain HA, so it would lose enzymatic activity after the polysaccharides reach a reduced length.[65] For all three hyaluronidase enzymes no reactivity towards heparin is observed. The enzymes do act on CS and HA. For hyaluronidase IV-S and I-S, HA is degraded more than unmodified CS. Hyaluronidase II degrades unmodified HA and CS with similar effectiveness. HA is composed of 4-linked β-D-glucuronic acid and 3-linked *N*-acetyl α-galactosamine units. CS consists of alternating 3-linked *N*-acetyl α-galactosamine units and 4-linked β-D-glucuronic with sulfated groups, while heparin consists of alternating 4-linked uronic acid and 4-linked α-glucosamine with α-L-iduronic acid (IdoA) as its major uronic acid type component.[80] Chitosan used in the PCNs is a copolymer of β-1,4-linked *N*-acetyl-D-glucosamine and D-glucosamine. The mammalian hyaluronidases used in this study are endo-β-*N*-acetylhexosaminidases that break down β-1,4 glycosidic linkages.[65] The presence of 4-linked β-D-glucuronic acid in CS explains why the hyaluronidases used are able to act on both HA and CS. The ability of hyaluronidases to act on CS is well documented.[63,77,81] Heparin does not have similar repeating units to HA so the hyaluronidases do not act on it.

PCN CS samples are more easily degraded by the hyaluronidase type II and IV-S enzymes, than GC CS samples, and the opposite is true for type I-S samples. The PCN are not as stable as the GC materials. The PCN are formed from electrostatic interactions and the GC consist of covalently bound GAGs. This may explain why the PCN CS samples are degraded more efficiently than GC CS samples for hyaluronidase II and IV-S. Since the PCNs are not as stable, they are more available functional groups to the enzymes in solution, and not reduced steric hinderance. This is not observed for

hyaluronidase I-S. We observe that hyaluronidase I-S favors HA more than CS. This may explain the observed difference between GC CS and PCN CS stability when exposed to hyaluronidase I-S. While GC CS contains an HA backbone PCN CS contains no HA. The presence of HA in the GC CS combined with the higher activity of hyaluronidase I-S towards HA results in higher glucose equivalent values as compared to PCN CS. It is also important to note that most of the mass of GC samples is CS and not HA (HA/CS – 15 mg/1000 mg; HA/HEP -15 mg/170 mg).[61]

The enzymatic activity toward PCN HEP is consistent with unmodified heparin and no cleavage is observed when exposed to the hyaluronidases. The GC HEP does however exhibit a small amount of degradation. GC HEP are the only heparin-containing samples to have any observable change in the presence of the enzymes. The observed activity is likely due to the presence of the HA backbone in the GC HEP.

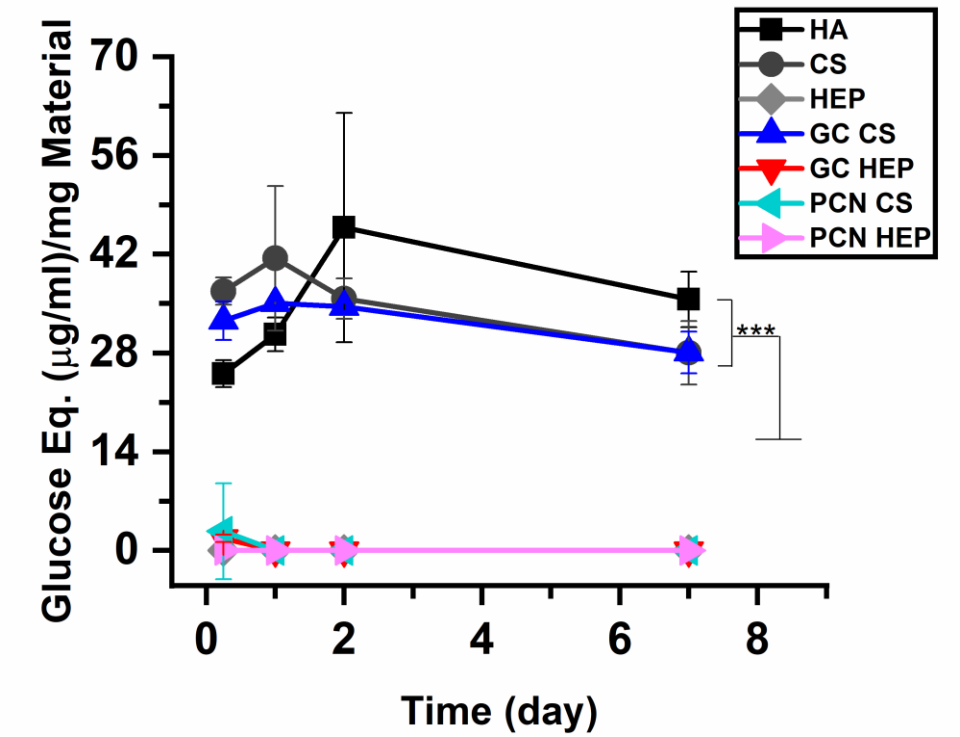


**Figure 3.3.** Relative enzymatic degradation of HA, CS, and HEP controls, and PG mimics when exposed to chondroitinase ABC. Values are converted to glucose equivalent (μg/mL) and normalized to mass of material in solution ($n$ = 3) (mean ± standard deviation). A one-way repeated-measures ANOVA with pairwise comparisons was conducted to determine differences between samples. Statistically significant differences are indicated by stars (* $p < 0.05$, ** $p < 0.005$, *** $p < 0.0005$).

Chondroitinase ABC is the most active enzyme used in our studies (Figure 3.3). After only 6 hours the concentration of reducing sugar ends available in solution is comparable to that of hyaluronidase-treated samples after 7 days. The quantity of reducing sugar ends in solution peaked around 24-48 h, and then decreased by day 7. As the glycosidic bonds in the GAGs are cleaved, reducing sugar ends (hemiacetal groups) are free in solution. These groups on the sugar can exist in an open form (even though it is not favorable). The aldehyde group on the open sugar can react with the water, making it unable to react with the pHBH in the detection assay after some time. Additionally, chondroitinase loses most of its enzymatic activity after 72 hours in solution

leading, to no new reducing sugar ends being introduced.[82] These factors may help explain the reduction of glucose equivalent from 2 to 7 days.

CS, HA, and GC CS samples all have similar enzymatic degradation when exposed to chondroitinase. Hyaluronic acid can be cleaved by chondroitinase ABC due to its similarities to CS, as described above. The lack of enzymatic degradation of heparin-containing samples can also be explained from the differences in structure between heparin and CS/HA as explained for hyaluronidase results. Unlike the results of the hyaluronidase experiments, there is no enzymatic degradation of PCN CS or GC HEP samples. Both PCN CS and GC HEP sample groups contain either HA or CS which should have been degraded by the enzyme. These samples do contain materials that do not react with chondroitinase ABC: heparin, and chitosan. The addition of these materials may have inhibited the enzyme activity. The GCs consist of an HA core with sidechains of HEP or CS grafted on. The overall mass of the GCs is mostly attributed to HEP (91.8%) or CS (98.5%).[61] The hyaluronic acid core of the GC HEP samples may be protected from chondroitinase ABC by the heparin side chains. PCN samples consist of a CS- or HEP-rich outer corona and a chitosan-rich core. The PCN samples should also contain an abundance of CS or HEP. Unlike the GC HEP samples, the PCN CS samples have CS more available to the enzymes on the outer corona of the PG-mimic. The chitosan-rich inner core may still inhibit the enzymatic degradation of the PCNs. This may be due to several reasons: the clustering of the CS on the PCN CS outer corona is too dense for the enzyme active site to interact with the glycosidic bonds of the CS; chitosan is not only confined to the core of the PCNs and may help block enzymatic cleavage of CS in the corona; or the hydrophobicity of chitosan may inhibit the enzyme interaction with the

PCNs. Chondroitinase ABC used in this study is larger (120 kDa) than the hyaluronidase enzymes (45-89 kDa).[63,81] The close association of CS and CHI in PCN CS samples, and HEP protecting the HA in GC HEP samples may explain the differences between hyaluronidase and chondroitinase results due to their size differences.

All the GAGs and PG mimics are resistant to enzymatic degradation by lysozyme at both concentrations tested (Figure 3.S2). There is a small change in absorbance from the pHBH assay for some sample types, but these values are close to the limit of detection (200-300 nmol).[74] Lysozymes are polycationic proteins that hydrolyze *N*-acetylglucosaminyl-*N*-acetylmuramic acid linkages.[73,79] None of the GAGs used contain *N*-acetylmuramic acid monomers, thus the lack of enzymatic activity on these materials is expected. The lack of enzymatic degradation by lysozyme would allow these materials to stay intact in the body when exposed to this innate immune system defense.

Figure 3.4 illustrates how the structure and composition of the PG mimics impacts their enzymatic degradation. PG mimics in these studies are hydrolyzed when exposed to enzymes that are specific to the GAGs they are composed of, if the enzymes are <120 kDa. The PG mimics are enzymatically degradable and degraded similarly to the unmodified GAGs. The hyaluronidase enzymes degrade CS and HA, but not HEP. Furthermore, the hyaluronidases are small. Therefore, they are able to degrade the hyaluronan backbone of both the GC CS and GC HEP PG mimics. However, they do not degrade the PCN HEP. In contrast, chondroitinase ABC is a much larger enzyme. Although it is capable of degrading both CS and HA in solution, it cannot degrade the PCN CS. This may be due to steric hinderance in the closely packed PCNs. The chondroitinase can degrade the CS in the side chains of the GC CS, but not the HA

backbone. HEP and both types of HEP-containing PG mimics are protected from degradation by chondroitinase ABC. The CS-containing mimics could be used in conjunction with hyaluronidases as a targeted drug delivery system, similar to previously described materials.[54,56,62] Enzymes that were specific to heparin were not used in these studies, but from our results we can infer that as long as the heparinases are relatively small, the HEP-containing PG mimics would be degraded by them. Further studies will need to be conducted to further evaluate these interactions.

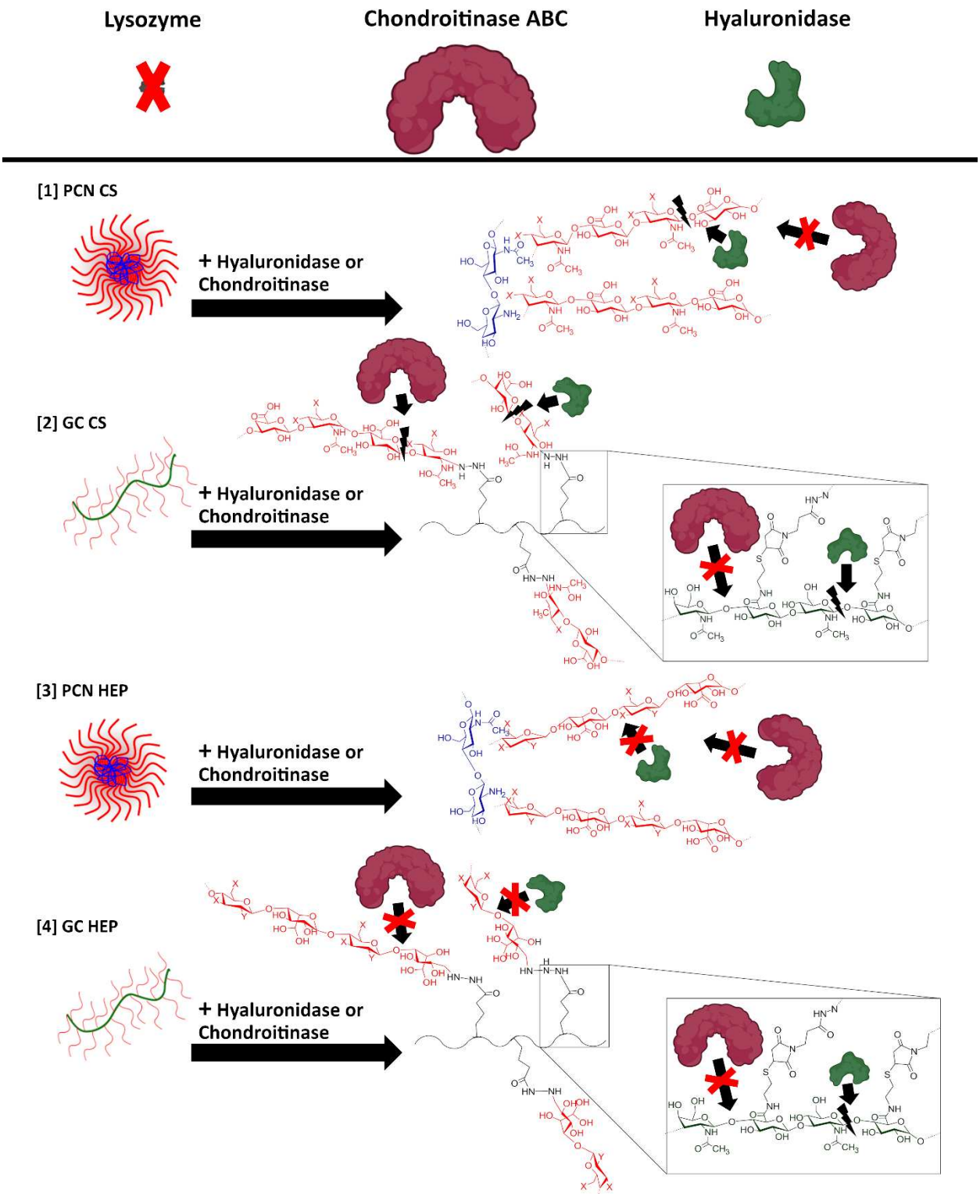


**Figure 3.4.** Schematic showing the enzymatic degradation of [1] PCN CS, [2] GC CS, [3] PCN HEP, and [4] GC HEP in solution. Lysozyme is denoted with a "X" through it because it did not act on any of the controls or PG mimics studied. Arrows with an X

represent no detectable enzymatic activity and arrows with blots represent breakage of glycosidic bonds on the GAGs.

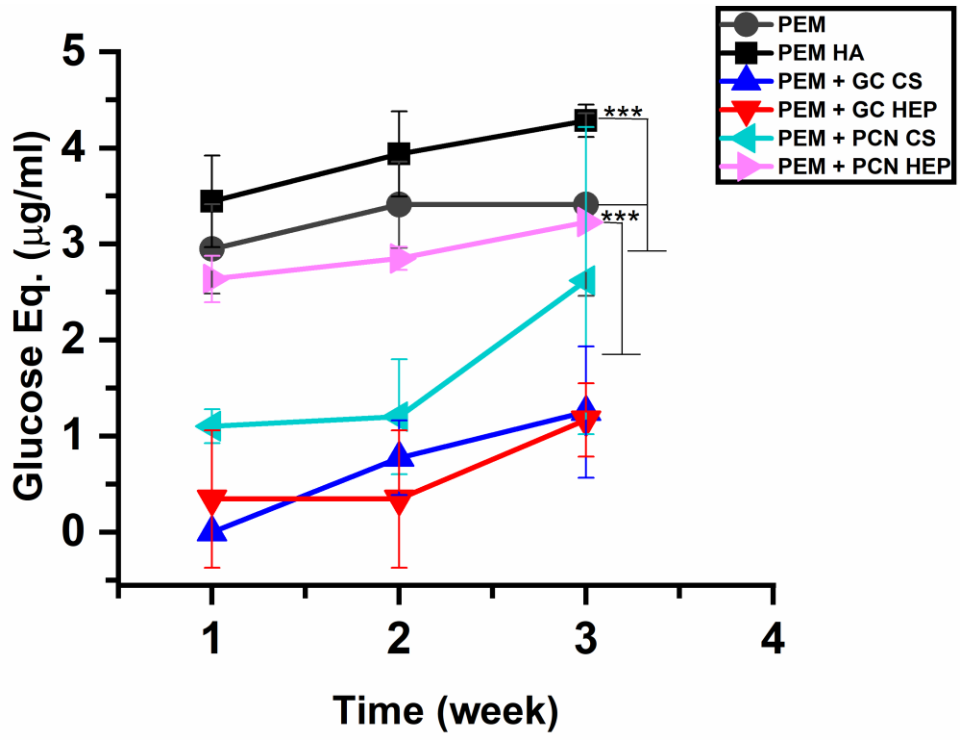


**Figure 3.5.** Relative enzymatic degradation of HA, CS, and HEP controls, and PG mimics on surfaces when exposed to hyaluronidase I-S. Values are converted to glucose equivalent (μg/mL) and normalized to mass of material in solution ($n$ = 3) (mean ± standard deviation). A one-way repeated-measures ANOVA with pairwise comparisons was conducted to determine differences between samples. Statistically significant differences are indicated by stars (* $p < 0.05$, ** $p < 0.005$, *** $p < 0.0005$).

### 3.3.2. Enzymatic degradation of surfaces

In addition to evaluating the PG mimics in solution, we evaluated them adsorbed onto PEM surfaces along with unmodified PEM surfaces. The enzymatic degradation of the surfaces is evaluated with hyaluronidase I-S only. This enzyme is chosen because hyaluronidase I is the most common hyaluronidase found in plasma.[65] Lysozyme was not used as this enzyme did not act on any of the GAGs or mimics evaluated, and

chondroitinase ABC was not used due to its short viability in solution.[82] Surfaces were evaluated against enzymatic degradation for 21 d, with enzyme solutions changed and collected every 7 d. The concentration of reducing sugar ends in solution was evaluated at 7, 14, and 21 d. Atomic force microscopy images were taken at day 0 and 21 d, and roughness measurements of the surfaces are compared across time and between enzyme-exposed and control samples.

The concentration of reducing sugar ends in solution is much lower for surface studies than studies conducted in solution. This is partially due to there being much less material available for the enzyme to act on. For solution studies, GAGs and mimics are dissolved at a concentration of 5 mg/mL, whereas the PEMs are only a few nm thick, containing only ng or μg quantities of material. Furthermore, in the PEM samples, the GAGs are confined to a surface and are not free in solution, reducing their availability for enzymatic cleavage. PEM surfaces terminated in HA (PEM HA) and CHI (PEM) show the greatest degradation due to exposure to the enzyme. This is followed by PCN-terminated surfaces. The GC-terminated PEMs have the least glucose equivalent in solution after 21 d of enzyme exposure (Figure 3.5).

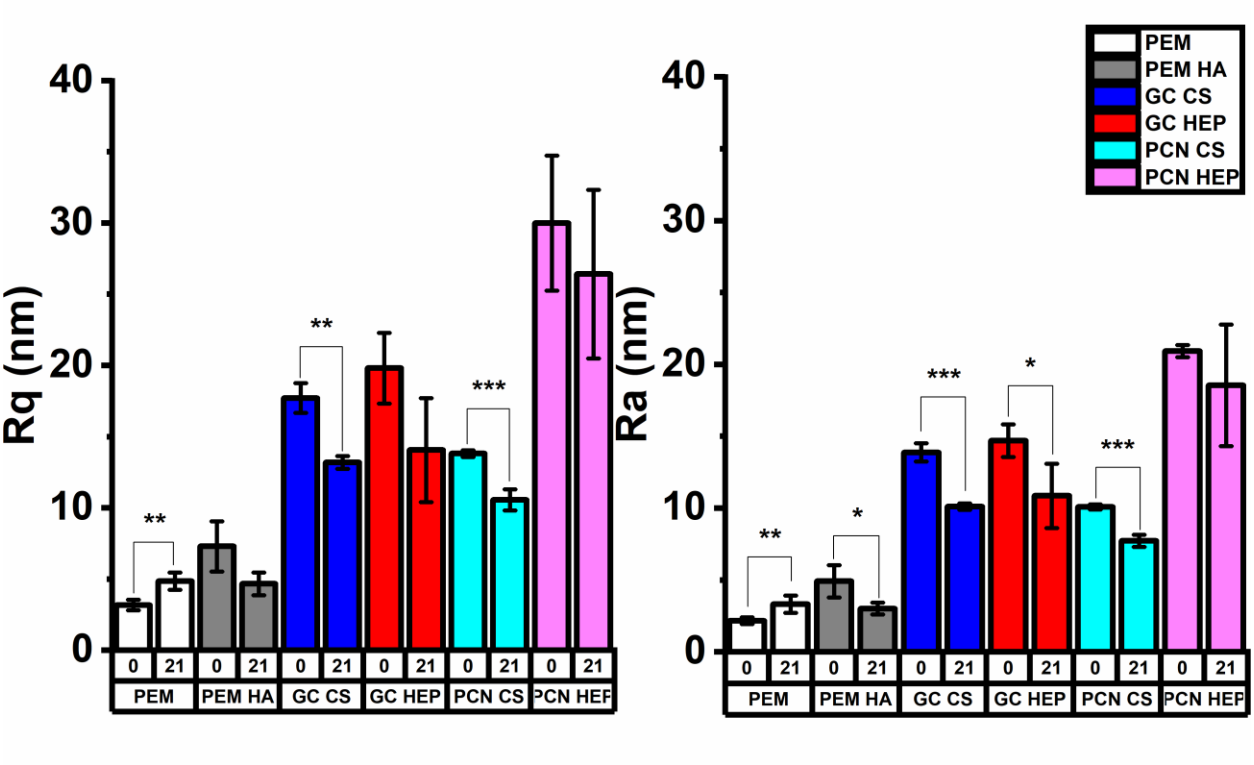


**Figure 3.6.** Roughness values for surfaces treated with hyaluronidase I-S for day 0 and 21 ($n$ = 6) (mean ± standard deviation). Paired $t$-tests were conducted to determine the change in samples before and after enzyme exposure. Statistically significant differences are indicated by stars (* $p < 0.05$, ** $p < 0.005$, *** $p < 0.0005$).

Atomic force microscopy images revealed that all surfaces (apart from PEM + enzyme), exposed to enzyme or not, become smoother (or have reduced roughness) after 21 d. This is visually apparent from AFM imaging (Figure 3.8) and quantifiable from Rq ($R_q = \sqrt{\frac{\Sigma_i (z_i - z)^2}{N}}$) and Ra ($R_a = \frac{1}{N}\sum_{i=1}^{N} |z_i - z|$) values (Figure 3.6, Figure 3.7 and 3.S3). The smoothing of all surfaces is due to the surfaces annealing in aqueous solution. When soaking in solution the GAGs in the PEMs have more mobility, allowing them to encounter opposing charges forming hydrogen and ionic bonds. These forces will cause surface layers to pull closer together resulting in a smoother surface.

Changes in surface roughness were analyzed at day 0 and day 21 for enzyme-exposed and control surfaces. For enzyme-exposed surfaces, there is only significant change in Rq between 0 and 21 days for PEM, PEM + GC CS, and PEM + PCN CS. All enzyme-exposed samples except for the PEM + PCN HEP have significantly different Ra values. All control surfaces (not exposed to enzymes), except for th PEM + PCN CS samples, show significant reduction in Ra and Rq values from day 0 to day 21. To further evaluate the change in surface roughness due to enzymatic exposure, change in roughness values were calculated (day 0 roughness values – day 21 roughness values) for all sample types. Change in roughness values are used to compare differences between enzyme and control surfaces. Exposure to enzymes significantly reduces the smoothing of PEM HA, and PEM + GC HEP surfaces, and increase the roughness of PEM surfaces. Both CS PG mimic-terminated surfaces show a significant increase in surface smoothing when enzymes are added to the surfaces. PCN HEP surfaces do not have a significant change in surface roughness, but the addition of the enzyme does seem to decrease surface smoothing.

Surfaces without PG mimics on them have the greatest amount of enzymatic degradation according to the pHBH assay results (Figure 3.5). These surfaces also have significant change in roughness between enzyme-treated and control groups (Figure 3.6 and 3.7). The lack of mimics on the surfaces may enable the enzymes to interact with HA in the PEMs more freely. The addition of mimics to the surface may cause some crowding that inhibits the enzymes. Hyaluronidase I-S seems to degrade HA more efficiently than CS, which also helps explain why CS-terminated PEMs result in lower glucose equivalent values (Figure 3.2 and 3.5). Roughness increases in only the PEM surfaces (Figure 3.7

and 3.8). These surfaces are terminated with a layer of chitosan instead of HA. The GAGs in the PEMs are not confined to any specific layer. Even though PEM samples are terminated with chitosan, the PEMs are not completely stratified, and HA is still exposed to the surface. The hyaluronidase in solution encounters exposed HA on the surface and degrades it. This results in an increase in surface roughness, as exposed HA regions degrade, while the surface-exposed chitosan-rich areas remain unchanged. Enzyme exposure to HA-terminated PEMs significantly reduces smoothing of the surfaces for a similar reason. The top surface of PEM HA samples may have patches of exposed chitosan. While the HA on the surface is degraded by the enzyme, surface chitosan is unchanged, introducing more roughness to the surface. This addition of roughness is not great enough to counteract the overall smoothing of the surface that occurs due to annealing, so there was still a net reduction in roughness from day 0 to 21.

PCN HEP surfaces show a higher amount of glucose equivalent in solution than GC HEP-terminated PEM surfaces. PCN HEP surfaces do not have any significant change in roughness due to enzyme exposure, but there is a trend of reduced smoothing for these surfaces, compared to controls with no enzyme exposure (Figure 3.6 and 3.7). The reduction of smoothing is significant for PG HEP terminated surfaces. The heparin in the PCNs or GCs themselves will not be affected by hyaluronidase exposure. Thus, all reducing sugar ends in solution are a result of enzymatic degradation of the HA in the PEM layers or core of GCs. For this reason, there would be an introduction of roughness to the HEP-containing surfaces. The exteriors of the PCN or GC HEP on the surface would not be affected by the enzymes. Enzymes would have to encounter the HA in the

PEM surface between PCNs and GCs. This would introduce more roughness by creating larger dips between the underlying PEM and the PG mimics adsorbed onto them.

Enzyme exposure to CS-terminated surfaces increases smoothing of the surfaces. As shown in Figure 3.2, hyaluronidases degrade both HA and CS. The CS-containing PG mimics are more available to the hyaluronidase for degradation than the HA in the PEM layers. The enzyme would then degrade the more available CS more often, smoothing the surface of the PCNs and GCs. This adds to the overall smoothing of the surface.

From pHBH assay results, the addition of GC to surfaces reduces enzyme activity more than the addition of PCN to surfaces. The GC protect the PEM surface from degradation more effectively than the PCN. This may be due to increased surface adsorption of the GC compared to the PCN. From AFM images, it does appear that the GC CS samples cover the surface more efficiently than PCN CS, but this is not visually apparent for HEP surfaces (Figure 3.8). The GC consist only of hydrophilic polyanions (HEP or CS and a core molecule of HA) while the PCNs have a core of a hydrophobic polycation (CHI). The zeta potential values of the PG mimics and PCNs are similar (Table 3.S1). The GC do have a larger hydrodynamic diameter than PCN particles (GC CS: 302 ± 5; GC HEP: 367 ± 3 vs. PCN CS:248 ± 2; PCN HEP: 284 ± 4) (Table 3.S1), which may influence the difference between these two sample types. After 21 days of enzyme exposure all surfaces are not fully degraded, and only small changes are observed in surface roughness. These surfaces will be desirable for long term surface/modification and tissue engineering applications.

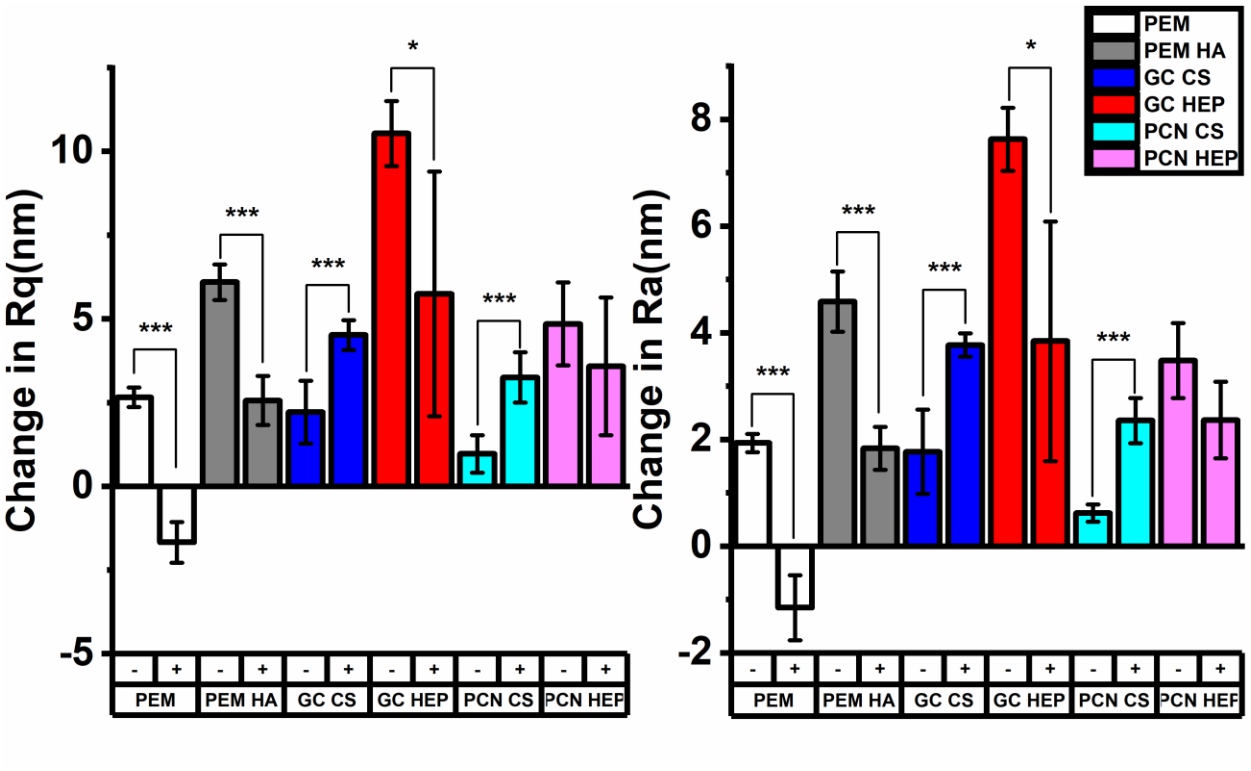


**Figure 3.7.** Change in Rq (nm) (right) and Ra (nm) (left) from day 0 to day 21 for samples exposed to diluent (-) and enzyme (+) solutions ($n$ = 6) (mean ± standard deviation). A negative value indicates an increase in roughness on samples surfaces where a positive value indicates a decrease in overall roughness. Unpaired $t$-tests were conducted to determine the differences between non-enzyme-treated samples and enzyme-treated samples. Statistically significant differences are indicated by stars (* $p < 0.05$, ** $p < 0.005$, *** $p < 0.0005$).

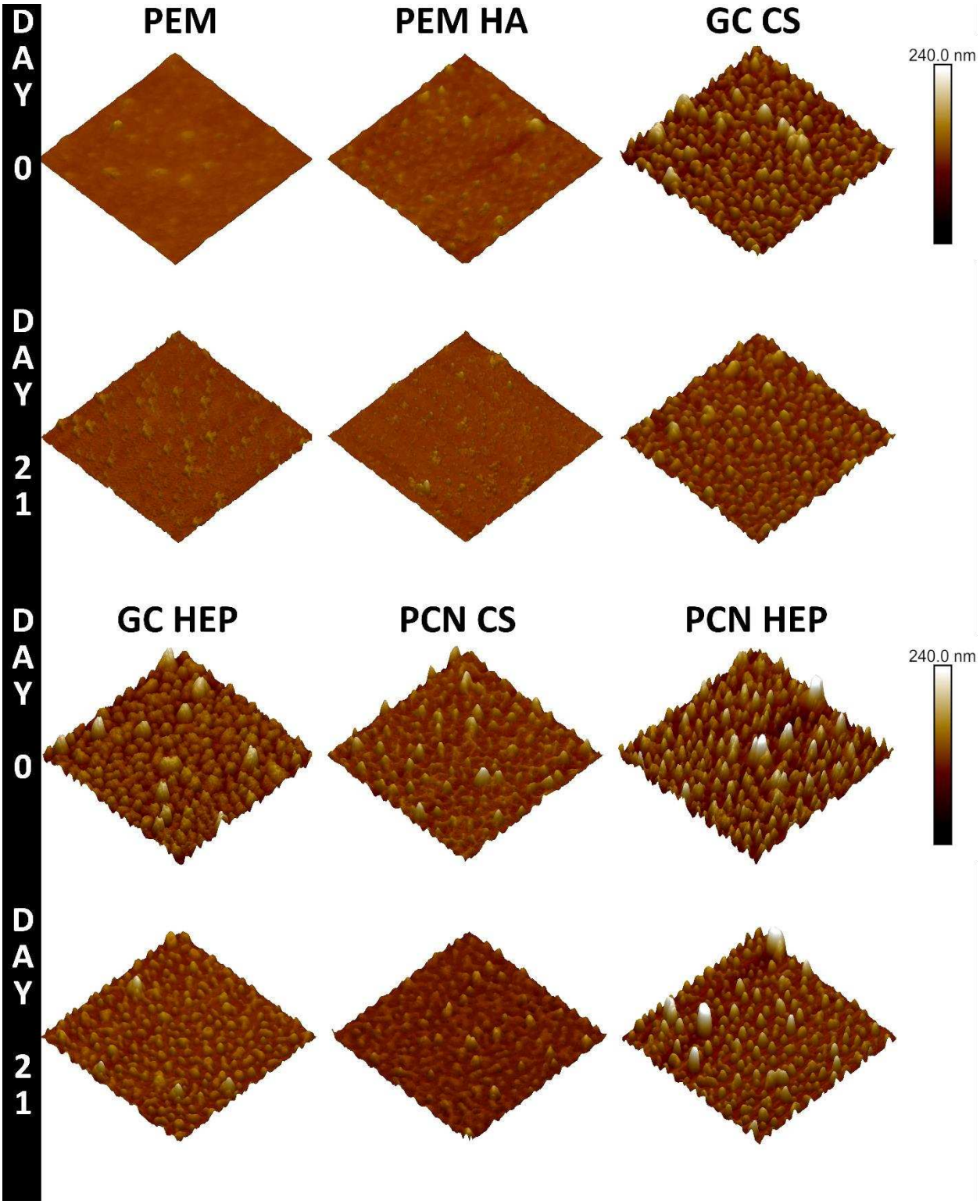


**Figure 3.8.** Representative images of surfaces before and after exposure to hyaluronidase I-S. Each image is a 5 µm x 5 µm area of the surface. Data scale incorporated is 0 to 240 nm in height.

## 3.4. Conclusion

In this work, the enzymatic stability of PG-mimics made using two different strategies is evaluated, for the first time. The CS- and HA-containing PG-mimics were degraded by all hyaluronidases. This shows that our materials are hydrolyzable by enzymes that are specific to the constituent GAGs. There were some differences between the GC CS and PCN CS samples depending on the hyaluronidase used. Hyaluronidase I-S tended to favor HA, and GC CS was cleaved more efficiently than PCN CS due to the presence of the HA backbone. The other two hyaluronidases showed the opposite affect (PCN CS > GC CS glucose equivalent value) which may be a result of the way the PCNs are constructed (electrostatic interactions) versus the GCs (covalent bonds). When exposed to chondroitinase ABC, there was variation in the degradation of the HA- or CS-containing mimics. The PCN CS and GC HEP were resistant to degradation via chondroitinase ABC, due to protecting the HA or CS via crowding. While the PG-mimics are enzymatically degradable, the arrangement of the macromolecular assembly of the PG-mimics may influence how these materials are cleaved depending on the size, charge, or other characteristics of the enzymes. From our results, we can assume the PG mimics would not persist in the body indefinitely. This may mean that periodic re-administration is required for long term applications. The products of the enzymatic hydrolysis are oligosaccharides that can be further metabolized, unlike synthetic polymers, which may degrade into non-natural byproducts.

The PG mimics such as GC and PCN have been incorporated onto surfaces for specific applications. The enzymatic durability of the PG-mimetic surfaces was also evaluated in this work. The PG-mimetic surfaces were all intact after 21 d of enzyme

exposure. There was no significant change in the thickness or surface coverage; we only observed changes in roughness of the surfaces. After 21 d of exposure to buffer with or without enzymes, the surface roughness was reduced, due to annealing. The addition of hyaluronidase I-S decreases this smoothing phenomenon on all surfaces excluding CS-terminated surfaces. These changes in surface roughness may influence the biological interactions of these surfaces overtime. The adsorption of PG-mimics onto the surfaces reduces the PEM degradation increasing their durability with respect to enzymatic degradation for weeks. The surfaces did not fail, delaminate, or expose the underlying substrate during 21 days of incubation with enzymes.

The proteoglycan-mimetic materials described in this work have already shown promise as biomaterials for a variety of applications, and the work done in these studies furthers our knowledge of their stability and enzyme reactivity.[16,34,44,58,59] The PG-mimics are enzymatically degradable and were more stable when adsorbed onto surfaces. The findings are related to the structures and compositions of the PG-mimics and PG-mimic surfaces, and the activities of the enzymes used. Interactions with enzymes will influence material longevity and function over time. These studies provide insight in how the structure of these materials is related to their enzymatic durability. We propose that these new insights could help drive future PG-mimic designs and applications, and that enzymatic stability of materials designed for biomedical applications should be considered in future work. This new understanding of their degradation profile is essential for proposing future applications of these materials for applications such as cardiovascular materials, orthopedic materials, and growth factor delivery applications.

## Citations


1. Hocking, A. M., Shinomura, T. & McQuillan, D. J. Leucine-rich repeat glycoproteins of the extracellular matrix. *Matrix Biol.* **17**, 1–19 (1998).

2. Iozzo, R. V. & Karamanos, N. Proteoglycans in health and disease: emerging concepts and future directions. *FEBS J.* **277**, 3863–3863 (2010).

3. Theocharis, A. D., Skandalis, S. S., Tzanakakis, G. N. & Karamanos, N. K. Proteoglycans in health and disease: novel roles for proteoglycans in malignancy and their pharmacological targeting: Proteoglycans as potential pharmacological targets. *FEBS J.* **277**, 3904–3923 (2010).

4. Kresse, H. & Schönherr, E. Proteoglycans of the extracellular matrix and growth control: EXTRACELLULAR MATRIX AND GROWTH CONTROL. *J. Cell. Physiol.* **189**, 266–274 (2001).

5. *Essentials of Glycobiology*. (Cold Spring Harbor Laboratory Press, 2015).

6. Yanagishita, M. Function of proteoglycans in the extracellular matrix. *Pathol. Int.* **43**, 283–293 (1993).

7. Sasisekharan, R., Raman, R. & Prabhakar, V. GLYCOMICS APPROACH TO STRUCTURE-FUNCTION RELATIONSHIPS OF GLYCOSAMINOGLYCANS. *Annu. Rev. Biomed. Eng.* **8**, 181–231 (2006).

8. Dudhia, J. Aggrecan, aging and assembly in articular cartilage. *Cell. Mol. Life Sci. CMLS* **62**, 2241–2256 (2005).

9. Roughley, P. J. & Lee, E. R. Cartilage proteoglycans: Structure and potential functions. *Microsc. Res. Tech.* **28**, 385–397 (1994).

10. Watanabe, H., Yamada, Y. & Kimata, K. Roles of Aggrecan, a Large Chondroitin Sulfate Proteoglycan, in Cartilage Structure and Function. *J. Biochem. (Tokyo)* **124**, 687–693 (1998).

11. Genetics Unit, Shriners Hospital for Children and Department of Surgery, McGill University, Montreal, Quebec, Canada *et al.* The involvement of aggrecan polymorphism in degeneration of human intervertebral disc and articular cartilage. *Eur. Cell. Mater.* **11**, 1–7 (2006).

12. Roughley, P. J. & Mort, J. S. The role of aggrecan in normal and osteoarthritic cartilage. *J. Exp. Orthop.* **1**, 8 (2014).

13. Genetics Unit, Shriners Hospital for Children and Department of Surgery, McGill University, Montreal, Quebec, Canada & Roughley, P. The structure and function of cartilage proteoglycans. *Eur. Cell. Mater.* **12**, 92–101 (2006).

14. Young, M. F., Bi, Y., Ameye, L. & Chen, X.-D. Biglycan knockout mice: New models for musculoskeletal diseases. *Glycoconj. J.* **19**, 257–262 (2002).

15. Roedig, H., Nastase, M. V., Wygrecka, M. & Schaefer, L. Breaking down chronic inflammatory diseases: the role of biglycan in promoting a switch between inflammation and autophagy. *FEBS J.* **286**, 2965–2979 (2019).

16. Place, L. W., Sekyi, M. & Kipper, M. J. Aggrecan-Mimetic, Glycosaminoglycan-Containing Nanoparticles for Growth Factor Stabilization and Delivery. *Biomacromolecules* **15**, 680–689 (2014).

17. Chandran, P. L. & Horkay, F. Aggrecan, an unusual polyelectrolyte: Review of solution behavior and physiological implications. *Acta Biomater.* **8**, 3–12 (2012).

18. Dreyfuss, J. L. *et al.* Heparan sulfate proteoglycans: structure, protein interactions and cell signaling. *An. Acad. Bras. Ciênc.* **81**, 409–429 (2009).

19. Alphonsus, C. S. & Rodseth, R. N. The endothelial glycocalyx: a review of the vascular barrier. *Anaesthesia* **69**, 777–784 (2014).

20. Reitsma, S., Slaaf, D. W., Vink, H., van Zandvoort, M. A. M. J. & oude Egbrink, M. G. A. The endothelial glycocalyx: composition, functions, and visualization. *Pflüg. Arch. - Eur. J. Physiol.* **454**, 345–359 (2007).

21. Melrose, J. *et al.* The Structure, Location, and Function of Perlecan, a Prominent Pericellular Proteoglycan of Fetal, Postnatal, and Mature Hyaline Cartilages. *J. Biol. Chem.* **281**, 36905–36914 (2006).

22. Okada, H., Yoshida, S., Hara, A., Ogura, S. & Tomita, H. Vascular endothelial injury exacerbates coronavirus disease 2019: The role of endothelial glycocalyx protection. *Microcirculation* **28**, e12654 (2021).

23. Kenagy, R. D., Plaas, A. H. & Wight, T. N. Versican Degradation and Vascular Disease. *Trends Cardiovasc. Med.* **16**, 209–215 (2006).

24. Wight, T. N. *et al.* Versican—A Critical Extracellular Matrix Regulator of Immunity and Inflammation. *Front. Immunol.* **11**, 512 (2020).

25. Weyers, A. & Linhardt, R. J. Neoproteoglycans in tissue engineering. *FEBS J.* **280**, 2511–2522 (2013).

26. Prudnikova, K. *et al.* Aggrecan-like biomimetic proteoglycans (BPGs) composed of natural chondroitin sulfate bristles grafted onto a poly(acrylic acid) core for molecular engineering of the extracellular matrix. *Acta Biomater.* **75**, 93–104 (2018).

27. Prudnikova, K. *et al.* Biomimetic Proteoglycans Mimic Macromolecular Architecture and Water Uptake of Natural Proteoglycans. *Biomacromolecules* **18**, 1713–1723 (2017).

28. Sharma, S., Panitch, A. & Neu, C. P. Incorporation of an aggrecan mimic prevents proteolytic degradation of anisotropic cartilage analogs. *Acta Biomater.* **9**, 4618–4625 (2013).

29. Pauly, H. M., Place, L. W., Haut Donahue, T. L. & Kipper, M. J. Mechanical Properties and Cell Compatibility of Agarose Hydrogels Containing Proteoglycan Mimetic Graft Copolymers. *Biomacromolecules* **18**, 2220–2229 (2017).

30. Wang, D.-A. *et al.* Multifunctional chondroitin sulphate for cartilage tissue–biomaterial integration. *Nat. Mater.* **6**, 385–392 (2007).

31. Goldberg, M., Langer, R. & Jia, X. Nanostructured materials for applications in drug delivery and tissue engineering. *J. Biomater. Sci. Polym. Ed.* **18**, 241–268 (2007).

32. Pumphrey, C. Y., Theus, A. M., Li, S., Parrish, R. S. & Sanderson, R. D. Neoglycans, Carbodiimide-modified Glycosaminoglycans: A New Class of Anticancer Agents That Inhibit Cancer Cell Proliferation and Induce Apoptosis. *Cancer Res.* **62**, 3722–3728 (2002).

33. Zhang, Q. *et al.* Preservation of the Structure of Enzymatically-Degraded Bovine Vitreous Using Synthetic Proteoglycan Mimics. *Invest. Ophthalmol. Vis. Sci.* **55**, 8153–8162 (2014).

34. Hedayati, M., Marruecos, D. F., Krapf, D., Kaar, J. L. & Kipper, M. J. Protein adsorption measurements on low fouling and ultralow fouling surfaces: A critical comparison of surface characterization techniques. *Acta Biomater.* **102**, 169–180 (2020).

35. Szente, L., Puskás, I., Csabai, K. & Fenyvesi, É. Supramolecular Proteoglycan Aggregate Mimics: Cyclodextrin-Assisted Biodegradable Polymer Assemblies for Electrostatic-Driven Drug Delivery. *Chem. - Asian J.* **9**, 1365–1372 (2014).

36. Place, L. W., Kelly, S. M. & Kipper, M. J. Synthesis and Characterization of Proteoglycan-Mimetic Graft Copolymers with Tunable Glycosaminoglycan Density. *Biomacromolecules* **15**, 3772–3780 (2014).

37. Kuberan, B., Gunay, N. S., Dordick, J. S. & Linhardt, R. J. Preparation and isolation of neoglycoconjugates using biotin-streptavidin complexes. *Glycoconj. J.* **16**, 271–281 (1999).

38. Bernhard, J. C. & Panitch, A. Synthesis and characterization of an aggrecan mimic. *Acta Biomater.* **8**, 1543–1550 (2012).

39. Merrett, K. *et al.* Synthetic neoglycopolymer-recombinant human collagen hybrids as biomimetic crosslinking agents in corneal tissue engineering. *Biomaterials* **30**, 5403–5408 (2009).

40. Chinol, M. *et al.* Biochemical modifications of avidin improve pharmacokinetics and biodistribution, and reduce immunogenicity. *Br. J. Cancer* **78**, 189–197 (1998).

41. Brito, A. *et al.* Minimalistic supramolecular proteoglycan mimics by co-assembly of aromatic peptide and carbohydrate amphiphiles. *Chem. Sci.* **10**, 2385–2390 (2019).

42. Sarkar, S. *et al.* Synthesis of macromolecular mimics of small leucine-rich proteoglycans with a poly(ethylene glycol) core and chondroitin sulphate bristles. *Carbohydr. Polym.* **166**, 338–347 (2017).

43. Hedayati, M. & Kipper, M. J. Atomic force microscopy of adsorbed proteoglycan mimetic nanoparticles: Toward new glycocalyx-mimetic model surfaces. *Carbohydr. Polym.* **190**, 346–355 (2018).

44. Vlcek, J. R., Hedayati, M., Melvin, A. C., Reynolds, M. M. & Kipper, M. J. Blood-Compatible Materials: Vascular Endothelium-Mimetic Surfaces that Mitigate Multiple Cell-Material Interactions. *Adv. Healthc. Mater.* 2001748 (2021) doi:10.1002/adhm.202001748.

45. Coburn, J. M., Gibson, M., Monagle, S., Patterson, Z. & Elisseeff, J. H. Bioinspired nanofibers support chondrogenesis for articular cartilage repair. *Proc. Natl. Acad. Sci.* **109**, 10012–10017 (2012).

46. Wen, Y. *et al.* Delivery of Dermatan Sulfate from Polyelectrolyte Complex-Containing Alginate Composite Microspheres for Tissue Regeneration. *Biomacromolecules* **13**, 905–917 (2012).

47. Murugesan, S., Park, T.-J., Yang, H., Mousa, S. & Linhardt, R. J. Blood Compatible Carbon Nanotubes − Nano-based Neoproteoglycans. **22**, 3461–3463 (2006).

48. Freudenberg, U. *et al.* A star-PEG–heparin hydrogel platform to aid cell replacement therapies for neurodegenerative diseases. *Biomaterials* **30**, 5049–5060 (2009).

49. Geckil, H., Xu, F., Zhang, X., Moon, S. & Demirci, U. Engineering hydrogels as extracellular matrix mimics. *Nanomed.* **5**, 469–484 (2010).

50. Kirker, K. R., Luo, Y., Nielson, J. H., Shelby, J. & Prestwich, G. D. Glycosaminoglycan hydrogel films as bio-interactive dressings for wound healing. *Biomaterials* **23**, 3661–3671 (2002).

51. Baier Leach, J., Bivens, K. A., Patrick Jr., C. W. & Schmidt, C. E. Photocrosslinked hyaluronic acid hydrogels: Natural, biodegradable tissue engineering scaffolds. *Biotechnol. Bioeng.* **82**, 578–589 (2003).

52. Nie, T., Akins, R. E. & Kiick, K. L. Production of heparin-containing hydrogels for modulating cell responses. *Acta Biomater.* **5**, 865–875 (2009).

53. Hempel, U. *et al.* Sulfated hyaluronan/collagen I matrices enhance the osteogenic differentiation of human mesenchymal stromal cells in vitro even in the absence of dexamethasone. *Acta Biomater.* **8**, 4064–4072 (2012).

54. Ghadiali, J. E. & Stevens, M. M. Enzyme-Responsive Nanoparticle Systems. *Adv. Mater.* **20**, 4359–4363 (2008).

55. Ulijn, R. V. Enzyme-responsive materials: a new class of smart biomaterials. *J. Mater. Chem.* **16**, 2217 (2006).

56. de la Rica, R., Aili, D. & Stevens, M. M. Enzyme-responsive nanoparticles for drug release and diagnostics. *Adv. Drug Deliv. Rev.* **64**, 967–978 (2012).

57. Hu, J., Zhang, G. & Liu, S. Enzyme-responsive polymeric assemblies, nanoparticles and hydrogels. *Chem. Soc. Rev.* **41**, 5933 (2012).

58. Zomer Volpato, F. *et al.* Preservation of FGF-2 bioactivity using heparin-based nanoparticles, and their delivery from electrospun chitosan fibers. *Acta Biomater.* **8**, 1551–1559 (2012).

59. Hedayati, M., Reynolds, M. M., Krapf, D. & Kipper, M. J. Nanostructured Surfaces That Mimic the Vascular Endothelial Glycocalyx Reduce Blood Protein Adsorption and Prevent Fibrin Network Formation. *ACS Appl. Mater. Interfaces* **10**, 31892–31902 (2018).

60. Boddohi, S., Moore, N., Johnson, P. A. & Kipper, M. J. Polysaccharide-Based Polyelectrolyte Complex Nanoparticles from Chitosan, Heparin, and Hyaluronan. *Biomacromolecules* **10**, 1402–1409 (2009).

61. Kipper, M. J. & Place, L. W. Preparation of Proteoglycan Mimetic Graft Copolymers. in *Macro-Glycoligands* (ed. Sun, X.-L.) vol. 1367 69–86 (Springer New York, 2016).

62. Slor, G. *et al.* Judging Enzyme-Responsive Micelles by Their Covers: Direct Comparison of Dendritic Amphiphiles with Different Hydrophilic Blocks. *Biomacromolecules* **22**, 1197–1210 (2021).

63. Menzel, E. J. & Farr, C. Hyaluronidase and its substrate hyaluronan: biochemistry, biological activities and therapeutic uses. *Cancer Lett.* **131**, 3–11 (1998).

64. Buhren, B. A. *et al.* Hyaluronidase: from clinical applications to molecular and cellular mechanisms. *Eur. J. Med. Res.* **21**, 5 (2016).

65. Jung, H. Hyaluronidase: An overview of its properties, applications, and side effects. *Arch. Plast. Surg.* **47**, 297–300 (2020).

66. Wohlrab, J., Finke, R., Franke, W. G. & Wohlrab, A. Clinical Trial for Safety Evaluation of Hyaluronidase as Diffusion Enhancing Adjuvant for Infiltration Analgesia of Skin with Lidocaine: *Dermatol. Surg.* **38**, 91–96 (2012).

67. Narayanan, R. & Kuppermann, B. D. Hyaluronidase for Pharmacologic Vitreolysis. in *Pharamacology and Vitreoretinal Surgery* (ed. Gandorfer, A.) vol. 44 20–25 (KARGER, 2009).

68. Baumgartner, G. & Hamilton, G. CHAPTER 19 - Clinical Use of Hyaluronidase in Combination Cancer Chemotherapy: A Historic Perspective. in *Hyaluronan in Cancer Biology* (ed. Stern, R.) 363–378 (Academic Press, 2009). doi:10.1016/B978-012374178-3.10019-5.

69. Raspa, A., Bolla, E., Cuscona, C. & Gelain, F. Feasible stabilization of chondroitinase abc enables reduced astrogliosis in a chronic model of spinal cord injury. *CNS Neurosci. Ther.* **25**, 86–100 (2019).

70. Muir, E., De Winter, F., Verhaagen, J. & Fawcett, J. Recent advances in the therapeutic uses of chondroitinase ABC. *Exp. Neurol.* **321**, 113032 (2019).

71. Yick, L.-W., Wu, W., So, K.-F., Yip, H. K. & Shum, D. K.-Y. Chondroitinase ABC promotes axonal regeneration of Clarke's neurons after spinal cord injury. *NeuroReport* **11**, 1063–1067 (2000).

72. Zuo, J., Neubauer, D., Dyess, K., Ferguson, T. A. & Muir, D. Degradation of Chondroitin Sulfate Proteoglycan Enhances the Neurite-Promoting Potential of Spinal Cord Tissue. *Exp. Neurol.* **154**, 654–662 (1998).

73. Hankiewicz, J. & Swierczek, E. Lysozyme in human body fluids. *Clin. Chim. Acta* **57**, 205–209 (1974).

74. Moretti, R. & Thorson, J. S. A comparison of sugar indicators enables a universal high-throughput sugar-1-phosphate nucleotidyltransferase assay. *Anal. Biochem.* **377**, 251–258 (2008).

75. Yick, L. Axonal regeneration of Clarke's neurons beyond the spinal cord injury scar after treatment with chondroitinase ABC. *Exp. Neurol.* **182**, 160–168 (2003).

76. Moharib, M. Alkalinized lidocaine and bupivacaine with hyaluronidase for sub-Tenon's ophthalmic block. *Reg. Anesth. Pain Med.* **25**, 514–517 (2000).

77. Stern, R. & Jedrzejas, M. J. Hyaluronidases: Their Genomics, Structures, and Mechanisms of Action. *Chem. Rev.* **106**, 818–839 (2006).

78. Cavallini, M., Gazzola, R., Metalla, M. & Vaienti, L. The Role of Hyaluronidase in the Treatment of Complications From Hyaluronic Acid Dermal Fillers. *Aesthet. Surg. J.* **33**, 1167–1174 (2013).

79. Mason, D. Y. & Taylor, C. R. The distribution of muramidase (lysozyme) in human tissues. *J. Clin. Pathol.* **28**, 124–132 (1975).

80. Pomin, V. H. NMR Chemical Shifts in Structural Biology of Glycosaminoglycans. *Anal. Chem.* **86**, 65–94 (2014).

81. Csóka, T. B., Frost, G. I., Wong, T. & Stern, R. Purification and microsequencing of hyaluronidase isozymes from human urine. *FEBS Lett.* **417**, 307–310 (1997).

82. Tester, N. J., Plaas, A. H. & Howland, D. R. Effect of body temperature on chondroitinase ABC's ability to cleave chondroitin sulfate glycosaminoglycans. *J. Neurosci. Res.* **85**, 1110–1118 (2007).

# CHAPTER 4: MODIFICATIONS TO POLYELECTROLYTE MULTILAYERS: IMPROVED MECHANICAL STABILITY AND HEMOCOMPATIBILITY[1]

## Overview

Developing materials that can inhibit coagulation at the blood-material interface is still a challenge for researchers despite decades of research. One approach taken to improve blood compatibility is coating substrate surfaces with polyelectrolyte multilayers (PEMs) which can act as a substrate by which nanoparticles can be adsorbed or from which drugs can be released. These surfaces have been extensively used due to their versatility and ease of use, but their mechanical stability against shear forces has yet to be evaluated. For the first time, we evaluated the mechanical durability of PEM surfaces against shear flow, and further modified these surfaces with polydopamine (PDA) and EDC-NHS chemistries to improve stability. The PDA EDC modified PEMs were found to be more stable than unmodified PEMs. To show that modifications made to the PEM surfaces to improve stability did not compromise hemocompatibility we evaluated surfaces against whole blood clotting directly onto surfaces, thromboelastography (TEG), and hemolysis. We tested PEM PDA EDC surfaces against PEMs modified with proteoglycan mimics (polyelectrolyte complex nanoparticles (PCN) and graft copolymers (GC)) which were previously developed in the lab to improve blood-material interactions. In this work we compared two design strategies: improved mechanical stability and targeted hemocompatibility.

[1]Modified version of manuscript in preparation to be submitted to *Applied Surface Science*.

We found that PEMs modified with PDA and EDC did not significantly influence interactions with donor blood. Additionally, the heparin (HEP) containing PG mimics were able to reduce clotting times with PCN HEP surfaces inhibiting clot formation all together. The differences in HEP containing surfaces was attributed to their construction and how that relates to their stability. Using PEMs, we were able to create surfaces with two design strategies: increased mechanical stability or hemocompatibility and compare them to determine what criteria should be used to create future blood compatible surfaces.

## 4.1. Introduction

Polyelectrolyte multilayers have been extensively used to modify biomaterials surfaces.[1–17] The popularity of these surfaces is in part due to their ease of construction, their versatility in the polymers used, and their ability to modify the surface chemistry of substrates while preserving microscale and nanoscale topographical features. PEM surfaces also provide substrates for nanoparticles adsorption or drug release.[3,4,7]

PEMs represent a platform technology from which blood compatibility of surfaces can be improved. For example, our group has proposed using PEM surfaces to mimic the biochemical composition and functions of the vascular endothelial glycocalyx for blood-contacting biomaterials. The endothelial glycocalyx is the inner lining of blood vessels which consists of a dense meshwork of negatively charged macromolecules (proteoglycans, glycosaminoglycans, and glycoproteins), and is considered the only truly blood compatible material.[18,19] Synthetic surfaces that have long-term blood compatibility comparable to the endothelial glycocalyx have not been fully developed.[20–22]

Surface modifications have shown promise in reducing blood coagulation locally. Approaches include designing: bioinert, thrombolytic, drug releasing, bioactive, and bioinspired surfaces.[20–22] Bioactive surfaces using heparin (HEP) have been successful enough to be produced commercially, but have limitations that prevent their long-term use.[23] We have designed PEM surfaces as mimics of the endothelial glycocalyx that reduce platelet adhesion and activation, reduce protein adsorption and polymerization, suppress pro-inflammatory responses from leukocytes and macrophages, and reduce bacterial attachment.[3,5,7,9,13] These biomimetic surfaces designed to mimic the topography and chemistry of the glycocalyx, are comprised of chitosan and hyaluronan polyelectrolyte multilayers as a substrate, with heparin- or chondroitin sulfate-containing proteoglycan mimics adsorbed onto their surfaces.[3,9,24] These materials have shown promise as blood-contacting materials, and their interactions with bacteria, platelets, blood proteins, and leukocytes have been evaluated.[3,24] We have also recently reported on their enzymatic stability.[17] Their interactions with whole human blood and their mechanical durability under flowing fluid has not yet been characterized. For blood-contacting applications, these surfaces may lose their functionality due to mechanical shear when in contact with flowing blood. In this work we propose PEM surfaces that are modified to be more mechanically stable, and we evaluate the clotting of whole blood in contact with these surfaces. We also demonstrate modifications to our PEM surfaces to better mimic the vascular endothelial glycocalyx.

Polydopamine (PDA) is a mussel-inspired chemistry, which has been extensively researched for applications in medicine.[25–33] Its adhesive properties have been exploited to adhere molecules and particles of interest to substrate surfaces.[26,27,29,32,34] For

example, Leung et al. used PDA to adhere covalent antithrombin-heparin complexes to poly(dimethyl siloxane) (PDMS) surfaces to improve their hemocompatiblity.[35] Others have used PDA for applications in the fields of cancer, neuroscience, bone tissue engineering, and wound healing among others.[36–42]

Due to PDA's versatility and widespread use, we selected it as component to improve the strength of attachment of our PEM surfaces to substrates. As an alternative, we also use a common carbodiimide chemistry (EDC) to form covalent crosslinks between carboxylic acid groups on hyaluronic acid (HA) amines in chitosan (CHI). We also created surfaces that use both PDA deposition and EDC crosslinking.

For the first time, we report on the evaluation of a PDA-containing and an EDC-NHS cross-linked glycocalyx-mimetic surface with respect to durability to fluid shear and blood compatibility. These PEM PDA EDC surfaces are compared with unmodified PEM, PEM PDA, and PEM EDC surfaces to determine how the modifications affect mechanical stability. The surfaces that were designed for mechanical improvement are also compared to surfaces designed to improve hemocompatibility against human whole blood. This work demonstrates surface designs driven by two competing technology needs—improved stability and improved hemocompatibility—with the aim of developing long-term blood-compatible surface.

## 4.2. Materials and Methods

### 4.2.1. Materials

Acetic acid was purchased from Acros, heparin sodium (HEP) (from porcine intestinal mucosa, 12.5% sulfur, approximately 14.7 kDa) was purchased from Celsus

Laboratories, and chitosan (CHI) from MP Biomedicals was used. Chondroitin sulfate sodium (CS) salt (from shark cartilage, 6% sulfur, 6-sulfate/4-sulfate = 1.24, Mw = 84.3 kDa), hyaluronan (HA) sodium salt (Mw = $1.5\times10^3$ kDa), cysteamine hydrochloride, tris(2-carboxyethyl) phosphine hydrochloride (TCEP), (2-(*N*-morpholino) ethanesulfonic acid (MES), *N*, *N*-dimethylformamide (DMF), and dopamine hydrochloride were purchased from Sigma Aldrich. Sodium phosphate dibasic, Tris(hydroxymethyl)aminomethane, *N*-(3-dimethylaminopropyl)-*N'*-ethylcarbodiimide hydrochloride (EDC), *N*-hydroxysuccinimide (NHS), *N*-[β-maleimidopropionic acid] hydrazide trifluoroacetic acid salt (BMPH), and Zeba desalting columns (7k MWCO) were acquired from Thermo Fisher. Sodium triacetoxyborohydride (STAB) was purchased from Alfa Aesar. Deionized water (18.2 MΩ cm), obtained from a Millipore Synthesis water purification unit, was used for all experiments using aqueous solutions.

### 4.2.2. Polydopamine deposition

Deposition of an initial polydopamine layer was achieved by modifying previously published methods.[43,44] Cleaned glass slides were oxidized using oxygen plasma (PlasmaTech model PE-25, for 8 min). Dopamine hydrocholoride (1 mg/mL) was dissolved in filtered tris buffer (22 µm filter) (pH 8.0) in a beaker shielded from light. An initial layer of dopamine and HA was deposited from a solution of 1 mg/mL PDA and 5 mg/mL HA. This solution was chosen after determining surface coverage achieved using a range of concentrations (Figure 4.S1). Because HA increases the solution viscosity, the PDA was dissolved first, and then the HA was slowly added until the HA concentration was 5 mg/mL. The combined solution was stirred for 30 min. The cleaned glass surfaces were then submerged in the dopamine/HA solution overnight. The resulting PDA/HA-

modified surfaces were cleaned by rinsing once with phosphate-buffered saline (PBS, pH 7.4) for 5 min, and rinsing three additional times with deionized water.

### 4.2.3. Polyelectrolyte (PEM) multilayer preparation

PEMs were prepared as previously described.[3,45] Briefly, chitosan (CHI) (1 mg/mL) and HA (0.5 mg/mL) solutions were prepared with acetate buffer (0.2 sodium acetate and acetic acid at pH 5.0). Solutions were stirred for at least 2 h at room temperature and were then filtered through 2.0 um PDVF syringe filters. Oxidized glass or PDA/HA modified glass surfaces were used as substrates for PEM deposition. The PEMs were constructed by alternating layers of a polyanion (HA) and polycation (CHI) with 3-min acetic acid rinse (pH 4.0; de-ionized water acidified with acetic acid) between adsorption steps (5 min). This procedure was repeated until a 15-layer, CHI-terminated PEM was produced.

### 4.2.4. Cross-linking of PEM layers

Adjacent HA and CHI in PEM layers were crosslinked using EDC and NHS to form amid bonds between the amine groups in HA and the carboxylic acid groups in HA. EDC (2.58 mg/mL) and NHS (3.86 mg/mL) were dissolved together in MES buffer (0.1 M MES, 0.5 NaCl, pH 6.0). The PEM samples were submerged in the cross-linking solution for at least 4 h and then submerged in a sodium phosphate dibasic solution (0.1 M) for at least 2 hrs. The resulting cross-linked surfaces were then rinsed three times with de-ionized water, for five minutes per rinse.

### 4.2.5. Preparation of graft copolymer (GC) proteoglycan (PG) mimics

PG-mimetic graft copolymers are composed of an HA backbone with side chains consisting of GAGs (HEP or CS). Synthesis of graft copolymers has been previously reported by our group.[17,46,47] The synthesis is a three-step process which consists of: HA backbone thiolation, backbone hydrazide activation, and coupling via reductive amination. During the first step, HA (250 mg) was activated with EDC (645 mg) and NHS (976 mg) in MES buffer (50 mL, pH 6.0). After the carboxylate functional groups are activated, cysteamine hydrochloride (880 mg) was added to the reaction mixture and bound to the activated HA (pH 7.2). The resulting thiolated HA (HA-SH) was then purified and lyophilized to be used in the second step of the synthesis process. Before backbone hydrazide activation, any disulfide bonds that may have formed in the HA-SH were reduced by combining purified HA-SH (100 mg) with TCEP (114 mg) in PBS (50 mL, pH 8.0). Buffer solutions were then changed using desalting columns (from PBS pH 8 to PBS pH 7.2). To attach a hydrazide group onto the HA, the bifunctional coupling agent containing a maleimide (to react with the thiol), and a hydrazide, BMPH (80 mg) was added to the solution. The HA-BMPH intermediate was purified and lyophilized. The third and final step is coupling the CS or HEP as side chains to the HA-BMPH backbone, via reaction of the reducing sugar end group with the hydrazide on the HA-BMPH. HA-BMPH (15 mg) and HEP (170 mg) or CS (1000 mg) were dissolved together in a DMF (10 mL) and acetic acid (0.35 mL) solution at a 1:1 molar ratio (thiolated side chain on the HA backbone to CS or HEP). The HA-BMPH and GAG solution was slowly heated to 85 °C, then 350 µL (5× over 8 h) of the reducing agent solution (STAB 0.1 g/mL) was added. This reaction was allowed to proceed overnight, and the final product was purified and

stored at 4 °C. Additional details and spectroscopic confirmation of the synthesis are provided in our previous publications.

### 4.2.6. Preparation of polyelectrolyte complex nanoparticle (PCN) PG mimics

Polyelectrolyte complex nanoparticles (PCN) were prepared as previously published by our group.[3,45,48,49] CHI (1mg/mL), HEP (1.5mg/mL), and CS (2.8 mg/mL) solutions were dissolved overnight in an acetate buffer solution (0.2 M sodium acetate and acetic acid at pH 5.0). After solutions were completely dissolved, they were filtered through 0.22 μm PDVF syringe filters. While 6 mL of CHI solutions were stirring at 1000 rpm, 36 mL of CS or 24 mL of HEP solutions were added. The solutions were allowed to stir for at least 3 h, after which they were allowed to settle overnight, to remove large aggregates. The remaining PCNs in solution were collected by decanting the solution from the settled aggregates.

### 4.2.7. Preparation of PEMs and PG mimic (both GC and PCN) adsorption on surfaces

Each PG mimic (GC or PCN) was dissolved in acetate buffer solution (0.2 M sodium acetate and acetic acid at pH 5.0) for at least 3 h at 1 mg/mL. The solutions were then moved to conical tubes and allowed to settle overnight before use. Solutions containing a PG mimic (HA-CS GC, HA-HEP GC, CHI-HEP PCN, or CHI-CS PCN) were exposed to CHI-terminated, 15-layer PEMs. The solution containing the PG mimic was added to the PEM for 4 min followed by a 3-min rinse. This rinsing procedure was repeated three times, and the samples were washed with a final de-ionized water rinse step for 30 s.

### 4.2.8. Construction of microfluidic channels containing experimental surface

Microfluidic channels were prepared using double-sided adhesive tape, and plastic cover slides. The construction of channels was modeled from previously described channels.[24] Briefly, the double-sided adhesive tape (Grace Bio-labs 620003) was cut to the size of glass slides. Two rectangular sections were excised from the tape. Each rectangle had dimensions of dimensions of l = 15 mm and w = 300 μm to create the channels. The double-sided tape pieces containing the channels were then adhered to glass slides (Fisher 12-544-4) that had been cleaned and charged using oxygen plasma. PEM and PG-mimic-modified PEM surfaces were then deposited directly on the glass surfaces that remained exposed in the open rectangular channels. After deposition of the surfaces the release layer of the adhesive was removed, and the surfaces were sealed with a plastic cover slip (VWR 82027-788), into which two holes were drilled to serve as inlet and outlet fluid ports. The resulting channels had a height of 300 μm. Channels were exposed to low vacuum, for at least 1 day prior to experimentation.

### 4.2.9. Flow studies and shear rate calculations

Water with 1% pen/strep solution was flowed through channels at a shear rate of 305.5 $s^{-1}$ for 2 hours using a (Masterflex Model 77201-60) rotary pump. The shear rate used is within the range of healthy vessels which can be as low as 10 $s^{-1}$ in veins to as high as 2000 $s^{-1}$ is the smallest arteries.[50] Shear rate calculations were made via MATLAB

software (version 9.9.0.123456) using **Equation 1**, which describes the wall shear rate for a Newtonian fluid flowing in rectangular pipes.

$$\gamma(x) = \frac{48Q}{w\pi^2 h^2} \frac{\sum_{n=1,3,5....}^{\infty} \frac{1}{n^2}\left[1 - \frac{\cosh\left(n\pi \frac{x}{h}\right)}{\cosh\left(n\pi \frac{w}{2h}\right)}\right]}{\left[1 - \sum_{n=1,3,5...}^{\infty} \frac{192h}{n^5\pi^5 w}\tanh\left(n\pi \frac{w}{2h}\right)\right]} \quad (1)$$

Here, $\gamma$ is the shear rate, $Q$ is the volumetric flow rate, $h$ is the channel height, and $w$ is the channel width. The coordinate x describes the position from the center of the channel, where $-w/2 \leq x \leq w/2$. Although blood being is a shear-thinning fluid (non-Newtonian), water was used in these studies for two reasons: shear-thinning fluids flowed through rectangular pipes form vortices, and blood behaves as a Newtonian fluid at high shear (wall shear rates greater than 100 $s^{-1}$).[51–53] After exposure to flow, the surfaces were dried in a desiccator overnight. After drying, the plastic cover slip was removed, creating open channels that can be evaluated using X-ray photoelectron spectroscopy.

### 4.2.10. Surface Characterization by atomic force microscopy (AFM)

Atomic force microscopy (AFM) was performed on the surfaces prepared on glass-bottom petri dishes (Ted Pella #14036) that were hydrated in DI water at room temperature, using a Bruker Bioscope Resolve atomic force microscope. The ScanAsyst mode was used, with a triangular silicon nitride tip with an average tip radius of 20 nm, a spring constant of 0.12 N/m, and a gold-coated reflective back side (DNP-10 B, Bruker). The peak force set point was set near 2 nN and was optimized using NanoScope

software. The scan rate was set to 0.7 Hz with a tapping frequency of 1-2 kHz. Representative images were taken at 5 μm × 5 μm areas on un-modified and modified PEM surfaces. Image analysis was preformed using NanoScope Analysis version 1.8.

#### 4.2.11. Surface characterization by X-ray photoelectron spectroscopy (XPS)

Changes in surface chemistry due to chemical modification and exposure to shear forces were analyzed using X-ray photoelectron spectroscopy (XPS) using a Physical Electronics 5800 Spectrometer (Chanhassen, MN). Spectra were obtained with a monochromatic Al K-α X-ray source ($hv$ = 1486.6 eV), a hemispherical analyzer, and multichannel detector. High-resolution spectra were obtained using 23.5 eV analyzer pass energy with 0.1 eV steps and an X-ray spot of 800 um. All spectra were taken at a photoelectron takeoff angle of 45°. Atomic percent values were obtained via MultiPak software, after spectra were smoothed and the background signal was subtracted. Spectra were plotted using Origin (version 9.6). For shear durability studies each channel ($n$ = 4 per group) was measured once in the center of the channel and atomic percent ratios were reported from these measurements as mean ± standard deviation.

#### 4.2.12. Donor blood collection

Blood isolation from healthy individuals who had refrained from taking thromboxane inhibitors for at least 2 weeks was approved by the Colorado State University Institutional Review Board (Protocol ID #19-9039H). For experimentation 2 donors were used in this study. Blood was drawn via venous phlebotomy, by a trained phlebotomist at Colorado State University Health and Medical Center. Blood was collected into 4.5 mL citrated BD Vacutainers venous blood collection tubes (12.35 mg of sodium citrate, 2.21 mg of citric acid). After collection, donor whole blood was coalesced

into a 50 mL conical tube and allowed to rest for 20 min before experimentation. All blood was used within 4 h following collection time.

#### 4.2.13. Sample sterilization

Samples were sterilized immediately before each study. Each sample was sterilized with a 70% ethanol solution for 15 minutes, and then washed 3× with sterile PBS (pH 7.4).

#### 4.2.14. Hemolysis measurements

Hemolysis measurements were performed using procedures modified from previously published work.[5,54] Donor blood collected in sodium citrated tubes was transferred to 15 mL conical tubes and centrifuged at 700 × *g* for 10 min at 15 °C. After initial centrifugation the supernatant was removed, and red blood cells (RBCs) were resuspended in sterile PBS (pH 7.4) to wash the cells. This washing step was repeated three times. Sterile samples (surfaces adsorbed onto 12 mm-diameter glass pucks; $n$ = 4) were transferred to 15 mL conical tubes and a 2% pure, washed RBCs and PBS solution (80 µL of RBCs per 4 mL PBS/sample solution) was added to the tubes, submerging the samples. Untreated glass was used as a negative control ($n$ = 4); RBCs submerged in DI water ($n$ = 4) were used as a positive control representing complete hemolysis. Conical tubes were incubated at 37 °C in a water bath for 3 h with gentle inversion of the tubes every 30 minutes. The sample solutions were then centrifuged at 700 × *g* for 10 min at 15 °C. From each tube, 100 µL of the supernatant solution was collected and transferred to a 96-well flat bottom plate. The absorbance representing the released hemoglobin was measured at 540 nm. Blank values were subtracted from reported absorbances. Reported values (mean ± standard deviation) were obtained from

*n* = 4 samples, which were calculated from the averages of two technical replicates for each sample.

### 4.3.15. Clotting characterization via Thromboelastography (TEG)

Sterile samples adsorbed onto 8 mm-diameter glass pucks were submerged in 1 mL of citrated human whole blood in 1.5 mL microcentrifuge tubes, shielded from light. Tubes were incubated at 37 °C on a shaker (100 RPM) for 30 minutes and then allowed to settle prior to experimentation. After resting, the blood was mixed by inversion and 340 mL of citrated human whole blood was transferred into TEG disposable cups with 20 mL of 0.2 M calcium chloride. TEG (Haemoscope 500, Haemonetics, Boston, Massachusetts) was then performed at 37 °C, and data collection was continued until clot maximum amplitude (MA) was detected or if there was no clot formation, after 1 hr. From TEG experiments a thromboelastograph was obtained, from which several clot formation parameters were calculated (**Figure 4.S2).** Reaction time (R) is the time from the beginning of the experiment until a 2-mm amplitude clot in blood is detected; initial clot formation time (K) is the time it takes for a 2-mm amplitude clot to grow in strength to a 20-mm amplitude clot; α-angle (A), is the angle formed between baseline (2 mm) and the imaginary line that is tangential to the area on the thromboelastograph curve that corresponds to clot time (K); and clot strength (MA) is the maximal amplitude of the TEG curve. Clot index (CI) values were calculated using the parameters above and **Equation 2**. [55] TEG studies were conducted on different days, due to the number of samples and time required. To ensure that samples evaluated at different times could be compared, all results (*n* = 4-5 samples or *n* = 8 samples for PEM) were normalized to control values (glass pucks) (*n* = 3) which were run during the same 4 h period, and blood was collected

from donors at the same time for each separate day. For each sample 1 TEG curve was obtained. Each TEG run took between 30 to 60 min between which the blood sat at room temperature.

$$\mathrm{CI} = -0.2454 * \mathrm{R} + 0.0184 * \mathrm{K} + 0.1655 * \mathrm{MA} - 0.0241 * \mathrm{A} - 5.0220 \qquad (2)$$

TEG studies were conducted on different days, due to the number of samples and time required. Blood was collected from donors at the same time for each separate day. For each sample 1 TEG curve was obtained.

### 4.2.16. Imaging surfaces exposed to whole blood by scanning electron microscopy (SEM)

Sterile samples adsorbed onto 12-mm diameter glass pucks were submerged in 340 mL of whole human blood collected from sodium citrate tubes in a 24-well plate. 20 mL of 0.2 M calcium chloride was added to each well, and then the samples were incubated at 37 °C at 100 RPMs. Samples were checked after 1 h of incubation and all had shown signs of significant clot formation. The surfaces were removed from the well and gently cleaned by rinsing three times (5 min) with PBS (pH 7.4). Samples were then fixed for scanning electron microscopy (SEM; JEOL JSM-6500F). The samples were fixed using a 3% glutaraldehyde, 0.1 M sodium cacodylate, and 0.1 M sucrose solution for 0.75 h at room temperature. The samples were then washed with a buffer (0.1 M sodium cacodylate, and 0.1 M sucrose) for 10 min. Subsequently, samples were dried with increasing concentrations of ethanol solutions (35%, 50%, 75%, and 100%) for 5 min each. To prepare samples for SEM imaging, samples were coated with 15 nm of gold and grounded with copper tape. Samples were imaged by SEM at 15 kV at multiple

magnifications (500x, 1000x, 2500x) at 3 separate areas on the sample surface. Representative images were chosen for each sample.

### 4.2.15. Statistical analysis

Statistical analysis was performed on XPS atomic composition data, hemolysis data, and TEG data using R (version 3.6.1). Data sets were tested for normality before comparative analysis. A one-way ANOVA with pairwise comparisons was performed on atomic composition data, and two-way ANOVA analyses with pairwise comparisons were performed on hemolysis and TEG data.

## 4.3. Results

### 4.3.1. Surface characterization of PDA and EDC-NHS modified surfaces

XPS and AFM were used to evaluate any chemical or topographical changes made to the surfaces due to PDA deposition or EDC-NHS crosslinking. **Figure 4.1** shows the XPS survey spectra of the modified and unmodified PEMs adsorbed onto the surface of glass. No silica peaks are present on surfaces modified with PDA or EDC or both, while unmodified PEM surfaces have small silica peaks, arising from the underlying glass substrate. These results show that even before exposure to flowing solutions, the PDA and EDC crosslinking improves the surface coverage compared to the unmodified PEMs at 15 layers. The oxygen, carbon, and nitrogen peaks are present on all surface types, and no additional peaks are found on modified surfaces. These results confirm that the modifications preserve the PEM chemistry and do not significantly modify the polysaccharide composition of the surfaces. The presence of the modified and unmodified PEM surfaces is also confirmed by AFM (**Figure 4.2**). The addition of the

PDA increases the overall roughness of the PEM surfaces, and the EDC-NHS cross-linking slightly smoothed the surfaces. Roughness values ($R_q$ and $R_a$) are reported in supplementary information **Table 4.S1**

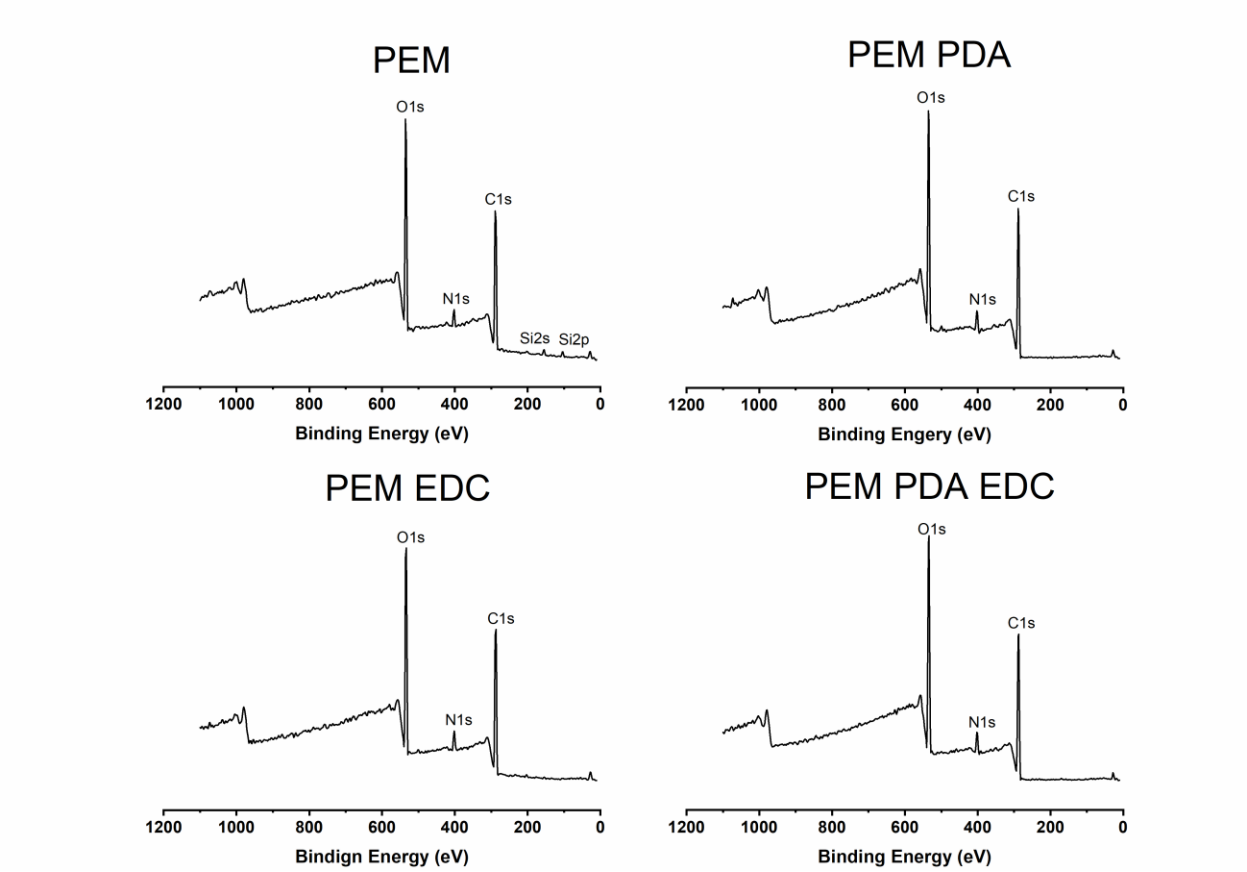


**Figure 4.1.** XPS survey spectra for PEM, PEM EDC, PEM PDA, and PEM PDA EDC surfaces. Peaks labeled on XPS spectra correspond to oxygen, carbon, nitrogen, and silica. Silica peaks were only present on untreated PEM surfaces, meaning that the surfaces treated with EDC and PDA more successfully masked the underlying surface chemistry of glass.

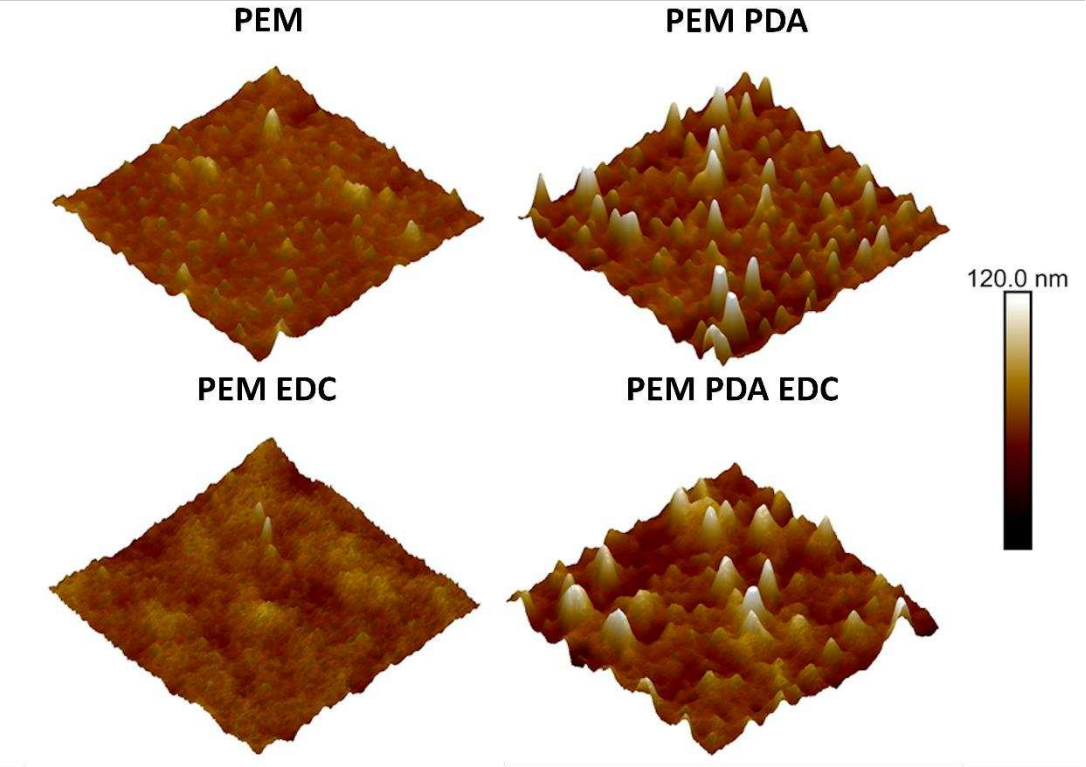


**Figure 4.2.** AFM images of a 5 μm × 5 μm square area of PEM, PEM EDC, PEM PDA, and PEM EDC PDA surfaces. The PDA deposition added roughness to the surfaces while the EDC-NHS crosslinking smoothed the surfaces. (Roughness values are reported in Table 4.S1 in the Supporting Information).

### 4.3.2. Surface chemistry after exposure to shear forces

After exposure to flow for 2 h, surfaces were evaluated via XPS to determine how much silica is still masked by the PEM layers. Survey XPS spectra are presented in **Figure 4.3**, showing that all surfaces have detectable silica (the limit of detection is 1 atomic percent), demonstrating that all surfaces were at least partially modified due to the shear forces of the flowing water. PEM PDA EDC surfaces have the smallest silica peaks on the survey spectra, indicating they withstood the shear forces better than the other surface types. High-resolution spectra were obtained and used to calculated atomic percent values for carbon, nitrogen, and silicon. These areas were combined as ratios

for each spectrum to normalize any charging effects that may occur. PEM PDA EDC surfaces have significantly higher C/Si ratio than PEM PDA surfaces, higher N/Si ratio than PEM and PEM PDA surfaces, and a significantly reduced C/N ratio compared to PEM surfaces. Higher C/Si and N/Si ratios corresponds to better surface coverage of the glass, and thus more stable surfaces. N/Si ratios may be a better measure of surface coverage, as carbon can be observed in the spectra of untreated glass, while nitrogen is absent from the untreated glass. The lower C/N ratio in the PDA samples is attributed to change in composition from the PDA. This may also indicate that the PDA is enriched at the surface following the flow exposure. Enriching the PDA near the surface may additionally alter the blood compatibility of these surfaces, as PDA has been used to improve the hemocompatibility of surfaces, either alone or in combination with other biomolecules.[1,8,25,28,30,33] Overall, the PEM PDA EDC surfaces are the most durable with regards to flow. We attribute the improved durability to both chemical crosslinking, enhancing the cohesion of the PEM layers, and PDA improving the adhesion to the glass substrate.[44] Despite these improvements, there is some evidence that exposure to flow disrupts the surface coverage

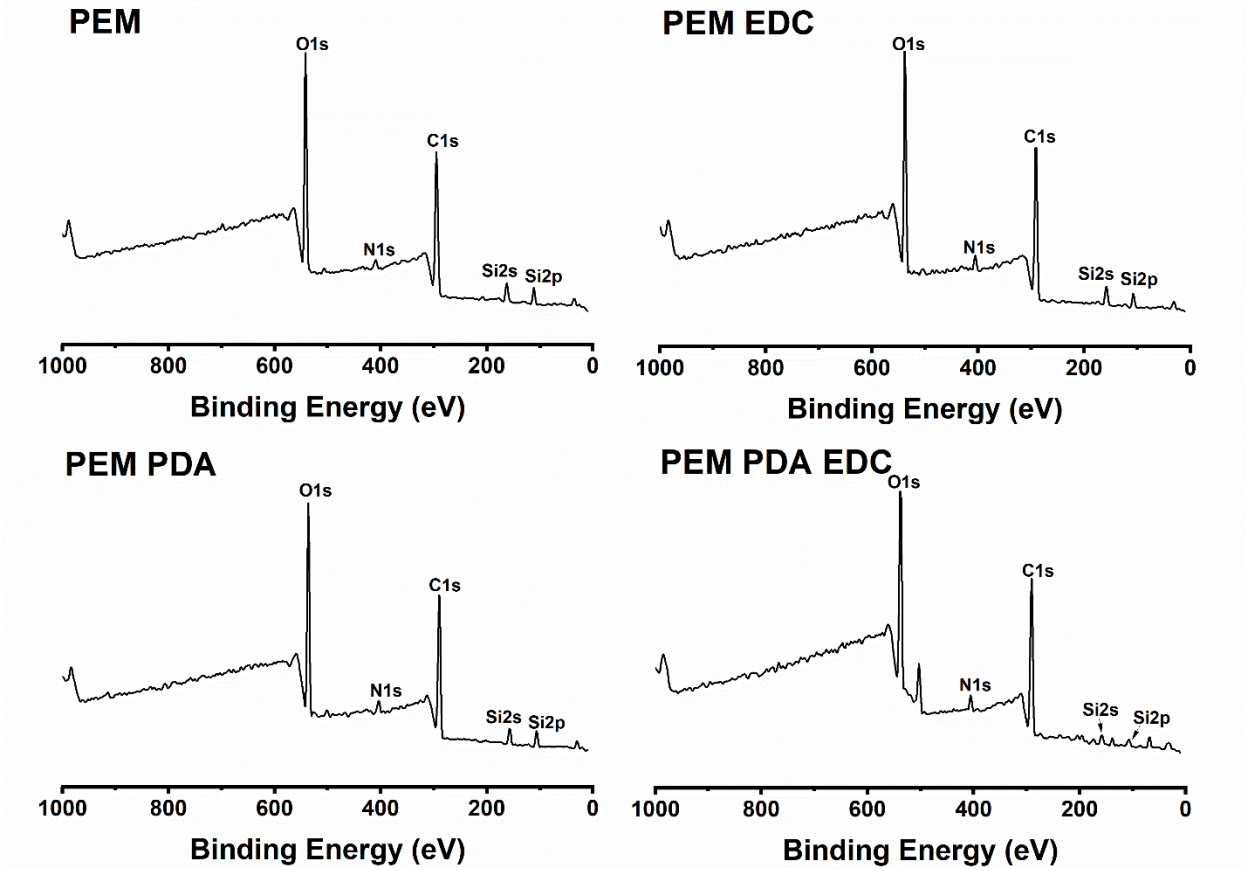


**Figure 4.3.** XPS survey spectra for PEM, PEM EDC, PEM PDA, and PEM PDA EDC surfaces after exposure to flow for 2 hrs. Peaks labeled on XPS spectra correspond to oxygen, carbon, nitrogen, and silica. Silica peaks present on all surfaces, meaning the flow of water sheared some of the surface.

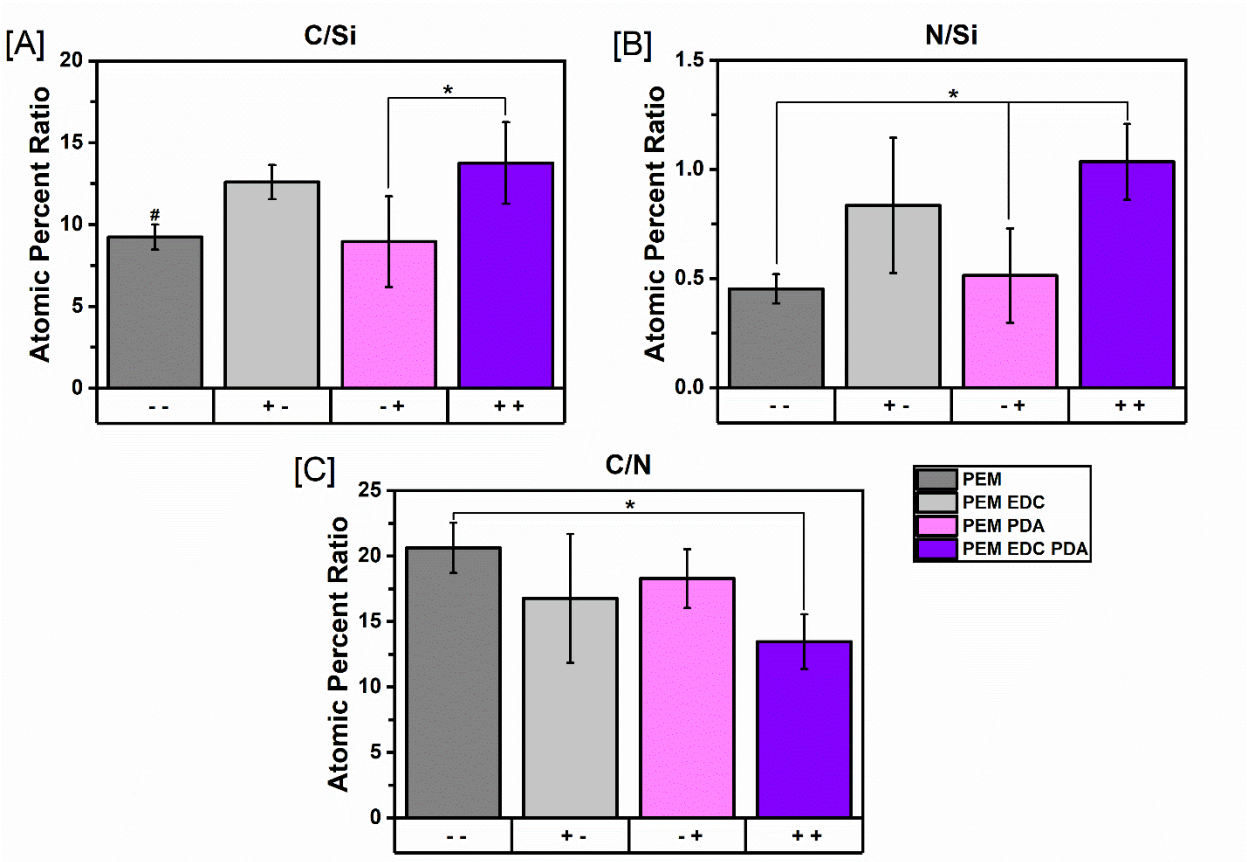


**Figure 4.4.** Atomic percent ratios (mean ± standard deviation of $n>5$) for [A] carbon/silica, [B] nitrogen/silica, and [C] carbon/nitrogen atom ratios calculated via MultiPak software from XPS high-resolution spectra. Spectra values were obtained for PEM, PEM EDC, PEM PDA, and PEM PDA EDC channels after exposure to flowing $H_2O$ (of 305.5 $s^{-1}$) after 2 hrs. of exposure ($n = 4$). A one-way ANOVA with post hoc Tukey test was performed on each set of ratios. (* $p < 0.05$). The # symbol on [A] denotes that there was no significant difference between PEM and PEM EDC PDA, but the $p$-value was close to 0.05 ($p$-value = 0.06). This data shows that the Si peak was reduced for PEM PDA EDC surfaces compared to other surface types, indicating resistance to shear flow.

### 4.3.3. Hemolysis evaluation

After evaluating how the modifications to our surfaces improve mechanical durability, we then evaluated how those changes influenced the surface interactions with blood. Additionally, we adsorbed our PG mimics to the surface of the unmodified PEMs

to determine how features that mimic the chemistry and topography of the endothelial glycocalyx can improve the PEM hemocompatibility. First hemolysis, the rupture of red blood cells, was evaluated (**Figure 4.5** and **Figure 4.S3**). Hemolysis can lead to complications such as hemoglobinemia, and anemia in severe cases.[56]

There are no significant differences between samples groups or between sample groups and the untreated glass control (**Figure 4.5** and **Figure 4.S3**). All groups, including the glass controls, are significantly different from the full hemolysis control (Figure 4.S3). Differing degrees of hemolytic capabilities of materials can be defined into different percent hemolysis brackets, where 0-2% hemolysis is considered non-hemolytic, 2-5% is considered slightly hemolytic, materials are said to be hemolytic but non-toxic at >5% but <10%, and hemolytic and toxic at >10%.[57–60] All surfaces tested were below the toxic range for hemolysis and most values fall within the slightly hemolytic range.

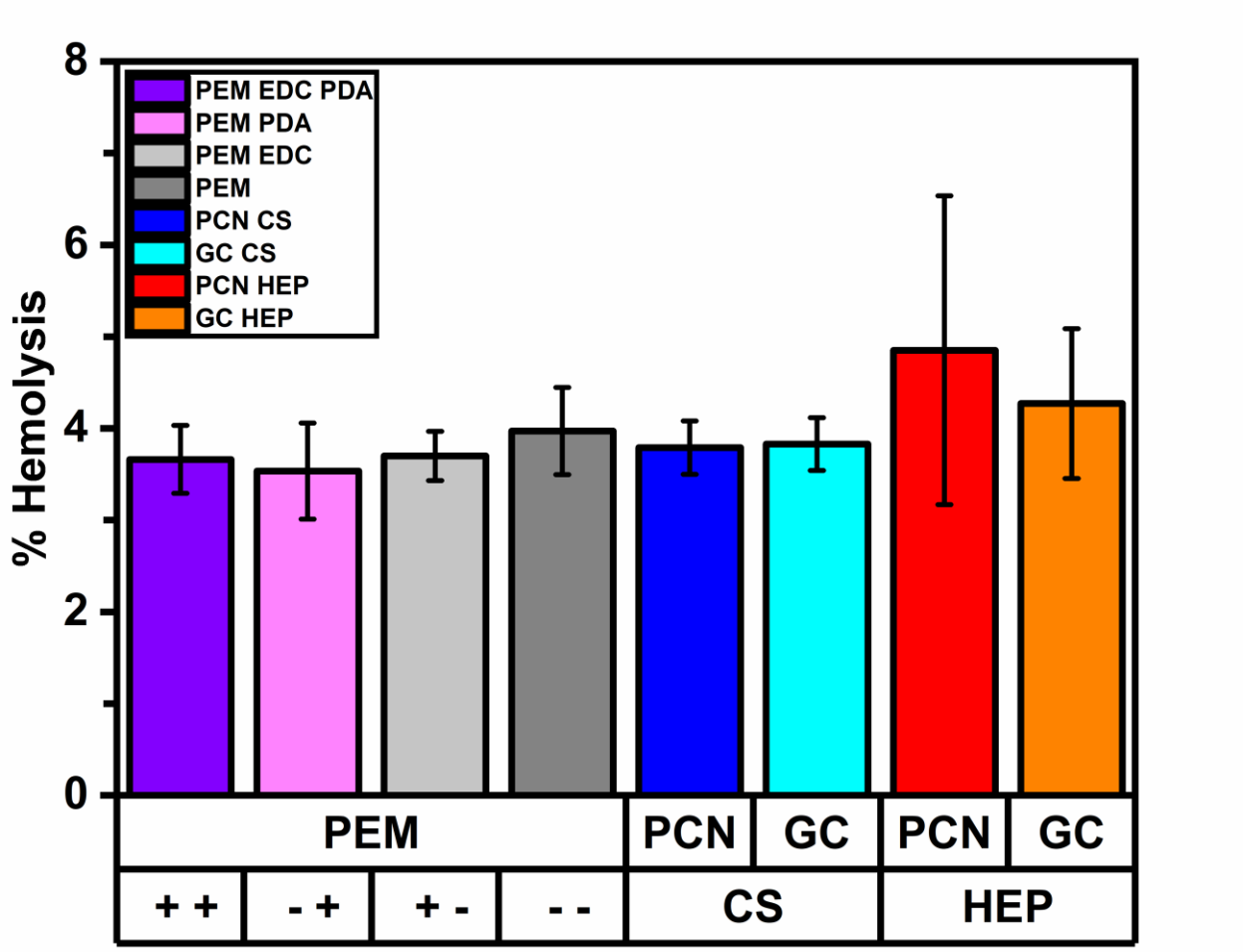


**Figure 4.5.** Percent hemolysis values for PEM EDC PDA, PEM PDA, PEM EDC, PEM, PCN CS, GC CS, PCN HEP, and GC HEP surfaces after 3 h exposure to RBC solutions (mean ± standard deviation) (n= 4). The "++" symbol corresponds to treatment with PDA and EDC, "- +" corresponds to treatment with PDA and not EDC, "+ -" corresponds to no PDA and treatment with EDC, and "- -" corresponds to untreated PEM. A two-way ANOVA with a pairwise comparisons was conducted to determine differences between surface chemistry/treatment (+ +, - +, + -, - -, CS, or HEP) and surface type (PEM, PCN, or GC).

### 4.3.4. Whole blood evaluations of modified surfaces

To evaluate how surfaces influenced whole blood clotting, surfaces were submerged in donor blood for 30 minutes and the blood was then evaluated via TEG. Thromboelastography is a technique that was first developed as a non-invasive method to guide transfusions in 1948, and since then has become a widely used clinical technique

to monitor blood coagulation parameters.[55,61] Thromboelastography uses the changes in viscosity of clotting blood to assign parameters that are relevant to different stages and components in blood coagulation (Figure 4.S2). These parameters are defined as: reaction time (R), clot time (K), α-angle (A), and clot strength (MA). These parameters reveal important information about clot dynamics on their own, and they are also used to calculate coagulation index values (CI), which assesses the overall coagulation status.[55]

**Figure 4.6** shows the control normalized values obtained for reaction time, clot time, α-angle, and clot strength form TEG analysis for different sample types, where glass pucks were used as controls. The reaction time corresponds to the cellular initiation phase of blood coagulation, during which factor XII is contact activated, which results in the production of thrombin and the resulting initial fibrin polymerization.[55,62–64] A normalized reaction time value of 1 corresponds to the control surface; a value greater than one indicates that activation is slowed (longer reaction time) and a value less than one indicates that activation is accelerated (shorter reaction time) compared to glass controls. HEP PCN terminated surfaces did not form a detectable clot after 1 hr. Additionally, reaction time is significantly increased for GC HEP terminated surfaces as compared to other surface treatments. These results reflect HEP's mechanism for inhibiting coagulation. HEP promotes the activity of anti-thrombin which inactivates thrombin and other activated factors, thus inhibiting fibrin formation and preventing clot initiation.[65,66] The PCNs are created by electrostatic interactions between HEP and CHI, whereas HEP is covalently bound to a HA backbone in the GCs. The HEP in the PCNs may more easily dissipate into the blood, while the HEP in the GCs may remain localized to the surface due to the difference between electrostatic and covalent bond strengths.

With respect to the interaction with antithrombin, HEP behaves as a classically recycled catalyst. Therefore, HEP released from the surfaces during the incubation with blood (prior to the TEG experiment) will continue to inhibit blood coagulation until it is removed or degraded. Normalized reaction time values for the non-HEP terminated surfaces are close to one, indicating that they are similar to the corresponding glass control values (**Table 4.S3** and Figure 4.6).

Clot time (K) corresponds to the amplification phase of coagulation, during which platelets are recruited to the site of clot formation. Recruited platelets become activated, and they subsequently release pro-coagulation factors leading to the conversion of fibrinogen to fibrin.[55,62–64] Clot time measurements are dependent in part on fibrinogen and platelet concentrations.[55,62–64] GC HEP terminated surfaces had a significantly increased clot time compared to other surface types. This is also related to the anticoagulant activity of HEP which can reduce the concentration of active fibrin in the blood. All the treated surfaces increase the clot time, compared to the untreated glass controls (Table 4.S3 and Figure 4.6).

The speed at which the propagation phase is initiated and carried out is partially characterized by α-angle (A).[55] The propagation phase of coagulation is characterized by platelet aggregation, a large spike in fibrin formation, and the polymerization of fibrin fibers on the surfaces of platelets to form a stable clot.[62–64] The change in α-angle is due to the speed of thrombin generation, fibrin deposition, and fibrin cross-linking.[55] GC HEP surfaces result in a reduced α-angle compared to other surfaces types, except for the PEM PDA surfaces which have a high variability in α-angle values. The reduced angle corresponds to a slower rate of thrombin generation and a slow progression of the

propagation phase of coagulation, which is also likely due to the anticoagulant activity of HEP.

The final parameter taken from the TEG curve is clot strength (MA). This parameter is the maximal mechanical strength of the resulting clot and depends on the abundance of GPIIb/IIIa interactions, fibrin cross-linking, and clot contraction.[55] Clot strength is affected by thrombocytopenia (low platelet counts) or anti-platelet agents (and fibrinogen concentration). GC HEP surfaces have significantly reduced clot strength to other sample types. When used clinically, HEP can be associated with thrombocytopenia which is a result of platelet aggregation due to HEP's interactions with platelet factor 4 (PF4).[67,68]

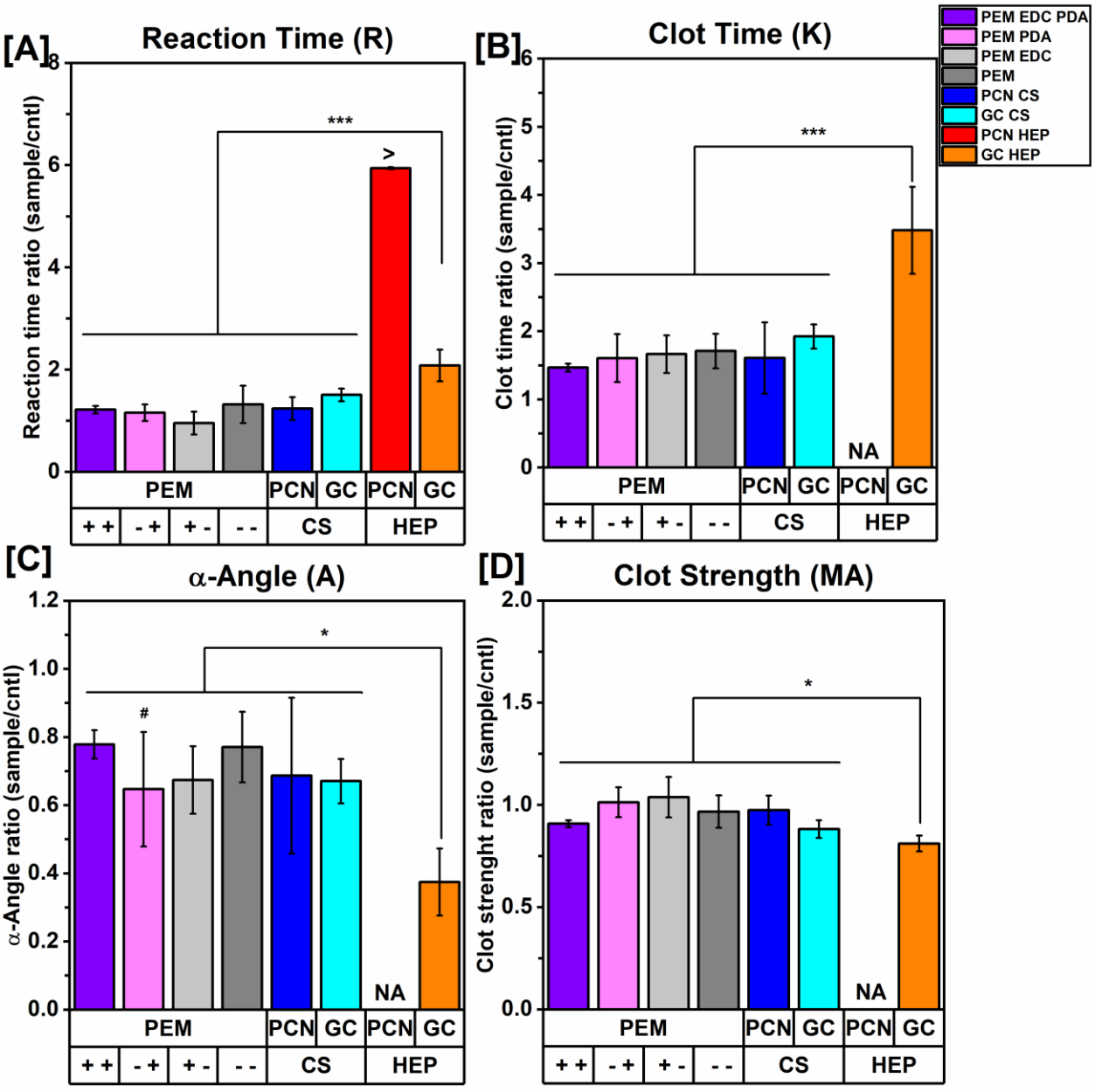


**Figure 4.6.** Values normalized to glass controls for [A] reaction time [B] clot time [C] α-angle [D] clot strength (mean ± standard deviation) (*n* = 4-5 for all samples except for untreated PEM which has an *n* = 8, and PCN HEP surfaces which did not clot) for PEM EDC PDA, PEM PDA, PEM EDC, PEM, PCN CS, GC CS, PCN HEP, and GC HEP surfaces. The "++" symbol corresponds to treatment with PDA and EDC, "- +" corresponds to treatment with PDA and not EDC, "+ -" corresponds to no PDA and treatment with EDC, and "- -" corresponds to untreated PEM. A two-way ANOVA with a pairwise comparisons was conducted to determine differences between surface chemistry/treatment (+ +, - +, + -, - -, CS, or HEP) and surface type (PEM, PCN, or GC). All differences in samples are due to chemistry/treatment and not surface type. Asterisks indicate the greatest significance value between one sample and all the other samples (*

$p < 0.05$; *** $p < 0.0005$). The # symbol on [C] denotes that there was no significant difference between GC HEP and PEM PDA. The addition of PCN HEP to the surface inhibited clot formation past 1 h, and the addition of GC HEP significantly influenced all parameters.

From the TEG parameters coagulation index values can be calculated to assess overall coagulation status. A normal clot index for young healthy individuals is defined as three standard deviations from the mean of zero (-3.0 to 3.0).[55] Deviations outside of this range may indicate an abnormal coagulation state with lower values indicating coagulopathy (impaired ability to clot) and higher values a hypercoagulable state (an abnormally increased tendency for blood clotting).[55] In **Figure 4.7** normalized clot index values are plotted with the normal range (adjusted to normalization of controls) as dashed black lines with the standard deviation due to controls as grey dotted lines. There were no significant differences between clot index values, despite GC HEP surfaces having significantly different values for parameters. PCN HEP samples were not included in this analysis as they did not form a clot and thus clot index values cannot be calculated. Median values for all clot indices (including controls, Table 4.S3) were within the normal clot index range. These findings show that exposure to these surfaces does not affect donor blood when not in direct contact with the surfaces, except for the PCN HEP surfaces.

The interaction with blood on the surfaces was also evaluated by allowing blood to clot directly onto samples for 1 h, and then fixing surfaces to be imaged with SEM. **Figure 4.8** shows that all surface types did not have direct clot formation on the surface whereas the glass control had substantial clot formation on the surface.[20] Additionally, HEP-terminated surfaces have activated leukocytes adhered to their surfaces, while other

surfaces do not. HEP binds stimulated leukocytes through its interactions with the integrin Mac-1.[69–71]

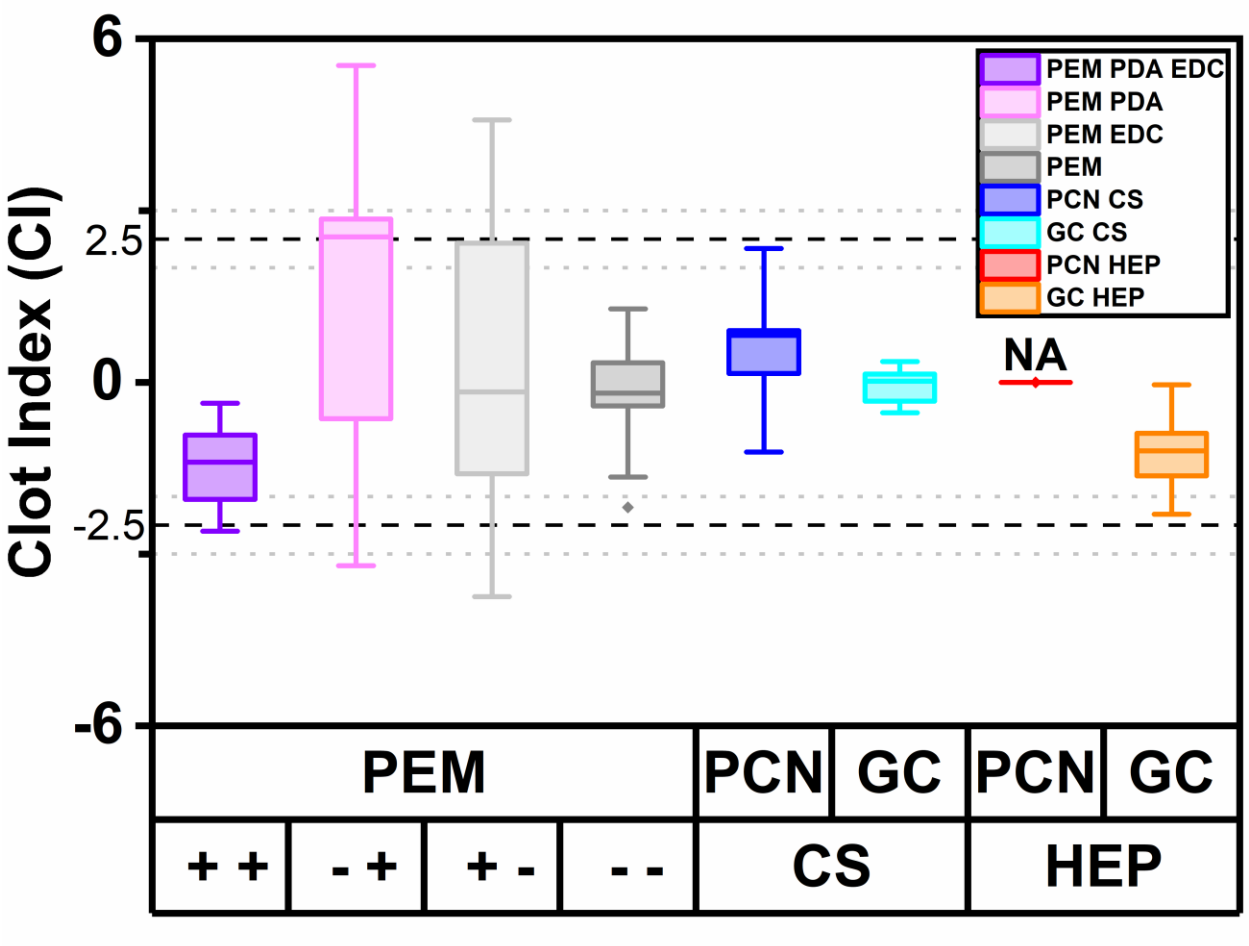


**Figure 4.7.** Clot index (CI) values were calculated from **Eq.1** using normalized values of reaction time, clot time, alpha angle, and clot strength for PEM EDC PDA, PEM PDA, PEM EDC, PEM, PCN CS, GC CS, PCN HEP, and GC HEP surfaces (n= 4-5 for all samples except for untreated PEM which has an n = 8, and PCN HEP surfaces which did not clot). For the box and whiskers plot: the brackets represent the standard deviation, the box area represents the area between 25% and 75% quartile, the solid line corresponds to the median, and diamonds are points that are outliers. The "++" symbol corresponds to treatment with PDA and EDC, "- +" corresponds to treatment with PDA and not EDC, "+ -" corresponds to no PDA and treatment with EDC, and "- -" corresponds to untreated PEM. The dashed, black lines at 2.5 and -2.5 represent the normal range for clot values normalized to control values (i.e., 3.0/CNTL CI and -3.0/CNTL CI), and the dotted, grey lines are ± standard deviation for those values. The addition of PCN HEP to the surface inhibited clot formation past 1 h, and GC HEP surfaces were only significantly

different from PCN CS surfaces. A clot value below the normal range signifies coagulopathy, and a clot value above the normal range indicates a hypercoagulable state.

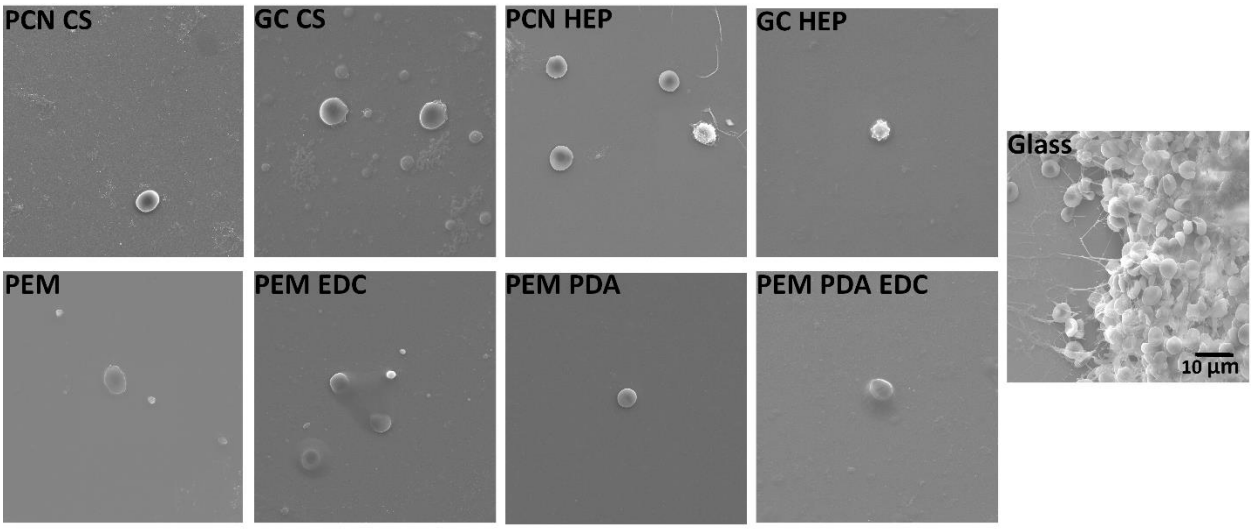


**Figure 4.8.** SEM images (1000x magnification) of surfaces after incubation with whole blood after 1 hr. All surfaces had reduced clot activity compared to glass control, but all blood in sample wells formed clots after 1 hr.

### 4.4. Discussion

The addition of PDA and EDC did increase surface durability of PEMs, but there is still evidence of surface modification resulting from fluid shear. The resulting surfaces may be more suitable for low-shear rate and no-shear rate applications (*e.g.*, blood bags) or short-term applications (*e.g.*, biosensors, microfluidic diagnostics).[72] The addition of PDA to the surface also changed the surface morphology by increasing nanoscale roughness. Increasing the roughness of the surfaces may have a beneficial effect on that the interactions of blood components with the surface. Pervious work has shown that increasing roughness of surfaces (by the addition of nanoparticles, nanotubes, and fibers) while keeping the chemistry the same can inhibit fibrin polymerization, decrease pro-inflammatory responses in leukocytes, platelet adhesion, and thrombogenicity.[7,9,24,73–76]

When comparing the PDA EDC surfaces to unmodified PEMs in whole blood and hemolysis experiments the modifications made to increase durability did not significantly change hemocompatibility. The addition of HEP to the surfaces did significantly influence the TEG parameters and caused leukocyte attachment. Additionally, in previous work we observed platelet aggregation on the surface of our PCN HEP samples.[3] The large aggregation of platelets is not observed in Figure 4.8 on our HEP-terminated surfaces. This difference may be due to differences in experimental set up. Previous work was conducted with platelet rich plasma where EDTA anti-coagulant was not inactivated. In the current work for SEM experiments we inactivated the sodium citrate which allowed formation of a large blood clot in the well, which is largely made of platelets. In the clot formation preferentially occurred in other parts of the well which outcompeted the HEP active sites for platelets

TEG was used to evaluate the systemic effects that exposure to the designed surfaces had on whole blood clot formation. For TEG experiments the samples were submerged in whole citrated blood. The citrate was not inactivated until the blood was transferred from the tubes containing the samples to the TEG cups. The blood was not allowed to clot until it was removed from the samples, and because the surfaces were able to clot (besides PCN HEP) we can say that they have a localized effect. PCN HEP surfaces seem to have a non-localized anti-coagulation effect. This may lead to systemic effects of anti-coagulation which can be associated with side-effects such as bleeding disorders.[77] These risks would need to be evaluated in future animal studies. The GC HEP surfaces did not have this effect, and though from the TEG parameters the anti-coagulation effects of HEP can be observed, the blood was able to clot in a normal clot

index range. These findings suggest that the GC HEP surfaces show the most promise in their ability to locally inhibit coagulation.

Taken together the PEM PDA EDC surfaces that were designed to improve PEM adherence to substrates were able to withstand shear forces better compared to unmodified PEMs, and the HEP-containing surfaces were able to influence blood coagulation. All surfaces besides PCN HEP surfaces were able to have a localized effect on the blood. The GC HEP surfaces were improved from the PCN HEP surfaces where the GC samples had a more localized approach. We were able to show that we can improve mechanical durability of the surfaces, the modifications to improve durability did not negatively influence blood compatibility, and the surfaces were able to be further modified to improve biological reactions. Future work could focus on combining PEM PDA EDC surfaces with GC HEP surfaces that are covalently adhered to the modified PEMs.

### 4.5. Conclusions

In this work we characterize new modified versions of our PEM surfaces that were made to increase their mechanical stability. The addition of PDA and EDC-NHS crosslinking created a more durable surface as demonstrated by XPS results after exposure to shear flow. The application of fluid shear modifies the structure of the surface coatings, exposing underlying substrate. While these surfaces show promise for blood-contacting applications, they should primarily be investigated for short-term applications, and applications for which there is low fluid shear. Future work could focus on adhering PEM surfaces to specific substrates with a more focused approach. We were also able to compare these surfaces to PEMs that are modified to have better interactions with the

surrounding biology by taking a biomimetic approach. GC HEP surfaces showed the most promise in influencing blood coagulation locally. PCN HEP surfaces inhibited coagulation altogether, even when the blood was no longer in contact with the surfaces indicating possible complications with the effects not being localized. Modifications to the PEM surfaces to increase durability did not have a significant effect on its interactions with whole blood. Future work may focus on PEM EDC PDA surfaces with GC HEP mimics covalently attached to surfaces, further improving the mechanical stability. The attachment strategy would have to be such that the biological function of the HEP is not compromised. Overall, the surfaces developed in this work show improvements form the untreated PEMs in their stability, and the adsorption of GC HEP to the surface has been identified as the best improvement to the PEM surfaces for use in future work. By combining two different approaches to surface design, we were able to evaluate what strategies could be combined to make future surfaces that will perform better when in contact with blood for long-term applications. Few researchers have evaluated materials for both durability and hemocompatibility and have evaluated two different design strategies for both. From this work we have developed new PEM PDA EDC surfaces that were designed for mechanical stability and compared them to surfaces that are designed for biocompatibility. Using this strategy, we were able to confirm increased mechanical stability, and have a clear direction for future surface combinations. Evaluating surfaces over several design criteria can push the development of future surfaces that are more blood compatible for long-term applications.

## Citations


1. Jin, Y. *et al.* A facile heparin/carboxymethyl chitosan coating mediated by polydopamine on implants for hemocompatibility and antibacterial properties. *Appl. Surf. Sci.* **528**, 146539 (2020).

2. Larkin, A. L., Davis, R. M. & Rajagopalan, P. Biocompatible, Detachable, and Free-Standing Polyelectrolyte Multilayer Films. *Biomacromolecules* **11**, 2788–2796 (2010).

3. Vlcek, J. R., Hedayati, M., Melvin, A. C., Reynolds, M. M. & Kipper, M. J. Blood-Compatible Materials: Vascular Endothelium-Mimetic Surfaces that Mitigate Multiple Cell-Material Interactions. *Adv. Healthc. Mater.* 2001748 (2021) doi:10.1002/adhm.202001748.

4. Wigmosta, T. B., Popat, K. C. & Kipper, M. J. Bone morphogenetic protein-2 delivery from polyelectrolyte multilayers enhances osteogenic activity on nanostructured titania. *J. Biomed. Mater. Res. A* **109**, 1173–1182 (2021).

5. Madruga, L. Y. C. *et al.* Carboxymethyl-kappa-carrageenan: A study of biocompatibility, antioxidant and antibacterial activities. *Int. J. Biol. Macromol.* **152**, 483–491 (2020).

6. Martins, A. F. *et al.* Chitosan/iota-carrageenan and chitosan/pectin polyelectrolyte multilayer scaffolds with antiadhesive and bactericidal properties. *Appl. Surf. Sci.* **502**, 144282 (2020).

7. Simon-Walker, R. *et al.* Glycocalyx-Inspired Nitric Oxide-Releasing Surfaces Reduce Platelet Adhesion and Activation on Titanium. *ACS Biomater. Sci. Eng.* **3**, 68–77 (2017).

8. Jiang, X., Wang, P., Liang, R. & Qin, W. Improving the Biocompatibility of Polymeric Membrane Potentiometric Ion Sensors by Using a Mussel-Inspired Polydopamine Coating. *Anal. Chem.* acs.analchem.9b00039 (2019) doi:10.1021/acs.analchem.9b00039.

9. Hedayati, M., Reynolds, M. M., Krapf, D. & Kipper, M. J. Nanostructured Surfaces That Mimic the Vascular Endothelial Glycocalyx Reduce Blood Protein Adsorption and Prevent Fibrin Network Formation. *ACS Appl. Mater. Interfaces* **10**, 31892–31902 (2018).

10. Facchi, S. P. *et al.* Polycationic condensed tannin/polysaccharide-based polyelectrolyte multilayers prevent microbial adhesion and proliferation. *Eur. Polym. J.* **130**, 109677 (2020).

11. Criado-Gonzalez, M., Mijangos, C. & Hernández, R. Polyelectrolyte Multilayer Films Based on Natural Polymers: From Fundamentals to Bio-Applications. *Polymers* **13**, 2254 (2021).

12. Boulmedais, F. *et al.* Polyelectrolyte multilayer films with pegylated polypeptides as a new type of anti-microbial protection for biomaterials. *Biomaterials* **25**, 2003–2011 (2004).

13. da Câmara, P. C. F. *et al.* Polyelectrolyte multilayers containing a tannin derivative polyphenol improve blood compatibility through interactions with platelets and serum proteins. *Mater. Sci. Eng. C* **112**, 110919 (2020).

14. Sabino, R. M., Mondini, G., Kipper, M. J., Martins, A. F. & Popat, K. C. Tanfloc/heparin polyelectrolyte multilayers improve osteogenic differentiation of adipose-derived stem cells on titania nanotube surfaces. *Carbohydr. Polym.* **251**, 117079 (2021).

15. Guillot, R. *et al.* The stability of BMP loaded polyelectrolyte multilayer coatings on titanium. *Biomaterials* **34**, 5737–5746 (2013).

16. Romero, R. *et al.* Coating cortical bone allografts with periosteum-mimetic scaffolds made of chitosan, trimethyl chitosan, and heparin. *Carbohydr. Polym.* **122**, 144–151 (2015).

17. Vlcek, J. R., Reynolds, M. M. & Kipper, M. J. Enzymatic Degradation of Glycosaminoglycans and Proteoglycan-Mimetic Materials in Solution and on Polyelectrolyte Multilayer Surfaces. *Biomacromolecules* acs.biomac.1c00720 (2021) doi:10.1021/acs.biomac.1c00720.

18. Alphonsus, C. S. & Rodseth, R. N. The endothelial glycocalyx: a review of the vascular barrier. *Anaesthesia* **69**, 777–784 (2014).

19. Reitsma, S., Slaaf, D. W., Vink, H., van Zandvoort, M. A. M. J. & oude Egbrink, M. G. A. The endothelial glycocalyx: composition, functions, and visualization. *Pflüg. Arch. - Eur. J. Physiol.* **454**, 345–359 (2007).

20. Liu, X. *et al.* Blood compatible materials: state of the art. *J. Mater. Chem. B* **2**, 5718–5738 (2014).

21. Reviakine, I. *et al.* Stirred, shaken, or stagnant: What goes on at the blood–biomaterial interface. *Blood Rev.* **31**, 11–21 (2017).

22. Hedayati, M., Neufeld, M. J., Reynolds, M. M. & Kipper, M. J. The quest for blood-compatible materials: Recent advances and future technologies. *Mater. Sci. Eng. R Rep.* **138**, 118–152 (2019).

23. Larm, O., Larsson, R. & Olsson, P. A New Non-Thrombogenic Surface Prepared by Selective Covalent Binding of Heparin Via a Modified Reducing Terminal Residue. *Biomater. Med. Devices Artif. Organs* **11**, 161–173 (1983).

24. Hedayati, M., Marruecos, D. F., Krapf, D., Kaar, J. L. & Kipper, M. J. Protein adsorption measurements on low fouling and ultralow fouling surfaces: A critical comparison of surface characterization techniques. *Acta Biomater.* **102**, 169–180 (2020).

25. Wang, B. *et al.* Antigenically shielded universal red blood cells by polydopamine-based cell surface engineering. *Chem Sci* **5**, 3463–3468 (2014).

26. Hauser, D., Septiadi, D., Turner, J., Petri-Fink, A. & Rothen-Rutishauser, B. From Bioinspired Glue to Medicine: Polydopamine as a Biomedical Material. *Materials* **13**, 1730 (2020).

27. Lee, H., Dellatore, S. M., Miller, W. M. & Messersmith, P. B. Mussel-Inspired Surface Chemistry for Multifunctional Coatings. *Science* **318**, 426–430 (2007).

28. Pop-Georgievski, O. *et al.* Nonfouling Poly(ethylene oxide) Layers End-Tethered to Polydopamine. *Langmuir* **28**, 14273–14283 (2012).

29. Mousavi, S. M., Zarei, M. & Hashemi, S. A. R. Polydopamine for Biomedical Application and Drug Delivery System. *Med. Chem.* **08**, (2018).

30. Yang, Y. *et al.* Polydopamine Modified $TiO_2$ Nanotube Arrays for Long-Term Controlled Elution of Bivalirudin and Improved Hemocompatibility. *ACS Appl. Mater. Interfaces* **10**, 7649–7660 (2018).

31. Kwon, I. S. & Bettinger, C. J. Polydopamine nanostructures as biomaterials for medical applications. *J. Mater. Chem. B* **6**, 6895–6903 (2018).

32. Liu, M. *et al.* Recent developments in polydopamine: an emerging soft matter for surface modification and biomedical applications. *Nanoscale* **8**, 16819–16840 (2016).

33. Hong, S. *et al.* Attenuation of the *in vivo* toxicity of biomaterials by polydopamine surface modification. *Nanomed.* **6**, 793–801 (2011).

34. Lee, H. A., Park, E. & Lee, H. Polydopamine and Its Derivative Surface Chemistry in Material Science: A Focused Review for Studies at KAIST. *Adv. Mater.* **32**, 1907505 (2020).

35. Leung, J. M. *et al.* Surface modification of poly(dimethylsiloxane) with a covalent antithrombin–heparin complex for the prevention of thrombosis: use of polydopamine as bonding agent. *J. Mater. Chem. B* **3**, 6032–6036 (2015).

36. Black, K. C., Yi, J., Rivera, J. G., Zelasko-Leon, D. C. & Messersmith, P. B. Polydopamine-enabled surface functionalization of gold nanorods for cancer cell-targeted imaging and photothermal therapy. *Nanomed.* **8**, 17–28 (2013).

37. He, S. *et al.* Antibiotic-decorated titanium with enhanced antibacterial activity through adhesive polydopamine for dental/bone implant. *J. R. Soc. Interface* **11**, 20140169 (2014).

38. Sun, X. *et al.* bFGF-grafted electrospun fibrous scaffolds via poly(dopamine) for skin wound healing. *J Mater Chem B* **2**, 3636–3645 (2014).

39. Ghorbani, F. *et al.* Decoration of electrical conductive polyurethane-polyaniline/polyvinyl alcohol matrixes with mussel-inspired polydopamine for bone tissue engineering. *Biotechnol. Prog.* **36**, (2020).

40. Tang, P. *et al.* Mussel-Inspired Electroactive and Antioxidative Scaffolds with Incorporation of Polydopamine-Reduced Graphene Oxide for Enhancing Skin Wound Healing. *ACS Appl. Mater. Interfaces* **11**, 7703–7714 (2019).

41. Huang, S., Liang, N., Hu, Y., Zhou, X. & Abidi, N. Polydopamine-Assisted Surface Modification for Bone Biosubstitutes. *BioMed Res. Int.* **2016**, 1–9 (2016).

42. Gholami Derami, H. *et al.* Reversible Photothermal Modulation of Electrical Activity of Excitable Cells using Polydopamine Nanoparticles. *Adv. Mater.* 2008809 (2021) doi:10.1002/adma.202008809.

43. Kang, S. M. *et al.* One-Step Multipurpose Surface Functionalization by Adhesive Catecholamine. *Adv. Funct. Mater.* **22**, 2949–2955 (2012).

44. Ryu, J. H., Messersmith, P. B. & Lee, H. Polydopamine Surface Chemistry: A Decade of Discovery. *ACS Appl. Mater. Interfaces* **10**, 7523–7540 (2018).

45. Hedayati, M. & Kipper, M. J. Atomic force microscopy of adsorbed proteoglycan mimetic nanoparticles: Toward new glycocalyx-mimetic model surfaces. *Carbohydr. Polym.* **190**, 346–355 (2018).

46. Kipper, M. J. & Place, L. W. Preparation of Proteoglycan Mimetic Graft Copolymers. in *Macro-Glycoligands* (ed. Sun, X.-L.) vol. 1367 69–86 (Springer New York, 2016).

47. Place, L. W., Kelly, S. M. & Kipper, M. J. Synthesis and Characterization of Proteoglycan-Mimetic Graft Copolymers with Tunable Glycosaminoglycan Density. *Biomacromolecules* **15**, 3772–3780 (2014).

48. Boddohi, S., Moore, N., Johnson, P. A. & Kipper, M. J. Polysaccharide-Based Polyelectrolyte Complex Nanoparticles from Chitosan, Heparin, and Hyaluronan. *Biomacromolecules* **10**, 1402–1409 (2009).

49. Place, L. W., Sekyi, M. & Kipper, M. J. Aggrecan-Mimetic, Glycosaminoglycan-Containing Nanoparticles for Growth Factor Stabilization and Delivery. *Biomacromolecules* **15**, 680–689 (2014).

50. Sakariassen, K. S., Orning, L. & Turitto, V. T. The impact of blood shear rate on arterial thrombus formation. *Future Sci. OA* **1**, fso.15.28 (2015).

51. Dodson, A. G., Townsend, P. & Walters, K. Non-Newtonian flow in pipes of non-circular cross section. *Comput. Fluids* **2**, 317–338 (1974).

52. Fournier, Ronald L. *Basic Transport Pheomena in Biomedical Engineering*. (Talor & Francis, 2017).

53. Moravec, S. & Liepsch, D. Flow investigations in a model of a three-dimensional human artery with Newtonian and non-Newtonian fluidS. Part I. *Biorheology* **20**, 745–759 (1983).

54. Henkelman, S., Rakhorst, G., Blanton, J. & van Oeveren, W. Standardization of incubation conditions for hemolysis testing of biomaterials. *Mater. Sci. Eng. C* **29**, 1650–1654 (2009).

55. Shaydakov, M. E., Sigmon, D. F. & Blebea, J. Thromboelastography. in *StatPearls* (StatPearls Publishing, 2021).

56. Maraj, R., Jacobs, L. E., Ioli, A. & Kotler, M. N. Evaluation of hemolysis in patients with prosthetic heart valves. *Clin. Cardiol.* **21**, 387–392 (1998).

57. Sovadinova, I., Palermo, E. F., Huang, R., Thoma, L. M. & Kuroda, K. Mechanism of Polymer-Induced Hemolysis: Nanosized Pore Formation and Osmotic Lysis. *Biomacromolecules* **12**, 260–268 (2011).

58. Fischer, D., Li, Y., Ahlemeyer, B., Krieglstein, J. & Kissel, T. In vitro cytotoxicity testing of polycations: influence of polymer structure on cell viability and hemolysis. *Biomaterials* **24**, 1121–1131 (2003).

59. Kwon, Y.-I. I., Vattem, D. A. & Shetty, K. Evaluation of clonal herbs of Lamiaceae species for management of diabetes and hypertension. 12.

60. Farooq, M. *et al.* Synthesis, characterization and modification of Gum Arabic microgels for hemocompatibility and antimicrobial studies. *Carbohydr. Polym.* **156**, 380–389 (2017).

61. Hartert, H. Blutgerinnungsstudien mit der Thrombelastographie, einem neuen Untersuchungsverfahren. *Klin. Wochenschr.* **26**, 577–583 (1948).

62. Hoffman, M. & Monroe, D. M. A cell-based model of hemostasis. *Thromb. Haemost.* **85**, 958–965 (2001).

63. Smith, S. A. The cell-based model of coagulation. *J. Vet. Emerg. Crit. Care* **19**, 3–10 (2009).

64. Hoffman, M. Remodeling the Blood Coagulation Cascade. *J. Thromb. Thrombolysis* **16**, 17–20 (2003).

65. Hemker, H. C., Al Dieri, R. & Béguin, S. Heparins: A Shift of Paradigm. *Front. Med.* **6**, 254 (2019).

66. Sanchez, J., Elgue, G., Riesenfeld, J. & Olsson, P. Studies of Adsorption, Activation, and Inhibition of Factor XII on Immobilized Heparin. *Thromb. Res.* **89**, 41–50 (1998).

67. Mikhailov, D., Young, H. C., Linhardt, R. J. & Mayo, K. H. Heparin Dodecasaccharide Binding to Platelet Factor-4 and Growth-related Protein-α. *J. Biol. Chem.* **274**, 25317–25329 (1999).

68. Ahmed, I., Majeed, A. & Powell, R. Heparin induced thrombocytopenia: diagnosis and management update. *Postgrad. Med. J.* **83**, 575–582 (2007).

69. Coombe, D., Watt, S. & Parish, C. Mac-1 (CD11b/CD18) and CD45 mediate the adhesion of hematopoietic progenitor cells to stromal cell elements via recognition of stromal heparan sulfate. *Blood* **84**, 739–752 (1994).

70. Diamond, M. S., Alon, R., Parkos, C. A., Quinn, M. T. & Springer, T. A. Heparin is an adhesive ligand for the leukocyte integrin Mac-1 (CD11b/CD1). *J. Cell Biol.* **130**, 1473–1482 (1995).

71. Peter, K. *et al.* Heparin Inhibits Ligand Binding to the Leukocyte Integrin Mac-1 (CD11b/CD18). *Circulation* **100**, 1533–1539 (1999).

72. Spijker, H. On the influence of flow conditions and wettability on blood material interactions. *Biomaterials* **24**, 4717–4727 (2003).

73. Fedel, M. Hemocompatibility of Carbon Nanostructures. *C — J. Carbon Res.* **6**, 12 (2020).

74. Merkle, V. M. *et al.* Hemocompatibility of Poly(vinyl alcohol)–Gelatin Core–Shell Electrospun Nanofibers: A Scaffold for Modulating Platelet Deposition and Activation. *ACS Appl. Mater. Interfaces* **7**, 8302–8312 (2015).

75. Leszczak, V., Smith, B. S. & Popat, K. C. Hemocompatibility of polymeric nanostructured surfaces. *J. Biomater. Sci. Polym. Ed.* **24**, 1529–1548 (2013).

76. S. Smith, B., Capellato, P., Kelley, S., Gonzalez-Juarrero, M. & C. Popat, K. Reduced in vitro immune response on titania nanotube arrays compared to titanium surface. *Biomater. Sci.* **1**, 322–332 (2013).

77. Mazzeffi, M. *et al.* Bleeding, Transfusion, and Mortality on Extracorporeal Life Support: ECLS Working Group on Thrombosis and Hemostasis. *Ann. Thorac. Surg.* **101**, 682–689 (2016).

# CHAPTER 5: CONCLUSIONS

## Overview

The following sections conclude this dissertation by summarizing the important findings in previous chapters and outlines how the work contributes to the field of blood contacting materials. This is done by highlighting key findings of the work and discussing their impacts. Future directions of this work are presented in this section.

## 5.1 Aims and their conclusions

In this work we aimed to design blood compatible surfaces using a biomimetic approach. In our work, we defined a material to be blood compatible if it can inhibit coagulation locally at the site of the blood-material interface and does not illicit an inflammatory response or cause toxicity for the duration of the materials use. Like others proceeding us, we were not able to create truly blood compatible materials that inhibited coagulation locally for long term applications. We successfully combined polyelectrolyte multilayers with two different proteoglycan mimics to match the surface chemistry and topography of the endothelial glycocalyx. These surface designs were further modified to include a natural platelet inhibitor, nitric oxide (NO) release. To achieve the goal of producing biomimetic surfaces that improve hemocompatibility we evaluated and improved the surface designs through 3 separate aims:

**Aim 1:** Incorporate NO with polyelectrolyte complex nanoparticle (PCN) surfaces and evaluate their cell-surface interactions to determine potential blood compatibility.

**Aim 2:** Establish structure function relationships between enzymes and proteoglycan mimics when absorbed onto polyelectrolyte multilayers (PEM) surfaces and suspended in solution.

**Aim 3:** Design more durable PEM surfaces and evaluate the modified PEMs along with graft copolymer (GC), and PCN surfaces on their whole blood interactions to determine if design strategies to improve durability hinder blood-material interactions.

In the first aim we were able to design biomimetic surfaces that were able to reduce unfavorable cell-material interactions associated with coagulation (platelets), inflammation (macrophages and leukocytes), and infection (gram-negative and gram-positive bacteria). There was no one material that combined topography, chemistry, and dynamic NO release in such a way that it outperformed the other surface types in reducing unfavorable biological interactions with all the experiments tested. We concluded that material scientists and engineers should be designing multifunctional surfaces to better combat the multiple modes of failure when interacting with the complexities of biology. In aim two we added a new proteoglycan mimic to our work (GCs) that were constructed via covalent attachment instead of electrostatic interactions (PCNs). The two different proteoglycan mimics were evaluated against enzymatic degradation. We were able to develop structure function relationships between the structure and chemistry of the PG mimics used and the size and activity of the enzymes. From results of the second aim, we concluded that the modified surfaces were still intact after 21 d exposure to enzymes even though the enzymes were still able to act on the surfaces. Furthermore, we propose that more work like this needs to be done to establish the longevity of biomaterials so they can be better assessed for their applications.

In aim 3 we were able to successfully create modified PEM surfaces that had increased durability by FILL IN description here. We found that the changes made to the PEMs to increase their durability did not impact the material-blood interactions when compared to unmodified PEMs. These surfaces did not perform as well as biomimetic surfaces to inhibit coagulation at the surface of the material. From this work we evaluated PEM durability against shear flow for the first time and found that PEM surfaces are not stable under flow and the addition of PDA deposition and EDC crosslinking can improve durability. These new surfaces with increased durability can now be utilized in future studies to be evaluated in animal models.

**5.2 Future work**

Building off the surface modifications established in Aims 1 and 3, will lead to the development of further improved surfaces. The surfaces that were modified to increase mechanical durability could be combined with the PCNs and GCs to create surfaces that are more mechanically durable and have the added addition of the PG mimics. This proposed work could evaluate if PG mimics could be covalently bound to PEM surfaces while maintaining their bioactivity. Methods of conjugation to bind PG mimics to the surface of PEMs should be evaluated in a way that balances the preservation of the chemical functionality of the CS and HEP with improved durability. The overall strength of attachment between PEMs and substrate surfaces could also be improved by taking a targeted approach in which the PEMs are modified to adhere to one material type for a specific blood contacting device/application. Additionally, the PEM releasing surfaces established in chapter 2 (aim 1) could be evaluated for their mechanical stability, and

different conjugation strategies can be developed to increase durability while maintaining nitric oxide release.

Two of the main limitations to using TGA-CHI with nitrosation as an NO source was its limited NO release and the potential chemical modifications on CS and HEP during the nitrosation process. Other NO sources (such as metal organic frameworks (MOFS)) could be combined with the surface modifications described in this dissertation to create long term NO releasing materials. The new NO sources should be designed to not interact with the multifunctional GAGs of the PEMs, PCNs, and/or GCs.

The materials developed in this work should be further evaluated in vivo using animal models. Testing surfaces using in vitro systems are useful to establish relationships between materials and specific cell types/proteins/cell groups and determine potential failure before using animals. In vitro systems are unable to replicate the exact conditions as in living organisms. The in vivo experiments would have to be evaluated with a specific application in mind (stents, extracorporeal membranes, etc..) and the surfaces tested would have to be evaluated for their durability and sanitization procedures and sterile packaging of samples will have to be developed.

### 5.3 Overall impact

The work done in this dissertation has established the importance of designing biomimetic surfaces that are multifunctional, the importance of evaluating the viability of blood contacting surfaces against multiple modes of failure (i.e.: multiple cell-material interactions, enzymatic and mechanical durability, and whole blood clotting). This research has developed and described several new surface types that have not been

established before. The design criteria and evaluations that we established to be vital in representing the complexity of biology can be applied by other researchers hoping to develop blood compatible materials. The surfaces developed in this work show promise as blood contacting materials and can be further tested for potential uses in medicine or diagnostics. The surfaces developed can also be further modified or repurposed for other applications as they have shown promise in inhibiting unfavorable biological interactions outside of the field of blood compatibility. This dissertation resulted in new surfaces that improved interactions with the surrounding biology by mimicked key components of the endothelial glycocalyx, and fully evaluated these surfaces against multiple modes of failure. While true blood compatibility was not achieved, the materials developed, and the relationships made between surface features and biological processes significantly contribute to the field of blood contacting materials.

APPENDIX 1: SUPPLEMENTARY INFORMATION CHAPTER 2

## Overview

This section contains supplementary information from chapter 2 that was published with the corresponding manuscripts.

## Chapter 2 Supplementary Information

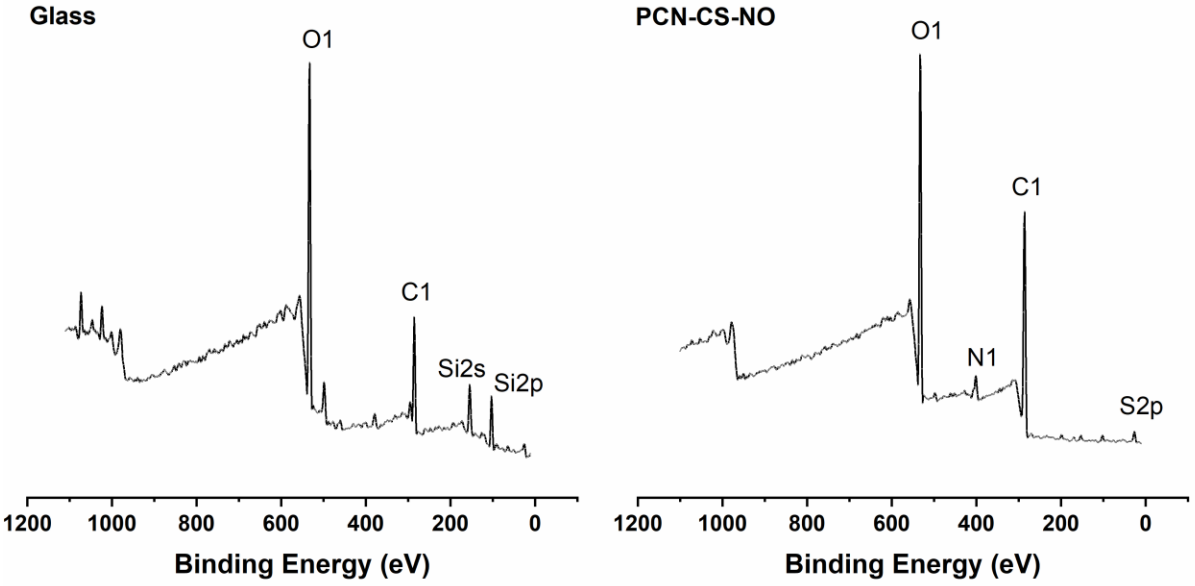


**Figure 2.S1**. Full XPS spectra for glass and PCN-CS-NO samples. O1s, N1s, C1s, Si2s, Si2p, and S2p peaks are labeled. The presence of N1s and S2p peaks indicates coverage of samples by our materials. The attenuation of Si peaks complete surface covered by PEMs and PCN.

**Table 2.S1**. Average Size, Polydispersity Index (PDI) and ζ potential plus/minus standard deviation of PCNs.

| PCN composition | hydrodynamic diameter [nm] | PDI | ζ potential [mV] |
|---|---|---|---|
| **CS – CHI TGA** | 250 ± 4 | 0.130 ± 0.007 | -33 ± 1 |
| **HEP – CHI TGA** | 238 ± 3 | 0.260 ± 0.008 | -25 ± 1 |

**Table 2.S2**. Root mean-square roughness, $R_q$ values (nm) of AFM images shown in Figure 2.3 of the main text. Two-factor ANOVA (with factors surface type and nitrosation) confirms that PCN addition, but not nitrosation leads to a significant difference in *Rq* ($p < 0.001$).

| | Root mean Square Roughness ($R_q$) [nm] | |
|---|---|---|
| **surface type** | **before treatment** | **after nitrosation** |
| **PEM** | 24.1 | 21.4 |
| **PCN-CS** | 45.5 | 34.4 |
| **PCN-HEP** | 47.6 | 37.7 |

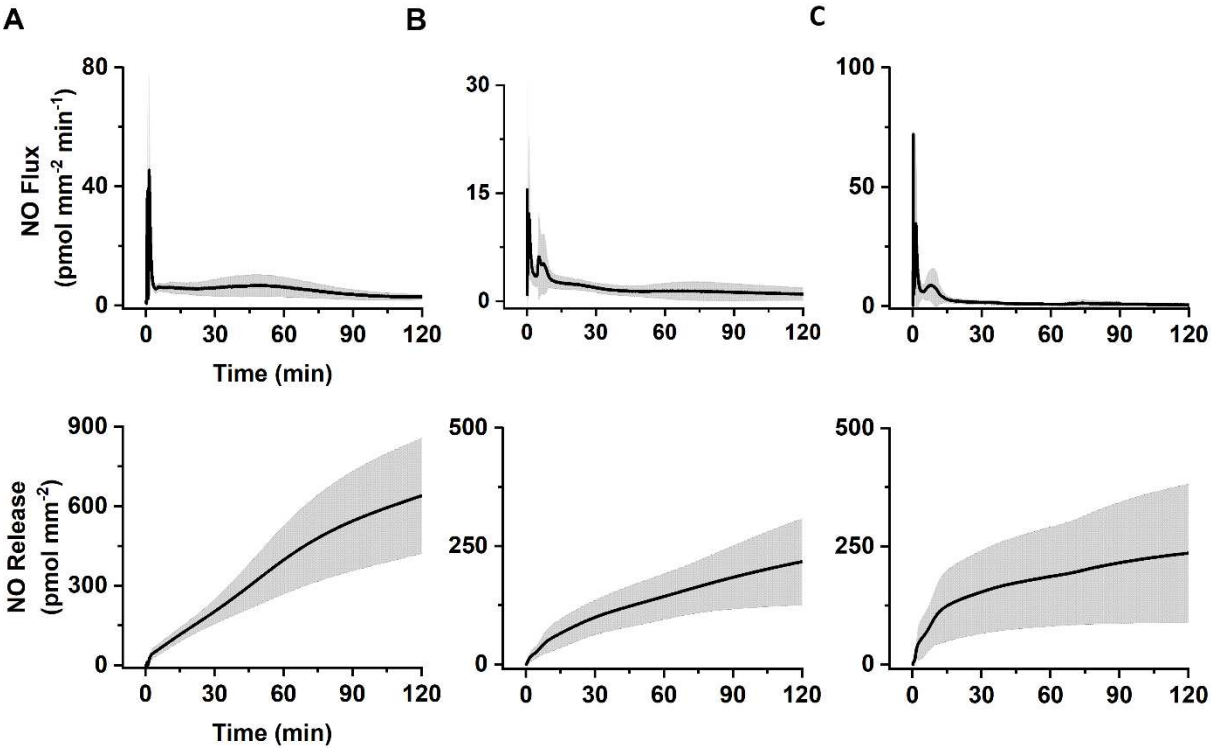


**Figure 2.S2**. NO flux (top row) and cumulative release (bottom row) for (A) PEM-NO, (B) PCN-CS-NO, and (C) PCN-HEP-NO.

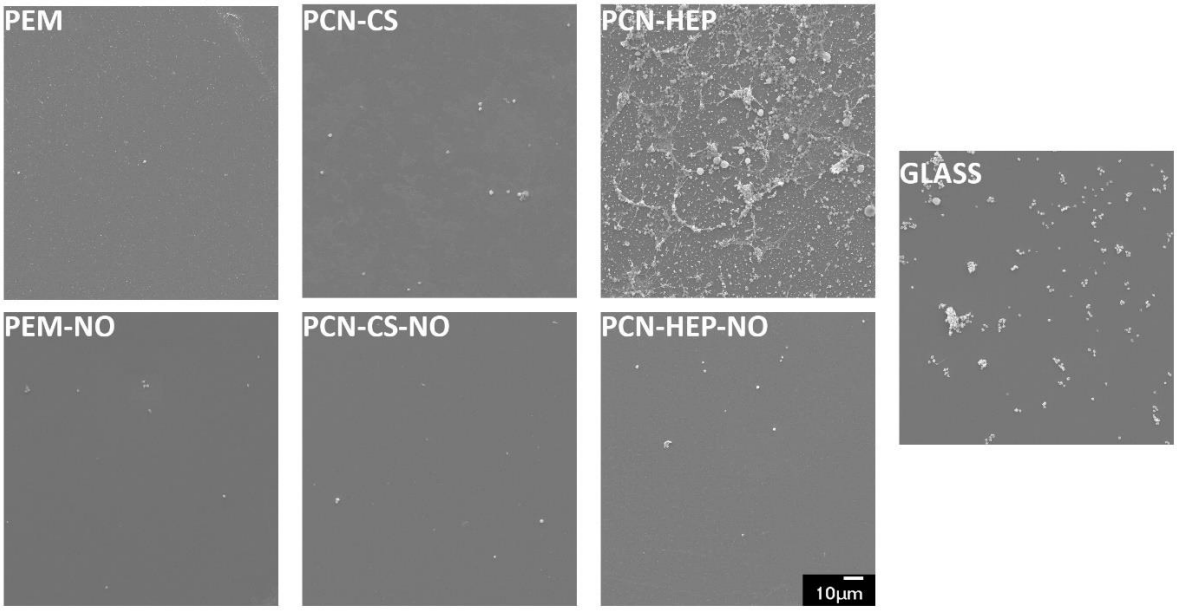


**Figure 2.S3**. Representative SEM images of samples and controls showing platelet adhesion onto surfaces.

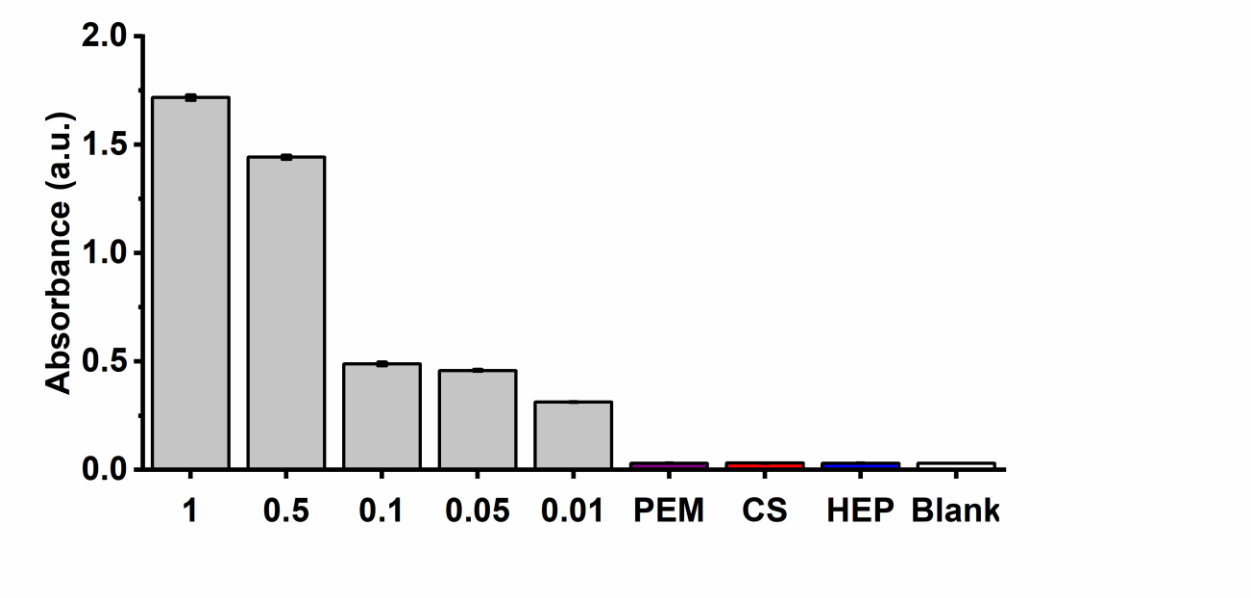


**Figure 2.S4**. Absorbance values for positive controls (1-0.01) in the units EU, negative control (blank), and samples for detection of endotoxins.

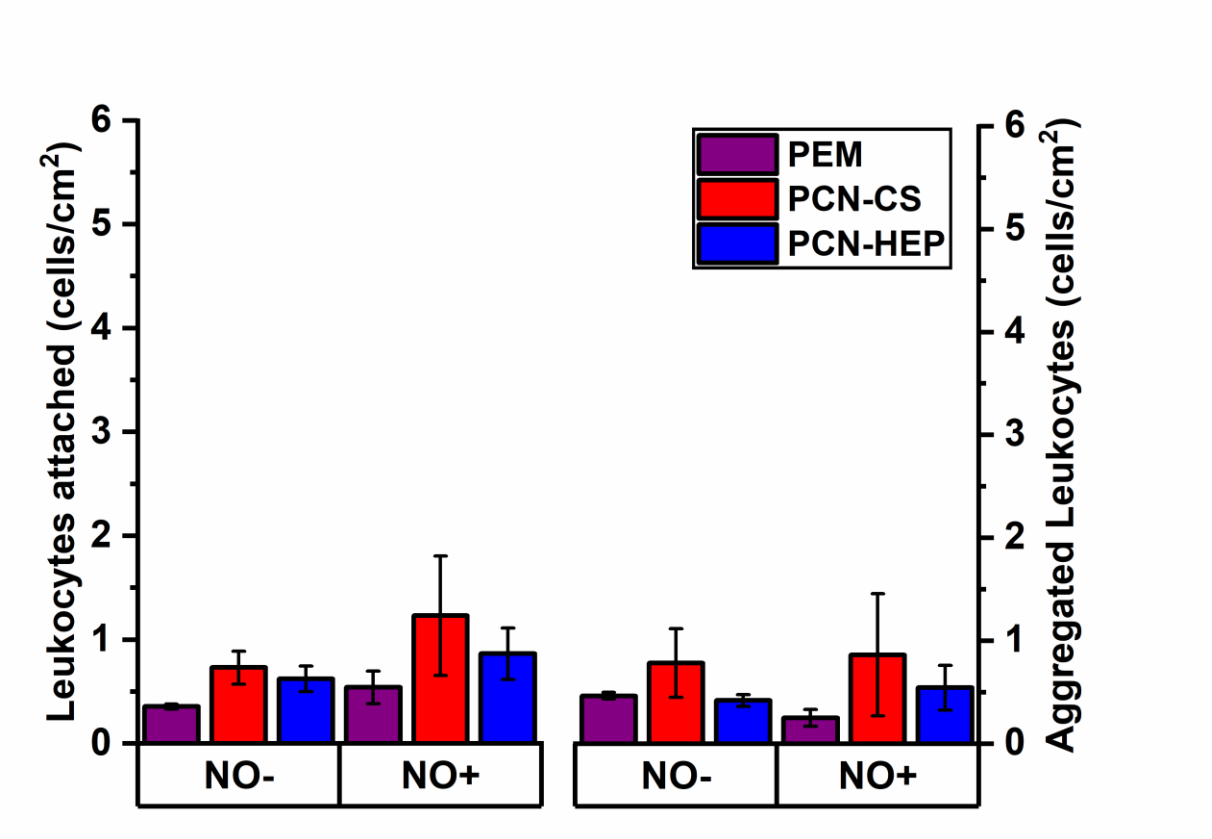


**Figure 2.S5**. Leukocyte attachment and aggregation after 4 d of incubation. Data are normalized to glass control. Two-factor ANOVA with post hoc Tukey test was conducted (on log-transformed data) where the factors are NO+/NO- and surface type. There are no significant differences.

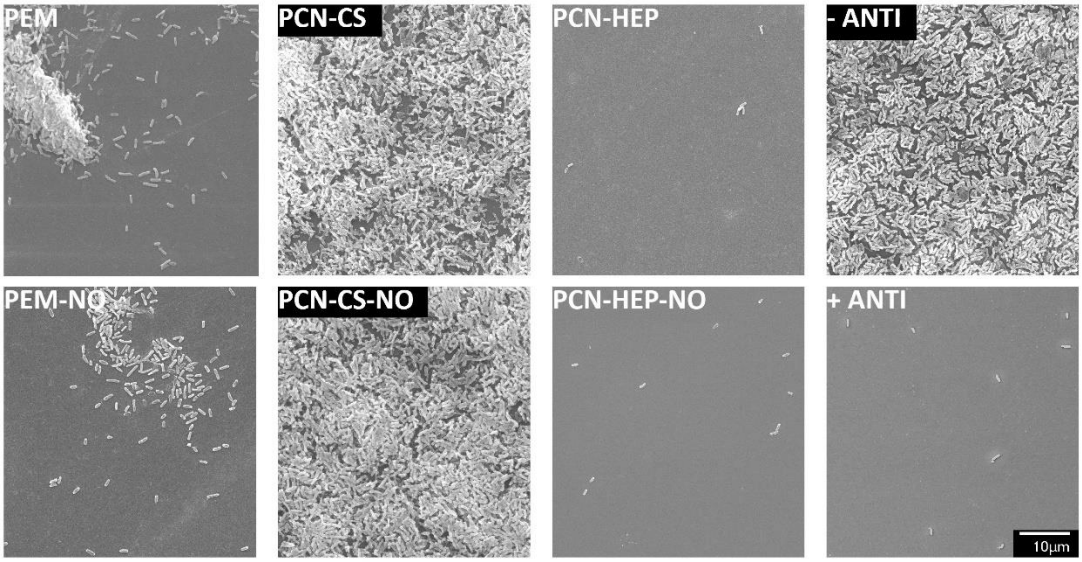


**Figure 2.S6**. Representative SEM images of samples and controls showing *Pseudomonas aeruginosa* attachment. Images are examples of samples after 6 h incubation at 37 °C.

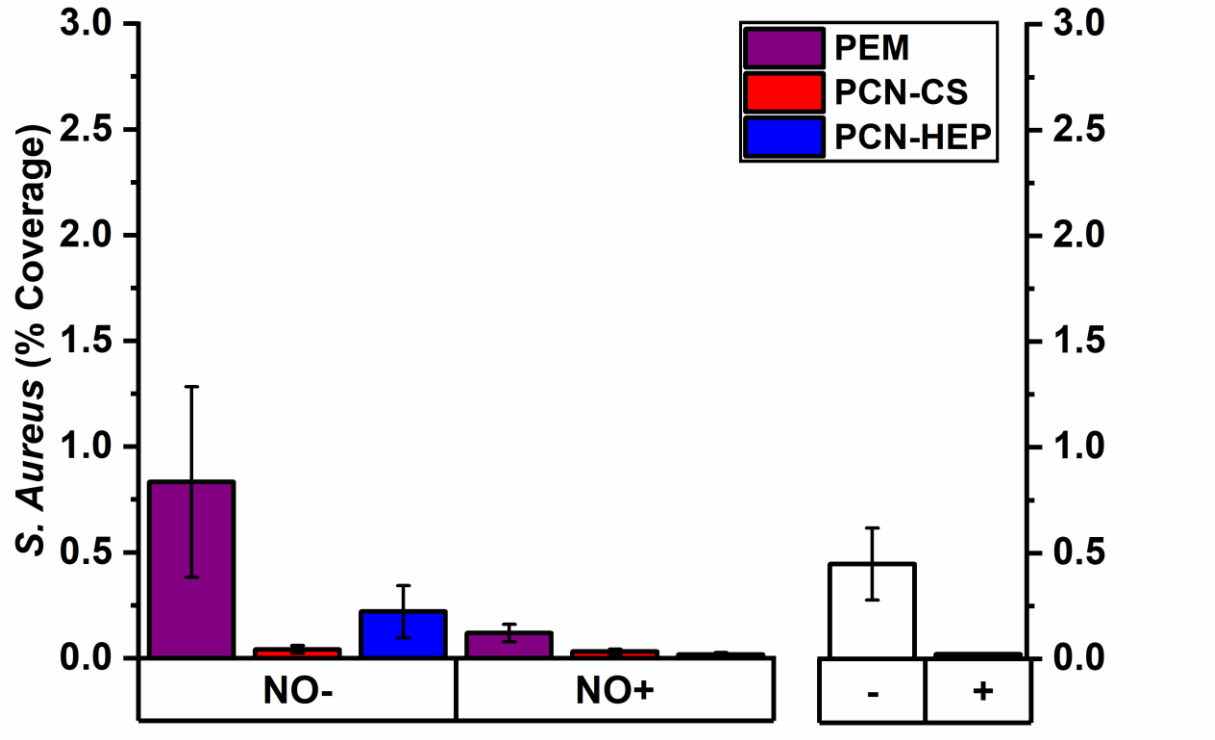


**Figure 2.S7**. *Staphylococcus aureus* attachment after 6 h of incubation. Two-factor ANOVA with post hoc Tukey test was conducted (on log-transformed data) of experimental samples, where the factors are NO+/NO- and surface type. There are no significant differences among experimental groups. Controls are bacteria with (+) and without (-) antibiotic treatment on polystyrene.

APPENDIX 2: SUPPLEMENTARY INFORMATION CHAPTER 3

## Overview

This section contains supplementary information from chapter 3 that was published with the corresponding manuscripts. It also contains data from additional experiments that were conducted but did not get published with the manuscript.

## Chapter 3 Supplementary Information

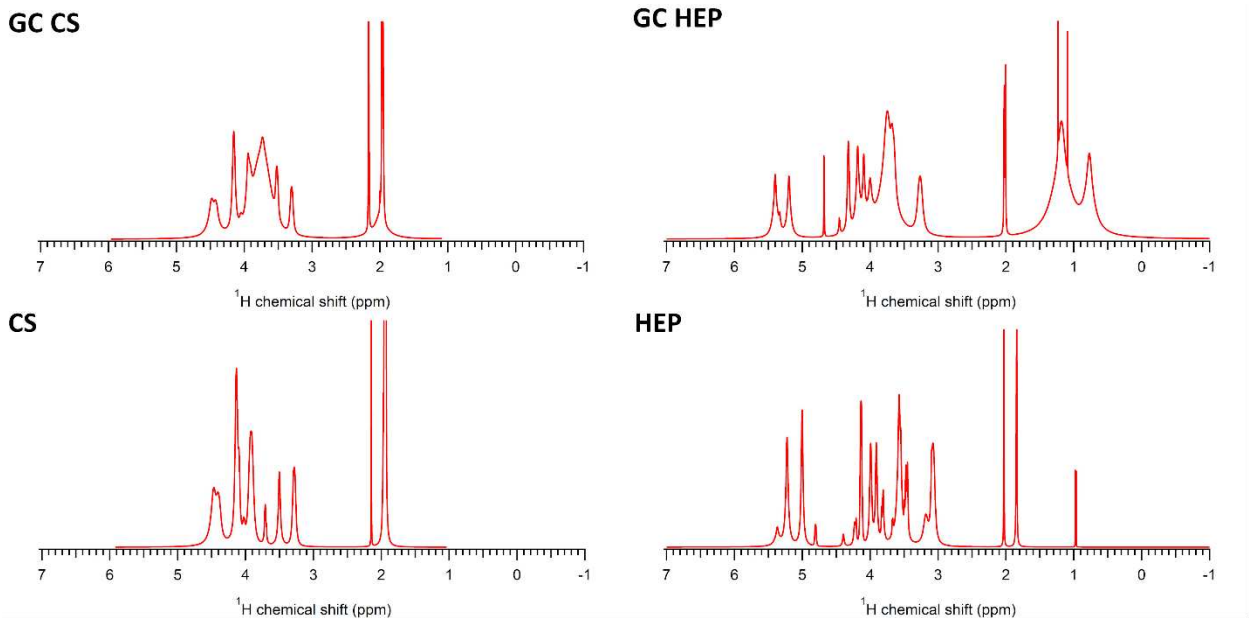


**Figure 3.S1.** $^1$H NMR spectra ($D_2O$ 400 MHz) of CS, HEP, and CS, HEP copolymers. Proton assignments in the untreated GAGs and copolymers can be made according to Pomin, V.H. *Anal. Chem.* 2013, 86, 65-94. Comparing the spectra confirms the conjugation of CS and HEP to the HA-BMPH backbone.

**Table 3.S1.** Average Size, Polydispersity Index (PDI), and ζ potential (mean ± standard deviation) of HA-CS and HA-HEP copolymers.

| Sample | Hydrodynamic diameter (nm) | PDI | Z-Potential (mV) |
|---|---|---|---|
| GC CS | 302 ± 5 | 0.351 ± 0.0085 | -32 ± 3.0 |
| GC HEP | 367 ± 3 | 0.342 ± 0.0175 | -20 ± 2.0 |
| PCN CS | 248 ± 2 | 0.135 ± 0.0104 | -25 ± 1.0 |
| PCN HEP | 284 ± 4 | 0.278 ± 0.0066 | -22 ± 0.2 |

**Table 3.S2.** *p*-Value results of a one-way repeated-measures ANOVA a with pairwise comparisons to compare samples exposed to hyaluronidases IV-S, I-S, and II.

| Enzyme: | Hyaluronidase IV-S | Hyaluronidase I-S | Hyaluronidase II |
|---|---|---|---|
| Sample comparison | p-value | p-value | p-value |
| HA-CS | 0.0006 | <0.0001 | 0.9925 |
| HA-HEP | <0.0001 | <0.0001 | <0.0001 |
| HA-GC CS | <0.0001 | <0.0001 | 0.0032 |
| HA-GC HEP | <0.0001 | <0.0001 | <0.0001 |
| HA-PCN CS | 0.0762 | <0.0001 | 0.0001 |
| HA-PCN HEP | <0.0001 | <0.0001 | <0.0001 |
| CS-HEP | 0.0020 | 0.0081 | <0.0001 |
| CS-GC CS | 0.7680 | 0.9989 | 0.0017 |
| CS-GC HEP | 0.0106 | 0.1479 | <0.0001 |
| CS-PCN CS | 0.5055 | 0.1264 | 0.0138 |
| CS-PCN HEP | 0.0007 | 0.0019 | <0.0001 |
| HEP-GC CS | 0.0468 | 0.0003 | 0.0211 |
| HEP- GC HEP | 0.9615 | 0.7595 | 0.2622 |
| HEP-PCN CS | <0.0001 | 0.7984 | <0.0001 |
| HEP-PCN HEP | 1.0000 | 1.0000 | 1.0000 |
| GC CS-GC HEP | 0.2142 | 0.0105 | 0.9000 |
| GC CS-PCN CS | 0.0037 | 0.0080 | <0.0001 |
| GC CS-PCN HEP | 0.0222 | <0.0001 | 0.0041 |
| GC HEP-PCN CS | <0.0001 | 1.0000 | <0.0001 |
| GC HEP-PCN HEP | 0.9718 | 0.6160 | 0.1256 |
| PCN CS-PCN HEP | <0.0001 | 0.6686 | <0.0001 |

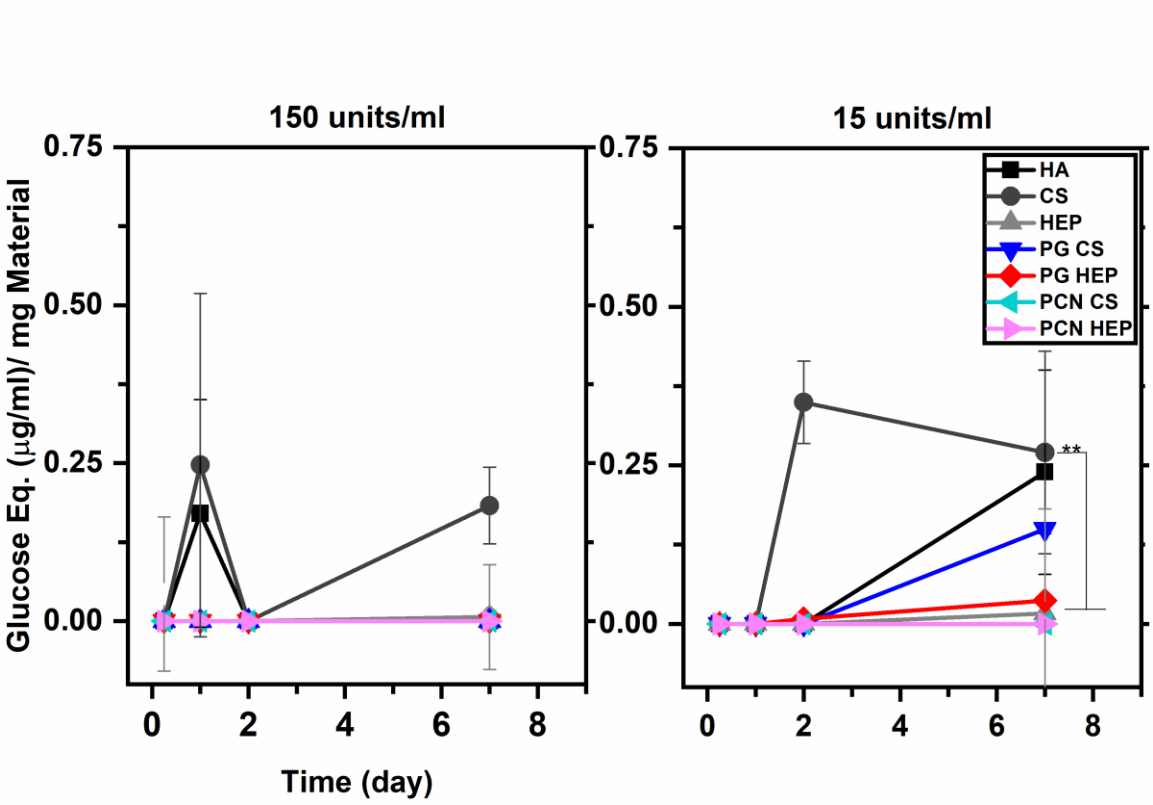


**Figure 3.S2.** Relative enzymatic degradation of HA, CS, and HEP controls, and PG mimics when exposed to lysozyme at concentrations of 150 units/mL and 15 units/mL. Values are converted to glucose equivalent (ug/mL) and normalized to mass of material in solution ($n$ = 3) (mean ± standard deviation). Statistically significant differences are indicated by stars and crosses (* $p < 0.05$, ** $p < 0.005$, *** $p < 0.0005$). A one-way repeated-measures ANOVA with pairwise comparisons was also conducted to determine differences between samples.

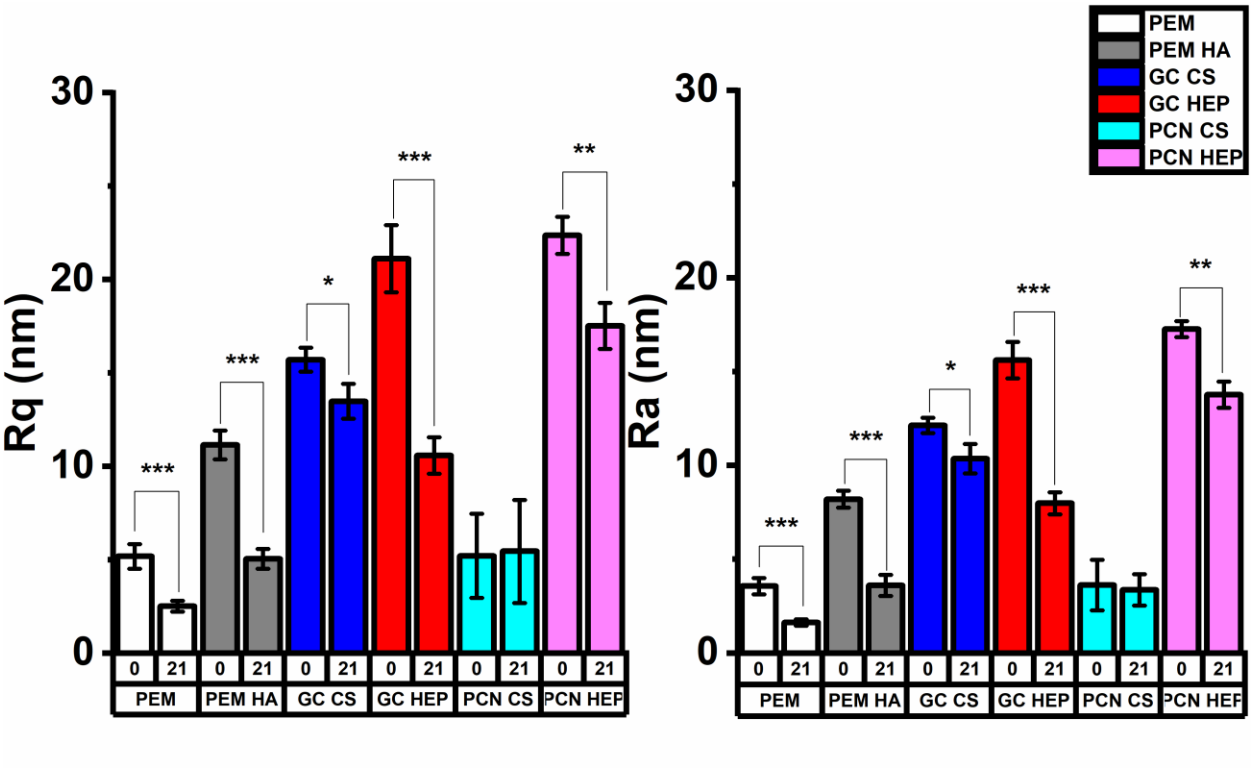


**Figure 3.S3.** Roughness values for surfaces treated submerged in enzyme dilutant for day 0 and 21 ($n$ = 6) (mean ± standard deviation). Paired $t$-tests were conducted to determine the change in samples before and after incubation in dilutant solution. Statistically significant differences are indicated by stars (* $p < 0.05$, ** $p < 0.005$, *** $p < 0.0005$).

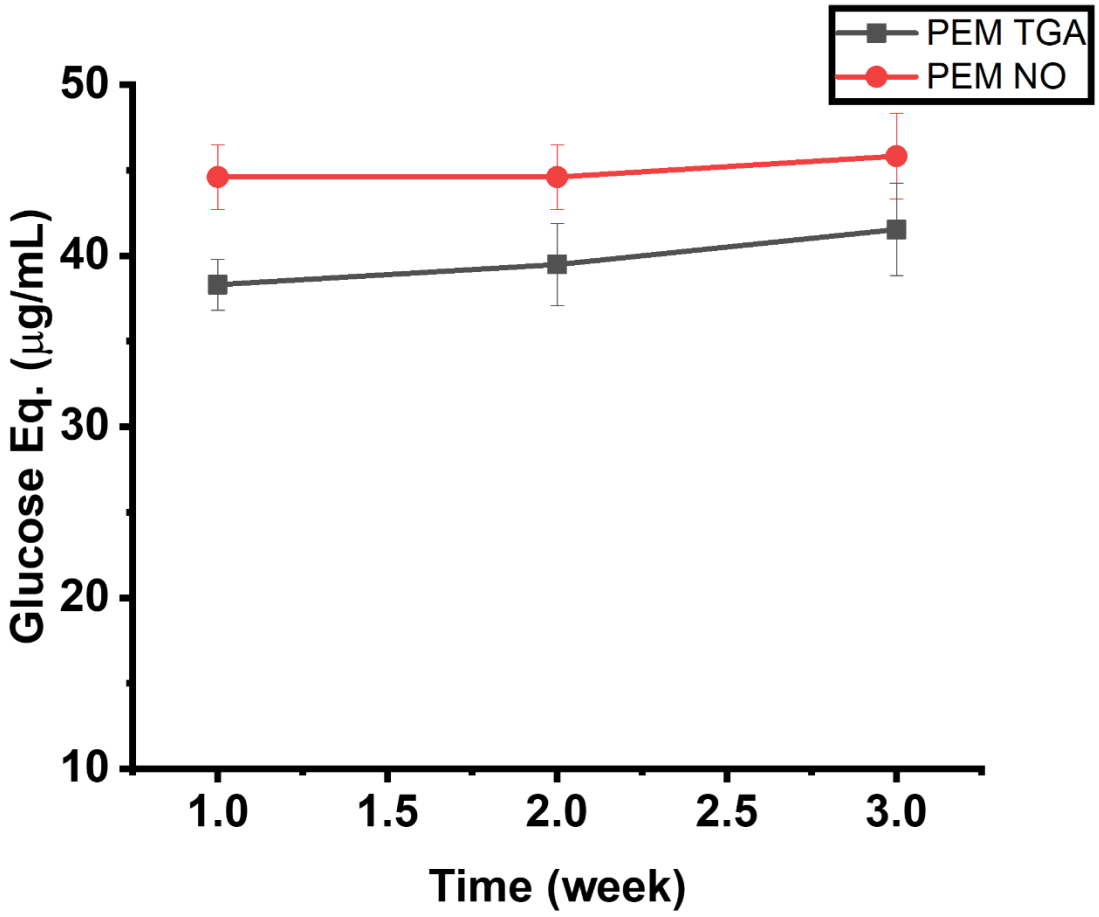


**Figure 3.S4.** Relative enzymatic degradation of PEM surfaces with chitosan thioglycolic acid (PEM TGA) and nitrosated PEM TGA (PEM NO) when exposed to hyaluronidase I-S. Values are converted to glucose equivalent (μg/mL)($n$ = 3) (mean ± standard deviation). A one-way repeated-measures ANOVA with pairwise comparisons was conducted to determine differences between samples. Statistically significant differences are indicated by stars (* $p < 0.05$, ** $p < 0.005$, *** $p < 0.0005$).

APPENDIX 3: SUPPLEMENTARY INFORMATION CHAPTER 4

## Overview

This section contains supplementary information from chapter 4 that will be published with the corresponding manuscripts. It also contains data from additional experiments that were conducted but will not be published with the manuscripts. This data may be used for future work.

## Chapter 4 Supplementary Information

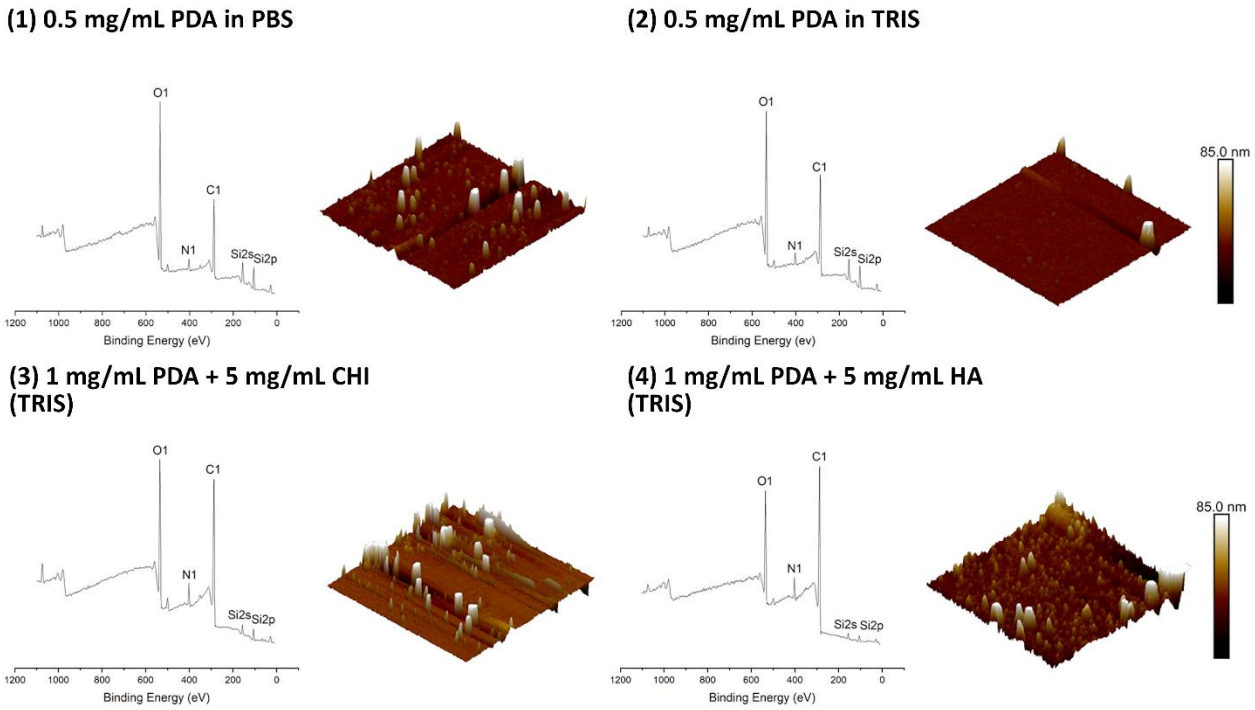


**Figure 4.S1.** XPS survey spectra and AFM images of glass surfaces treated with (1) 0.5 mg/mL PDA in PBS buffer pH 7.4, (2) 0.5 mg/mL PDA in Tris(hydroxymethyl)aminomethane (TRIS) buffer pH 8.0, (3) 1 mg/mL PDA + 5 mg/mL chitosan (CHI) in TRIS pH 8.0, and (4) 1 mg/mL PDA + 5 mg/mL hyaluronic acid (HA). Peaks labeled on XPS spectra correspond to oxygen, carbon, nitrogen, and silica. AFM images are of a 5x5 µm area.

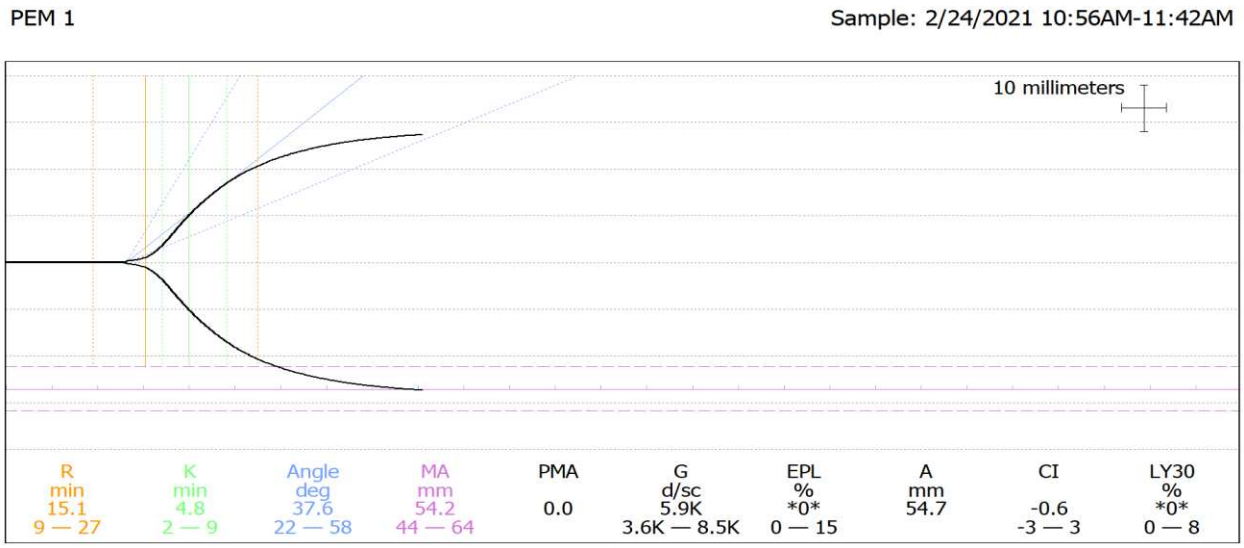


**Figure 4.S2.** Thromboelestograph obtained from TEG analysis, from which reaction time (R) (orange), clot time (K) (green), α-angle (A) (blue) and clot strength (MA) (purple) were calculated.

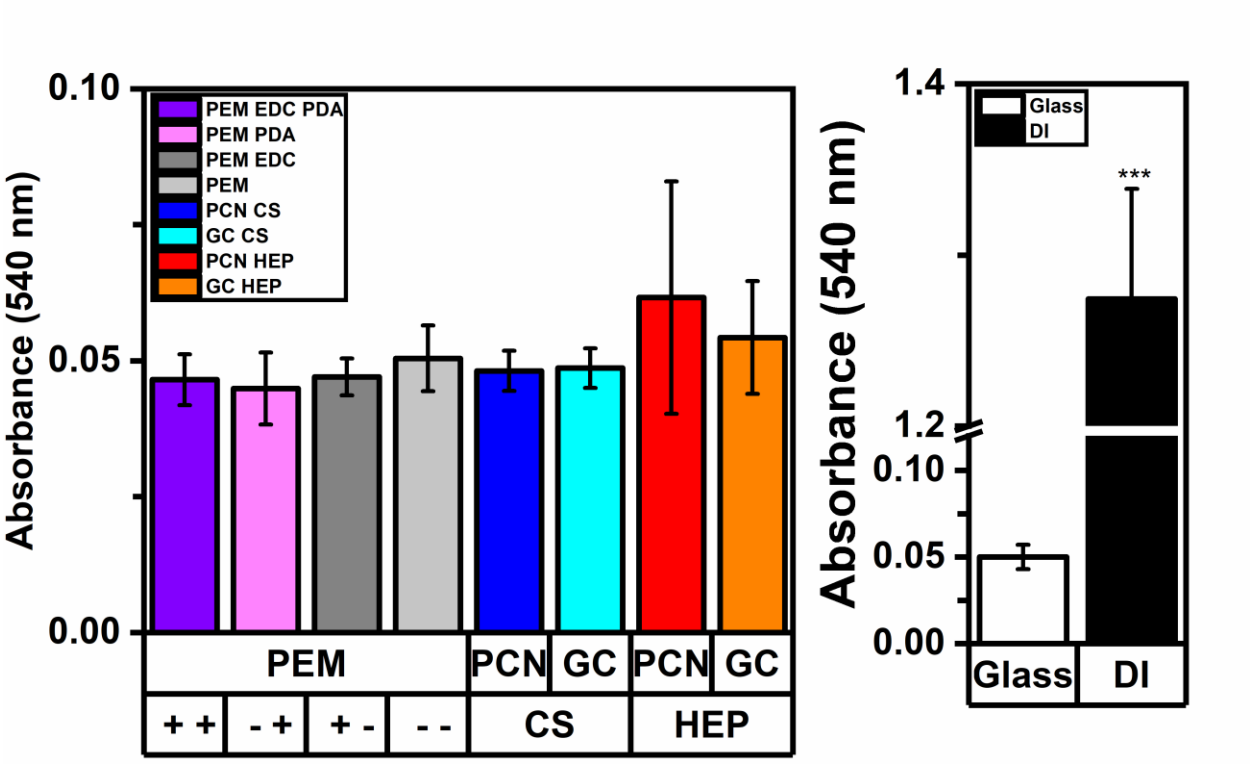


**Figure 4.S3.** Hemolysis absorbance values for PEM EDC PDA, PEM PDA, PEM EDC, PEM, PCN CS, GC CS, PCN HEP, and GC HEP surfaces (left) and untreated glass and full hemolysis controls (DI)(right) after 3 h exposure to RBC solutions (mean ± standard deviation) (n= 4). The "++" symbol corresponds to treatment with PDA and EDC, "- +" corresponds to treatment with PDA and not EDC, "+ -" corresponds to no PDA and treatment with EDC, and "- -" corresponds to untreated PEM. A two-way ANOVA with a

pairwise comparisons was conducted to determine differences between surface chemistry/treatment (+ +, - +, + -, - -, CS, or HEP) and surface type (PEM, PCN, or GC). A one-way ANOVA with a pairwise Tukey test was conducted to determine differences between samples and the full hemolysis control. Asterisks indicate the greatest significance value between one sample and all the other samples (* $p < 0.05$, ** $p < 0.005$, *** $p < 0.0005$).

**Table 4.S1.** Roughness (Rq and Ra) values (mean ± standard deviation) taken from AFM images (5x5 um) of PEM, PEM EDC, PEM PDA, and PEM PDA EDC.

| Sample | Rq (nm) | Ra (nm) |
|---|---|---|
| PEM | 5.57 ± 0.38 | 3.66 ± 0.43 |
| PEM EDC | 5.28 ± 0.43 | 4.00 ± 0.50 |
| PEM PDA | 12.48 ± 2.02 | 8.20 ± 1.29 |
| PEM PDA EDC | 11.66 ± 1.32 | 7.99 ± 0.91 |

**Table 4.S2.** Area under the curve ratios (mean ± standard deviation) for carbon/silica, carbon/nitrogen, and nitrogen/silica calculated from curve fitting of XPS high resolution spectra. Spectra values were obtained for PEM, PEM EDC, PEM PDA, and PEM PDA EDC channels after exposure to flowing $H_2O$ after 2 h of exposure (n = 4).

| Sample | C/Si | C/N | N/Si |
|---|---|---|---|
| **PEM** | 9.96 ± 0.75 | 13.51 ± 2.19 | 0.70 ± 0.10 |
| **PEM EDC** | 13.8 ± 1.40 | 13.61 ± 2.68 | 1.04 ± 0.12 |
| **PEM PDA** | 9.34 ± 3.30 | 12.17 ± 1.06 | 0.76 ± 0.34 |
| **PEM PDA EDC** | 15.26 ± 2.97 | 9.11 ± 0.94 | 1.66 ± 0.34 |

**Table 4.S3**. TEG parameter and CI values for all glass controls used throughout TEG experiments.

| Sample | Reaction time (R) | Clot time (K) | α-angle (A) | Clot strength (MA) | Clot Index (CI) |
|---|---|---|---|---|---|
| **Glass CNTLs** | 11.76 ± 3.68 | 3.76 ± 0.16 | 54.71 ± 17.68 | 57.3 ± 1.07 | 0.54 ± 0.13 |

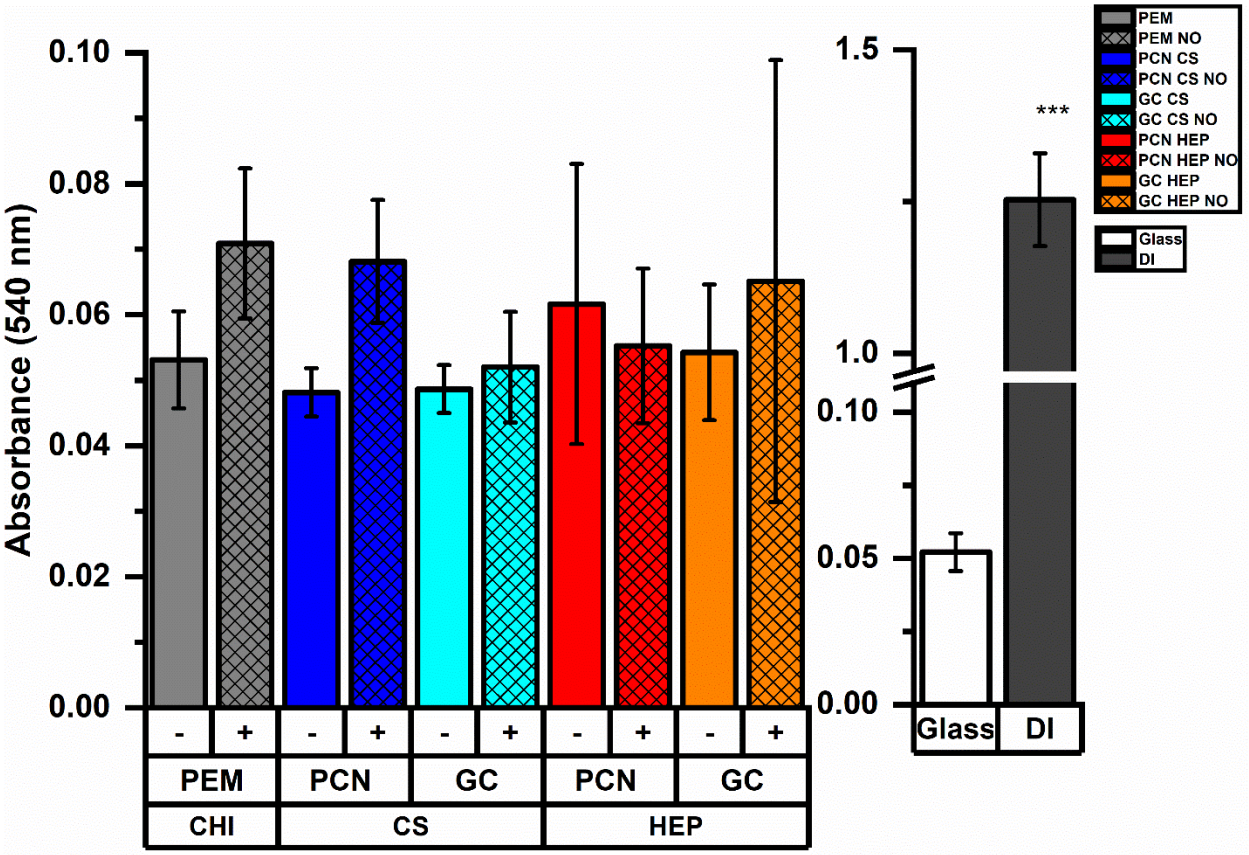


**Figure 4.S4.** Absorbance values at 540 nm from hemolysis samples after 3h exposure to RBC solutions for PEM, PCN CS, GC CS, PCN HEP, GC HEP with and without nitric oxide release and glass and DI water (full hemolysis) controls (mean ± standard deviation) (n= 4). The "-" symbol corresponds to no nitric oxide release and "+" corresponds to nitric oxide release. A three-way ANOVA with a pairwise comparisons was conducted to determine differences between surface chemistry/treatment (CHI, CS, or HEP), surface type (PEM, PCN, or GC), and nitric oxide release (- or +). A one-way ANOVA was used to compare all other surface types to controls. Asterisks indicate the greatest significance

value between one sample and all the other samples (* $p < 0.05$, ** $p < 0.005$, *** $p < 0.0005$).

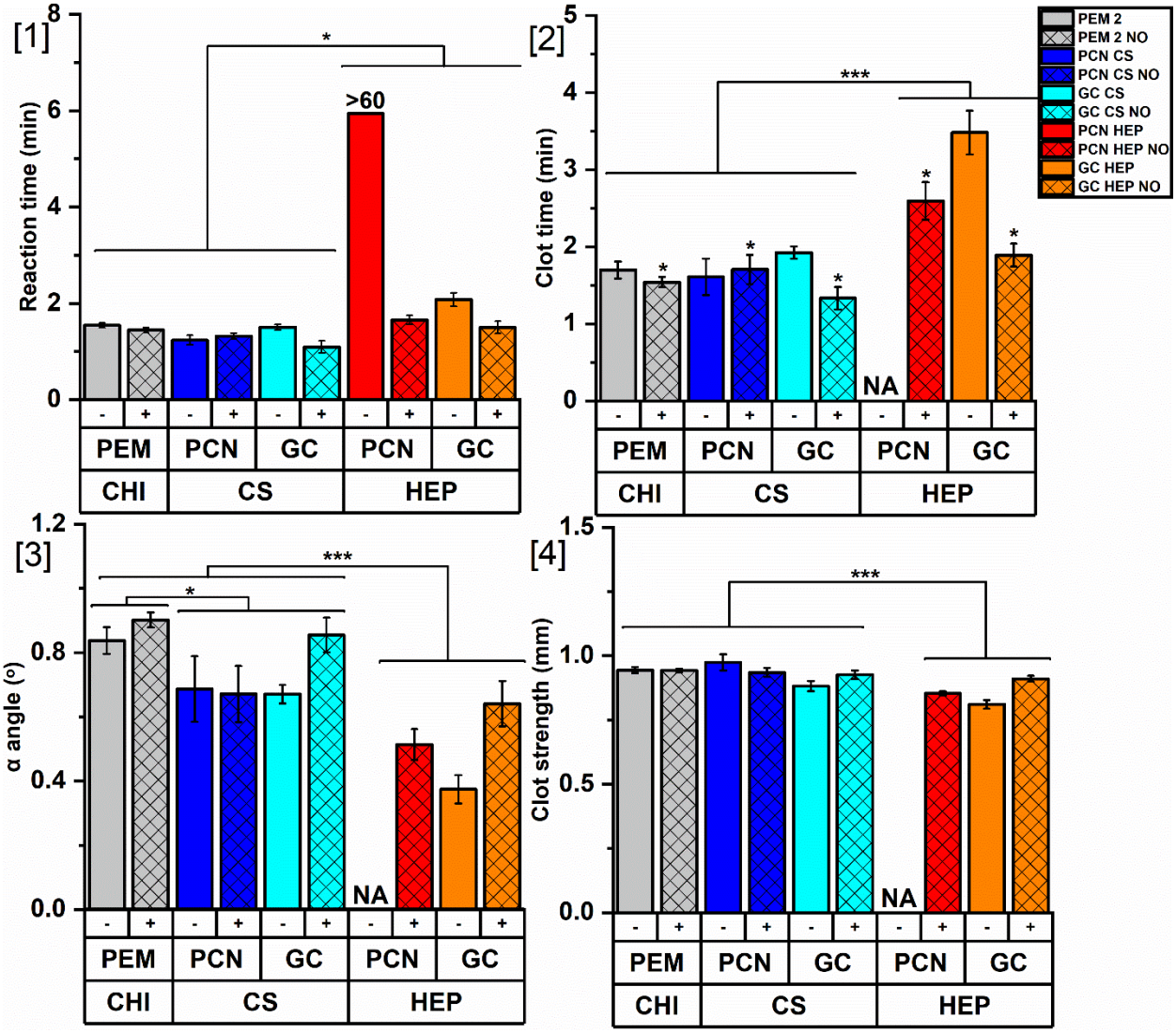


**Figure 4.S5.** Values normalized to glass controls for [1] reaction time [2] clot time [3] α-angle [4] clot strength (mean ± standard deviation) (n= 4-5 for all samples except PCN HEP surfaces which did not clot) for PEM, PCN CS, GC CS, PCN HEP, GC HEP with and without nitric oxide release. The "-" symbol corresponds to no nitric oxide release and "+" corresponds to nitric oxide release. A three-way ANOVA with a pairwise comparisons was conducted to determine differences between surface chemistry/treatment (CHI, CS, or HEP), surface type (PEM, PCN, or GC), and nitric oxide release (- or +). Asterisks indicate the significance value between different treatment groups (* $p < 0.05$, ** $p < 0.005$, *** $p < 0.0005$). The addition of PCN HEP to the surface inhibited clot formation past 1 h so PCN HEP was not included in statistical analysis for clot time, alpha angle, and clot strength. The addition of HEP significantly influenced all parameters. Nitric oxide release reduced clot time. The addition of CS significantly reduced α angle as compared to CHI surfaces, and HEP reduced α angle compared to both CS and CHI surfaces.

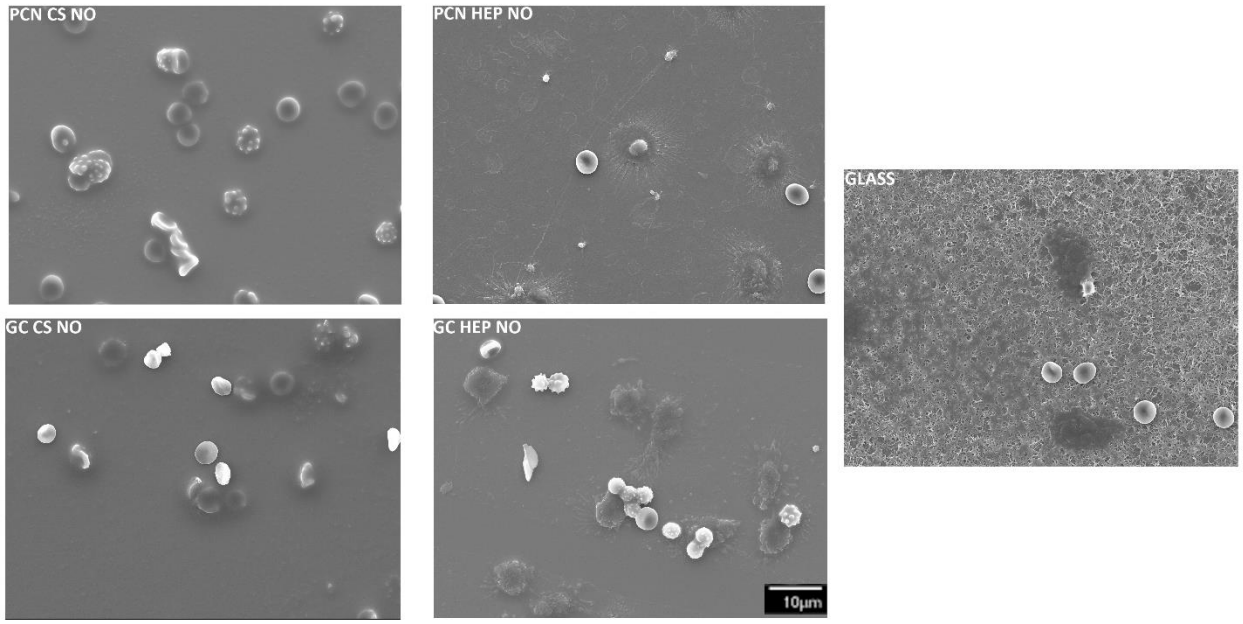


**Figure 4.S6.** SEM images (1000x magnification) of surfaces after incubation with whole blood after 1 hr. All surfaces had reduced clot activity compared to glass control, but all blood in sample wells formed clots after 1 hr.